INTERNATIONAL SCHOOL FOR ADVANCED STUDIES
ELEMENTARY PARTICLE THEORY SECTOR

STATISTICAL PHYSICS CURRICULUM
Academic Year 2010/2011

TOPOLOGICAL QUANTUM COMPUTATION, ANYONS AND NON-ABELIAN GAUGE POTENTIALS

THESIS SUBMITTED FOR THE DEGREE OF
Doctor Philosophiae

Advisors:
Prof. Giuseppe Mussardo
Dr. Andrea Trombettoni

Candidate:
Michele Burrello

26th September 2011

We shall not cease from exploration
And the end of all our exploring
Will be to arrive where we started
And know the place for the first time.

T. S. Eliot, Four Quartets, Little Gidding **V**

Abstract

This thesis deals with the study of topological quantum computation and the possible realization of non-Abelian anyons in cold atomic gases. Two main topics are investigated: the first subject is the quantum hashing technique to approximate unitary operators by braiding non-Abelian anyons, the second one is the analysis of systems of multicomponent ultracold atoms in the presence of an effective non-Abelian gauge potential giving rise to a quantum Hall regime.

The common frame of these topics is the emergent study of topological phases of matters, driven by the necessity to overcome the Landau-Ginzburg paradigm to describe strongly correlated quantum systems such as the quantum Hall ones. To achieve this goal it is crucial to involve seemingly distant branches of knowledge such as conformal field theories, topological field theories, integrable models, knot theory, tensor category theory but also quantum information and computation, in order to deepen our understanding of the new and exciting experimental and numerical results given by the analysis of different systems sharing these topological properties.

Due to the deep interdisciplinary character of this wide research field it seems natural to face it from different points of view. This choice is reflected in the structure of this thesis where I present first a more abstract study of the theory of non-Abelian anyons and its application to topological quantum computation, and then I analyze more concrete examples of ultracold atomic systems that are suitable to show non-Abelian anyons as local excitations.

The first main topic of this thesis is the quantum hashing algorithm to solve the problem of the quantum compiling: the quantum hashing is a technique to obtain a fast approximation of a target quantum gate in the unitary group SU(2) represented as a product of the elements of a universal basis. The hashing exploits the structure of the icosahedral group in order to reduce the algorithm to a search over a finite number of elements and one of its main advantages is the possibility of iteration to obtain accurate representations of the targets. To describe this algorithm we mainly refer to the case of Fibonacci anyons, however the technique is much more general and can be extended not only to different anyonic theories but also to arbitrary quantum computation setups.

Given the importance of the physical realization, detection and manipulation of non-Abelian anyons, the second part of this thesis is devoted to a possible realization of non-Abelian quantum Hall states. The systems I analyze are constituted by ultracold atomic gases subjected to artificial external non-Abelian gauge fields which mimic a spin-orbit coupling. I show that such potentials, acting on atoms

with an effective pseudospin, may give rise to many-body quantum Hall states and, under certain conditions, to non-Abelian excitations. In particular I consider a realistic gauge potential for which the Landau levels can be exactly determined: the non-Abelian part of this vector potential lifts the pseudospin degeneracy of the Landau levels and, in the presence of strong repulsive interactions, the ultracold atomic gas is generally described by deformed Laughlin states. However, at the degeneracy points of these deformed Landau levels, non-Abelian quantum Hall states appear and explicit analytical results can be obtained: these ground states, including a deformed Moore-Read state that is characterized by Ising anyons as quasiholes, are studied for both fermionic and bosonic gases.

The work here presented is based on the following papers:

[1] M. Burrello, H. Xu, G. Mussardo and X. Wan, *Topological Quantum Hashing with the Icosahedral Group*, Physical Review Letters **104**, 160502 (2010).

[2] M. Burrello, G. Mussardo and X. Wan, *Topological Quantum Gate Construction by Iterative Pseudogroup Hashing*, New Journal of Physics **13**, 025023 (2011).

[3] M. Burrello and A. Trombettoni, *Non-Abelian Anyons from Degenerate Landau Levels of Ultracold Atoms in Artificial Gauge Potentials*, Physical Review Letters **105**, 125304 (2010).

[4] M. Burrello and A. Trombettoni, *Ultracold Atoms in U(2) non-Abelian Gauge Potentials Preserving the Landau Levels*, arXiv:1108.0839 (2011) (to be published in Physical Review A).

Contents

Chapter 1

Introduction

1.1 Topological order

The fascinating phenomenon of the Quantum Hall Effect, discovered by von Klitzing, Dorda and Pepper in 1980 [5], constitutes one of the most remarkable and unexpected development of condensed matter physics in the last decades. Its importance is not only related to the incredible accuracy of the quantization of the Hall conductivity, which is a striking manifestation of quantum phenomena at the mesoscopic scale, but it relies also on its connection with fundamental principles of physics. The theoretical challenge imposed by the understanding of the Quantum Hall Effect required to build a new paradigm in our knowledge of condensed matter systems: since the works by Laughlin [6] and Thouless [7] it was clear that a satisfactory explanation of such a robust and universal phenomenon had to be built on as much solid theoretical bases, as gauge invariance [6] and topological invariance [7, 8].

The topological properties of the quantum Hall conductivity became even more important after the experimental observation of the Fractional Quantum Hall Effect (FQHE), conducted by Tsui, Stormer and Gossard in 1982 [9]. This discovery made evident the existence of several quantum Hall states, characterized by different physical properties and labelled by their filling factor ν, which can be regarded as different phases of a phase diagram. Nevertheless, their classification cannot be simply related to a local order parameter as prescribed by the usual Ginzburg-Landau approach, but requires the novel idea of a *topological order*, a long-range order of topological origin (see the reviews [10, 11]). Such condensed phases of matter are topological invariant, at least at small enough temperatures, and their properties are insensitive to local perturbation such as impurities or deformations. This behaviour, however, is not related to a given symmetry of the Hamiltonian describing the quantum Hall systems, but emerges as an effective symmetry at low energy. Therefore the order parameter classifying these phases doesn't arise from a broken symmetry of the Hamiltonian, as in the Ginzburg-Landau theory, but must be described in terms of non-local observables that define a new kind of ordering, universal and robust against arbitrary perturbation. To a certain extent we can thus consider the existence of a topological order as the contrary of a sym-

metry breaking: topological order does not require any preexisting symmetry of the Hamiltonian but it brings to new conservation laws of the system [12].

The topological nature of the quantum Hall states becomes explicit thanks to the description of such systems with an effective topological field theory in the low energy regime [13]. In particular quantum Hall systems can be modelled by Chern-Simons field theories (see [14] for a review), topological field theories of the kind first studied by Witten [15, 16]. One of the advantages of this approach is to allow an abstract description of the different topological excitations of the quantum Hall systems, namely the anyonic quasiholes or quasiparticles we will discuss in the following, under the light of knot theory [16, 17, 18, 19] or tensor category theory [12, 20].

The most puzzling characteristic of FQHE is perhaps the fractional charge of the gapped excitations in these systems. This phenomenon, together with the electronic incompressibility that derives from the exceptional stability of the observed plateaux at fractional filling, cannot be explained in terms of non-interacting electrons. The most important contribution in the understanding of the structure of such states is due to Laughlin [21], who managed to describe the $\nu = 1/3$ plateau in terms of the well-known wavefunction named after him. After his seminal work it became clear that the charged excitations of the fractional quantum Hall states aren't, in general, fermions or bosons, but obey more exotic anyonic statistics [22]. Moreover, with generalizations of the Laughlin wavefunction, it is possible to build hierarchies of states which describe the quantum Hall plateaux with an odd denominator filling [23].

Yet another experimental milestone of the study of the Quantum Hall Effect gave rise to new and deeper theoretical investigations. In 1987 Willett *et al.* [24] observed a quantum Hall plateau having an even denominator filling, the celebrated $\nu = 5/2$ quantum Hall state. This state cannot be directly related to the previously studied wavefunctions and brought to the necessity of finding new tools in the descriptions of such systems. Even if, so far, there is no completely unambiguous description of the $\nu = 5/2$ state, the main proposals done are based on the idea by Moore and Read [25] of writing the quantum Hall wavefunctions as correlation functions of Conformal Field Theories (CFTs). In particular they proposed a new wavefunction, the Pfaffian state, adopting the Ising minimal model to describe the $\nu = 5/2$ state. This brings to the revolutionary notion of non-Abelian anyons that we will analyze in the following chapter.

CFTs [26] are a useful tool to analyze quantum Hall states, and, in general, to investigate systems showing a topological order. Their relation with the Quantum Hall Effect was already implicit in the Chern-Simons description of these systems, since it can be shown that such topological field theories can be mapped in CFTs [16]. After the work by Moore and Read, CFTs had been successfully used to describe both quantum Hall states and their edge modes, and their study can be put at the basis of most of the anyonic models (see [20] and references therein).

The connection between CFTs and topological order gave rise to many models showing topological properties beside the Quantum Hall Effect. The simplest examples are constituted by the celebrated Kitaev's models: the toric code giving rise to Abelian anyons [27], and the honeycomb lattice model characterized by

non-Abelian Ising anyons [12]. Both of them are spin models on a lattice whose topological structure emerges studying the characteristics of the ground state and its low energy excitations. More abstract and general models featuring a topological order can be built starting from loop or RSOS models [28, 29, 30], and, finally, their most general formulation can be accomplished through the so called sting-net models [18, 19] that emphasize the mathematical framework underlying topological phases and allow to realize a Hamiltonian for every tensor category theory. Moreover it has been shown that such structures can be generalized also in three dimensions and their partition function can be expressed in terms of knot invariants [31].

Since the works by Kitaev, Freedman and Wang [32, 33, 34, 27] it was realized by several authors [35, 36, 37, 38, 39, 40, 41, 42] that topological order can be regarded also as a resource. Quantum systems showing topological properties can be exploited to overcome the decoherence phenomena and the intrinsic noise sources that affect all the main schemes to achieve quantum computation. This is the main idea at the origin of *Topological Quantum Computation*: to encode and manipulate information in a topologically protected way, insensitive to local sources of errors (see the reviews [20, 43]). In particular the possibility of storing information is related to the topological degeneracy of the ground states typical of systems characterized by Abelian anyonic excitation, as, for example, the toric code [27]; whereas the construction of quantum gates relies on the nontrivial braiding properties of non-Abelian anyons we will analyze in the following.

Topological quantum computation and the study of topological states of matter evolved together in the last decade. The appealing quantum computation schemes offered by the manipulation of non-Abelian anyons prompted the research of new physical systems suitable to present such quasi-particles as excitations above their ground state. Beside the previously mentioned studies on Quantum Hall Effect, based on two-dimensional electronic gas in high-mobility semiconductor structures, in the last years new theoretical and experimental proposals were considered, in order to obtain physical systems with nontrivial topological properties. Among them I would like to mention the studies on quantum Hall regime in cold atomic gases (see [44] for an extensive review) and the works on p-wave superconductors [45] that are strongly related to the $\nu = 5/2$ Hall state [46]. Finally the new research field on topological insulators allowed to extend the notion of topological order to several physical systems and models characterized by different symmetries (see [47, 48] and references therein) and it seems to offer the possibility of realizing Majorana fermions (and therefore non-Abelian Ising anyons) in one-dimensional systems characterized by both an s-wave superconductor pairing and a strong spin-orbit interaction [49, 50, 51].

Anyons are the main feature linking these systems and their existence is intrinsically related to a non trivial topological order. Moreover, they are the key to encode and manipulate information in topological quantum computation; therefore, in the next section, I will introduce their main characteristics and the mathematical tools to describe them.

1.2 Anyons and the braid group

A main feature of quantum theories is the idea of indistinguishable particles, which implies that the exchange of two identical particles in a system is a symmetry which can be related to a unitary operator on the Hilbert space describing that system. In a three-dimensional space the well known spin-statistics theorem states that particles must be bosons or fermions, and their exchange operator is described respectively by the identity or by the multiplication of a factor -1. In two spacial dimensions, however, the spin-statistics theorem does not hold and this opens the possibility of having a much wider variety of particle statistics: indistinguishable particles that are neither bosons nor fermions are called *anyons*.

In general we can state that, for fermions or bosons, a system of identical particles can be described by states which depend only on the permutation of these particles. The wavefunctions describing these states are independent on the past configurations of the particles and, in particular, on the worldlines describing the past evolution of the system. The permutation group, in this case, is enough to identify every possible configuration of the system and the main feature that characterizes the behaviour of bosons and fermions is that the operator σ associated to the exchange of two particles is its own inverse: $\sigma^2 = 1$.

Anyons are described, instead, by the more general *braid group*. The time evolution of a two-dimensional system of identical particles is defined by the pattern of the worldlines of these particles which constitute the strands of a braid (see Fig. 1.1). Since the worldlines are forbidden to cross, such braids fall into distinct topological classes that cannot be smoothly deformed one to another. In this case the exchange of two particles can happen counterclockwise, σ, or clockwise, σ^{-1}, and, in general, $\sigma^2 \neq 1$. Moreover the temporal order of the exchanges is important because different orders bring to non-equivalent braids, and this is the basis of the topological degeneracy of anyonic systems.

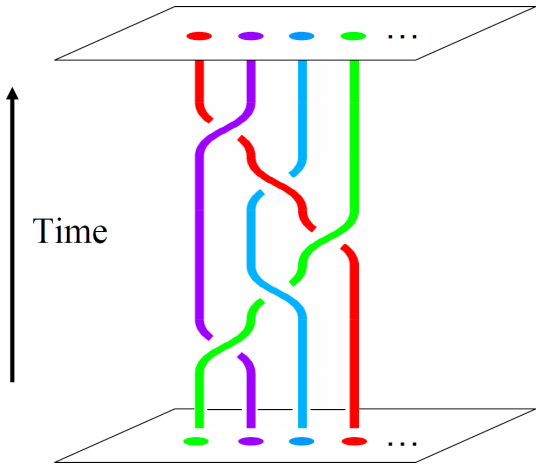

Figure 1.1: The worldlines of anyons in a two dimensional space are represented by braids constituted by the ordered exchanges σ of the particles.

Let us briefly summarize the main characteristics of the braid group, which will

be useful to the purpose of topological quantum computation. A more extensive introduction to the subject can be found in [52]. The braid group is generated by the counterclockwise exchange operators σ_i between the pair $(i, i+1)$ of neighboring particles. If we consider the possible braids of n strands, corresponding to the worldlines of n anyons, this group is characterized by the following relations:

$$\sigma_i\sigma_j = \sigma_j\sigma_i \quad \text{if} \quad |i-j| > 1\,, \tag{1.1}$$

$$\sigma_i\sigma_{i+1}\sigma_i = \sigma_{i+1}\sigma_i\sigma_{i+1} \quad \text{for} \quad i = 1, ..., n-2 \tag{1.2}$$

The first equation just states that the exchanges of disjoint pairs of anyons commute, whereas (1.2) is the Yang-Baxter relation which can be easily verified observing Fig. 1.2: both the terms in the equation represent two particles exchanging their position by encircling a third one.

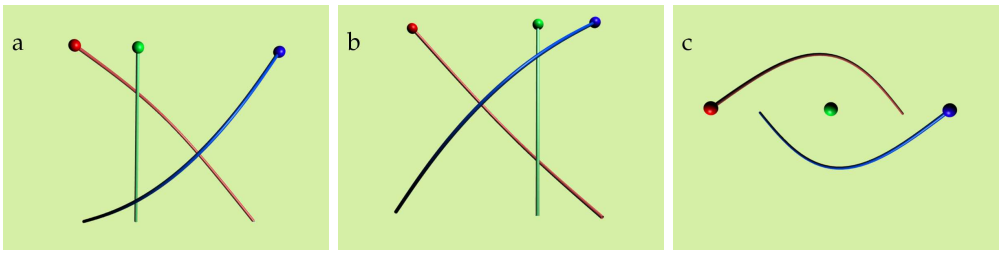

Figure 1.2: The Yang-Baxter relation 1.2 is illustrated: **a)** represents the anyonic worldlines in 2+1 dimensions corresponding to the left hand side of Eq. 1.2, **b)** corresponds to the right hand side and **c)** depicts the trajectories of the anyons on the plane.

The braid group admits an infinite number of unitary irreducible representations: the Abelian anyons are indistinguishable particle that transform as a one-dimensional representation of the braid group; in this case each generator of the braid group is associated with the same phase $e^{i\theta}$, in particular the case $\theta = 0$ corresponds to bosons whereas $\theta = \pi$ corresponds to fermions. The Abelian anyons, first studied by Wilczek [53], are present as localized and gapped quasiholes and quasiparticles in the Abelian states of FQHE and, in general, are characterized by a fractional charge, as first observed in 1995 [54].

The peculiar statistics of Abelian anyons can be understood once we consider them as composite particles constituted by a unitary flux $\Phi_0 = hc/e$ and a fractional charge, which, in the most common case of a Laughlin state at filling ν, corresponds to $e^* = \nu e$. This description allows us to associate an Aharonov-Bohm phase to their exchange: when an Abelian anyons moves around another quasihole corresponding to a flux quantum, the resulting Aharonov-Bohm phase acquired by their wavefunction is $e^*\Phi_0/\hbar c = 2\pi\nu$. Therefore the exchange of two Abelian anyons is characterized by a phase $\nu\pi$ and the fractional charge determines the statistics of such particles (see [55, 56, 57] for extensive introductions about anyons in FQH systems). There are cases, however, in which the statistics cannot be easily deduced only from the Aharonov-Bohm effect and must be calculated explicitly through the interplay between Berry phases and the monodromy of the wavefunctions involved [22].

The existence of quasiholes with a fractional charge can be easily related to the quantum Hall conductance through a simple gedanken experiment due to Laughlin: let us consider a sample of quantum Hall liquid at filling factor ν and imagine to pierce it with an infinitely thin solenoid as in Fig. 1.3, creating an annulus. Adiabatically increasing the magnetic flux $\Phi_B(t)$ inside the solenoid from 0 to Φ_0 causes, by Maxwell's laws, an azimuthal electric field $E \propto \frac{d\Phi_B}{dt}$ to arise. This electric field generates, in turn, a radial current whose intensity $j = \sigma_H E = \nu E e^2/h$ is determined by the fractional Hall conductance. Once the flux reaches the value Φ_0, the total amount of charge transferred from the inner edge of the annulus to the outer one is $e^* = \nu e^2 \Phi_0/hc = \nu e$ and this amount of charge can be considered as the charge of the excitation created through the insertion of a flux quantum. This simple argument shows that an excitation characterized by a flux quantum has a fractional charge proportional to the filling factor of the quantum Hall liquid considered. Therefore the existence of quasiholes with a fractional charge is intrinsically related to the fractional Hall conductance simply by Maxwell's equations.

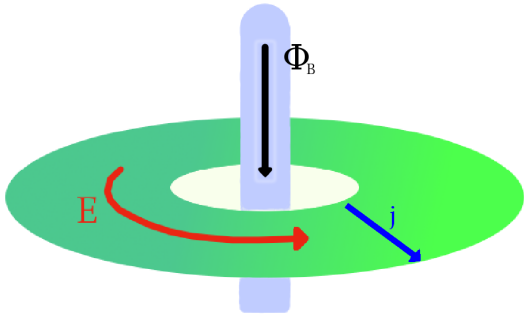

Figure 1.3: The adiabatic insertion of a magnetic flux in a quantum Hall liquid induces an azimuthal electric field which, in turn, implies a radial flow of a charge νe due to the quantum Hall conductance.

The last property of Abelian anyons I would like to mention is the topological degeneracy that, in principle, characterizes systems with a nontrivial topology. In every anyonic model there is a ground state corresponding to the absence of anyons. On the plane such state is unique, but on two-dimensional surfaces with nontrivial topology, such as the torus, this vacuum state becomes degenerate [52]. Such degeneracy depends on the existence of non-local operators that commute with the Hamiltonian but do not commute with each other. The most celebrated example of this degeneracy is found in the so called toric code [27]: in this case the Abelian anyons are constituted by electric and magnetic charges, whereas the non-local operators correspond to drag different Abelian anyons along the two possible inequivalent circumferences of the torus. These operators do not affect the energy but allow to divide the ground state space into four topological sectors that cannot

be locally distinguished. In this way one can store information in a topologically protected way inside such a system, however the Abelian nature of the system makes it unsuitable to manipulate this information.

So far we discussed the characteristics of Abelian anyons and we mentioned that, from a mathematical point of view, their behaviour corresponds to a one-dimensional representation of the braid group, whereas from the physical point of view, their statistics is usually described through suitable wavefunctions related to different Abelian quantum Hall states. There are, however, also higher-dimensional representations of the braid group that give rise to non-Abelian anyons: particles whose exchanges are defined by nontrivial unitary operators, corresponding to the braid generators σ_i, that, in general, do not commute with each other.

In particular the non-Abelian states of matter are characterized by a novel topological degeneracy: a collection of non-Abelian anyonic excitations with fixed positions spans a multi-dimensional Hilbert space and, in such a space, the quantum evolution of the multi-component wavefunction of the anyons is realized by braiding them. As we will discuss in the next chapter, the quantum dimension of this space is determined by peculiar characteristics of the considered anyonic model; and the operators defined by the exchange of these particles can be naturally represented by unitary matrices and constitute the building blocks to realize a topological quantum computation [20].

The signature of the anyonic properties of the quantum Hall excitations is their nontrivial evolution under braiding; therefore it is natural to probe this behaviour via interference measurements (see [20, 56, 58] and references therein for detailed reviews on the subject). Interferometry allows not only to detect the charge value of the excitations through the Aharonov-Bohm effect, but also to distinguish whether their nature is Abelian or non-Abelian. Concerning the charge measurements, for the $\nu = 1/3$ quantum Hall state the charge $e^* = e/3$ was first observed in 1995 [54]; after that, more precise observations were achieved by using measurements of quantum shot noise [59]. Regarding the $\nu = 5/2$ state there are several measurements of the fractional charge $e/4$ of the elementary excitations based both on shot noise and interferometry (see, for example, [60, 61]); and recently, some convincing indication about its non-Abelian nature was obtained [62], coherently with the Moore and Read description of the bulk and edge states. From the quantum computation point of view, interference could provide a useful tool to distinguish the different states obtained after the braidings of several non-Abelian anyons, therefore it corresponds to the state measurement required for computation and it constitutes the main instrument to investigate anyons.

The following step towards the creation of a topological quantum computer would be the experimental realization of a system that allows us not only to detect non-Abelian anyons, but also to manipulate their positions in order to physically implement topologically protected quantum gates through their ordered braidings. Unfortunately, gaining such a control in the semiconductor quantum Hall systems we mentioned seems to be a prohibitive task; therefore we are justified in the search for new alternative systems characterized by non-Abelian anyons.

1.3 Outline of the thesis

This thesis deals with two main works: the first part, comprehending Chapters 2 and 3, is devoted to topological quantum computation and concerns subjects that we could consider connected with the *software* of a quantum computer and with its implementation through non-Abelian anyons; the second part, instead, presents a new class of physical systems, namely cold atomic gases in artificial non-Abelian gauge potential, that, under certain constraints, can be suitable to obtain novel quantum Hall states with anyonic excitations; therefore Chapter 4 can be considered more related to the search for a possible *hardware* for topological quantum computation.

In Chapter 2 I will summarize the main features of non-Abelian anyon models in order to underline the main characteristics that allow for a topological quantum computation and to provide the reader with the essential tools to deal with the abstract description of non-Abelian anyons. Therefore, I will describe the main elements of anyonic models that constitute a common background of different theories ranging from conformal minimal models, to tensor category theory and to knot theory. In particular I will analyze, as an example, one of the simplest non-Abelian models, the Fibonacci anyons (see [63] for an introduction), which are suitable to implement a universal quantum computation. More comprehensive studies on anyonic models can be found in [12, 20, 52, 58].

Chapter 3 is based on my work done with the collaboration of Giuseppe Mussardo, Xin Wan and Haitan Xu [1, 2]. In this chapter I will first present the problem of *quantum compiling* [39], namely the search for an ordered sequence of elementary quantum operators to approximate a target quantum gate. This problem is extremely interesting for topological quantum computation since the exchange operators of Fibonacci anyons provide a natural basis for a universal quantum computation. As we will see, the compiling problem can be easily solved by a brute-force approach (namely to search among all the possible sequences up to a certain length for the best one); this kind of algorithm, however, requires a runtime which is exponential in the accuracy requested, and thus, it is unfeasible to reach high precisions. I will present an alternative solution to the compiling problem of single-qubit gates named *quantum hashing*: this procedure allows to obtain accurate representations of the target quantum gates in a shorter time, by exploiting the composition rules of a finite subgroup of SU(2). In particular we will use the icosahedral group to approximate arbitrary single-qubit gates in terms of braids of Fibonacci anyons.

Chapter 4 concerns the work done in collaboration with Andrea Trombettoni [3, 4]. Here I will analyze cold atomic gases subjected both to an effective magnetic field and to an artificial non-Abelian gauge potential affecting a spin-like inner degree of freedom. First we will investigate the classification of U(2) gauge potentials that bring to a proper Landau level structure in the single-particle problem; then we will discuss how it is possible to obtain a particular example of U(2) gauge potential starting from the so-called tripod atoms [64] and, finally, we will analytically solve both the single-particle and the many-body problem. In particular we will show that the non-Abelian part of the vector potential lifts the

spin-degeneracy and brings, in general, to deformed Laughlin ground states; there are however degeneracy points of the Landau levels where more complex quantum Hall states appear, including non-Abelian ones such as a deformed Pfaffian state, and we will study these ground states for both fermions and bosons.

Chapter 2

Anyon Models

In this chapter we will investigate the theoretical structure of anyon models emphasizing the elements that are essential to the purpose of topological quantum computation. In the last section we will describe, as an example, the model of Fibonacci anyons, which is not only the simplest non-Abelian anyon model, but also the main example of anyons supporting universal quantum computation, as we will discuss in Chapter 3.

The mathematical structure underlying anyon models is extremely rich and it is related to the study of unitary tensor categories, whose discussion is far beyond the purpose of this thesis. Here we will analyze only the main feature of anyon models; broader introductions to the subject can be found in [12, 20, 52, 58].

The structure of anyon models originated from CFT [26] and can be understood under the light of conformal models. The connection between FQHE and CFT is very strong: as we already mentioned trial wavefunctions for the bulk of quantum Hall liquids can be retrieved by two-dimensional correlation functions in CFTs; moreover, the edge states in QHE are successfully described by 1+1 dimensional CFTs. CFTs are therefore powerful tools to investigate the topological order of anyon models and provide the basic instruments that are necessary for their complete description. In particular the definition of an arbitrary anyon model relies on the following elements which are strictly related to several features of CFTs:

- **Topological superselection sectors**: each anyon model is defined starting from the set of all the possible anyons in the model. Every different anyon is characterized by a topological charge (or spin) and corresponds to a primary field (in the holomorphic sector);

- **Fusion Rules**: the outcome of the fusion between two anyons with arbitrary topological charges can be described by the fusion rules of the corresponding primary fields;

- **Associativity Rules** (F matrices): the fusion process of 3 anyons can be related to a 4-point correlation function in a CFT. The different fusion channels in the anyon model correspond to different expansions of the correlation function in the conformal blocks: the F matrices allow in both cases to de-

scribe the process choosing different fusion channels and thus are related to the crossing symmetry in conformal models;

- **Braiding Rules** (R matrices): the braiding rules for the anyons are strictly connected to the monodromy of the corresponding primary fields in the holomorphic sector.

2.1 Fusion rules and quantum dimensions

The first ingredient to define an anyon model is a finite set $\mathcal{C}$ of superselection sectors which are labelled by conserved topological charges and can be related to the primary fields (in particular to their holomorphic components) in a given CFT. Among them, every anyon theory presents the vacuum (or identity) sector, $1 \in \mathcal{C}$, corresponding to the absence of a topological charge. These topological sectors characterize the properties of the anyons included in the model and must obey a commutative and associative fusion algebra that states the possible topological charges obtained considering a pair of anyons:

$$a \times b = \sum_{c \in \mathcal{C}} N_{ab}^{c} c \tag{2.1}$$

where, in general, the fusion multiplicities N_{ab}^{c} are non-negative integers and specify the number of different ways the charges a and b can give the charge c as an outcome. However, to the purpose of this thesis, it will be sufficient considering these coefficient to be 0 or 1. The identity sector 1 is defined by the relation $N_{a1}^{c} = \delta_{ac}$ and, in the models we will consider, every topological sector is its own conjugate (*self-duality*): $N_{aa}^{1} = 1$ (even if, in general, for every charge a there exists an anti-charge $\bar{a}$).

The commutativity and associativity of the fusion algebra imply that:

$$N_{ab}^{c} = N_{ba}^{c} \tag{2.2}$$

$$\sum_{e} N_{ab}^{e} N_{ec}^{d} = \sum_{f} N_{af}^{d} N_{bc}^{f}, \tag{2.3}$$

moreover, in the case of self-duality of all the charges, $N_{ab}^{c} = N_{ac}^{b}$ and, for each charge a, we can define a symmetric fusion matrix $N_a \equiv N_{ab}^{c}$ that describes the fusion outcome of an arbitrary state with the charge a.

The theory is non-Abelian if there is at least a pair of charges a and b such that:

$$\sum_{c} N_{ab}^{c} > 1 \tag{2.4}$$

and the charge a corresponds to a non-Abelian anyon if $\sum_c N_{aa}^{c} > 1$, whereas a is Abelian if $\sum_c N_{ab}^{c} = 1$ for every b.

For every outcome c of the fusion $a \times b$ we can associate a fusion space V_{ab}^{c} whose dimension is given by N_{ab}^{c} (1 in the models we will examine). When we consider

a set of different anyons $a_1, ..., a_n$ whose total charge is c, the Hilbert space of the states describing this system can be decomposed in the following form:

$$V^c_{a_1 \dots a_n} = \bigoplus_{b_1,\dots,b_{n-1}} V^{b_1}_{a_1 a_2} \otimes V^{b_2}_{b_1 a_3} \otimes V^{b_3}_{b_2 a_4} \otimes \dots \otimes V^{c}_{b_{n-2} a_n}. \tag{2.5}$$

This Hilbert space cannot be decomposed in the tensor product of subsystems corresponding to the initial anyons a_i but rather it is described in terms of a direct sum of tensor products of the fusion spaces. The dimension of the Hilbert space $V^c_{a_1 \dots a_n}$ can be expressed in terms of the fusion matrices N_{a_i}:

$$\dim \left(V^c_{a_1 \dots a_n} \right) = (N_{a_2} N_{a_3} \dots N_{a_n})^c_{a_1} \tag{2.6}$$

If we assume that all the anyons a_i are of the same sector a, we obtain an expression for the dimension of the Hilbert space describing n non-Abelian anyons with charge a:

$$D_{a,n} = \sum_c \left(N_a^{n-1} \right)^c_a \simeq d_a^n \tag{2.7}$$

where we introduced the *quantum dimension* d_a associated to anyons with a charge a. Such quantum dimension can be defined as the Perron-Frobenius eigenvalue of the matrix N_a and, in general, it is not an integer number. For non-Abelian anyons $d_a > 1$ and it is important to notice that from the fusion relations one can derive

$$d_a d_b = \sum_c N^c_{ab} d_c \tag{2.8}$$

that generalizes the usual relations of the dimensions of the irreducible representations of the unitary groups. The previous relation can be written also as $N_a \vec{d} = d_a \vec{d}$ where $\vec{d} = d_a, d_b, ...$ with $a, b, ... \in \mathcal{C}$ is the eigenvector associated to the eigenvalue d_a of the fusion matrix N_a. The norm of the vector $\vec{d}$

$$\mathcal{D} = \sqrt{\sum_{i \in \mathcal{C}} d_i^2} \tag{2.9}$$

is the total quantum dimension of the anyon model.

The equation (2.7) relates the dimension of the Hilbert space of n equal anyons with their quantum dimension: to the purpose of topological quantum computation we can therefore state that the quantum dimension of an anyon refers to the quantity of information that a system of such anyons can store; besides, it is interesting to notice that such information is encoded in a non-local and topological protected way: in fact, to label each state in the Hilbert space, it is necessary to consider the sequence b_i of the fusion outcomes in (2.5), that, involving all the anyons in the system, is a non-local observable. In order to understand better the structure of this kind of Hilbert space it is useful to introduce the Brattelli diagrams which allow to easily count all the orthogonal states in the system. Let us consider as an example the model of *Ising anyons*, corresponding to the $\mathcal{M}_{4,3}$ conformal minimal model [26, 65]. The superselection sectors are the vacuum

1, the spin sector σ (non-Abelian Ising anyon) and the fermionic sector ε. The corresponding (nontrivial) fusion rules are:

$$\sigma \times \sigma = 1 + \varepsilon\,, \qquad \sigma \times \varepsilon = \sigma\,, \qquad \varepsilon \times \varepsilon = 1. \tag{2.10}$$

From these rules it is easy to calculate the quantum dimensions exploiting the equation (2.8):

$$d_\varepsilon = 1\,, \qquad d_\sigma^2 = 1 + 1 \quad \Rightarrow \quad d_\sigma = \sqrt{2} \tag{2.11}$$

In the basis $(1, \varepsilon, \sigma)$ the fusion matrix N_σ reads:

$$N_\sigma = \begin{pmatrix} 0 & 0 & 1 \\ 0 & 0 & 1 \\ 1 & 1 & 0 \end{pmatrix} \tag{2.12}$$

This non-Abelian fusion matrix can be represented through the diagrams in Fig. 2.1.

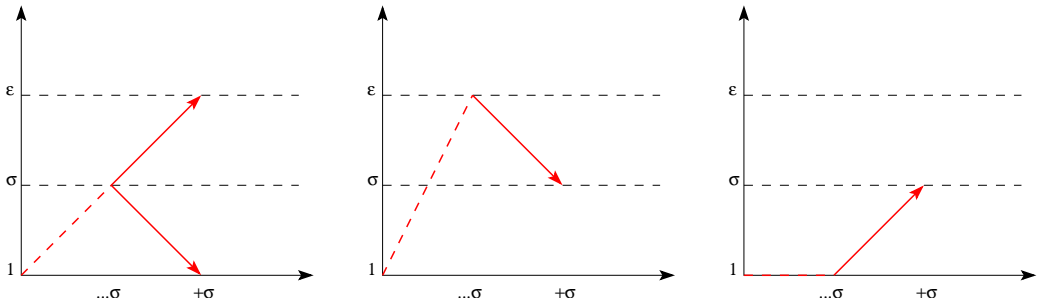

$\sigma \times \sigma = 1 + \varepsilon$ $\qquad$ $\varepsilon \times \sigma = \sigma$ $\qquad$ $1 \times \sigma = \sigma$

Figure 2.1: The Brattelli diagrams for the fusion rules of the non-Abelian Ising anyon σ are shown.

The Brattelli diagrams help us to describe the Hilbert space of a set of non-Abelian anyons. Let us consider a chain of σ anyons (see Fig. 2.2): the total charge of the first two of them can be either 1 or ε, therefore the first pair of Ising anyons is correctly described by a two-state Hilbert space, that highlights the quantum dimension $d_\sigma = \sqrt{2}$ of a single Ising anyon. Adding a third σ to the first pair, the total charge must be σ, since the Ising anyons are characterized by an odd parity unlike the vacuum and fermionic sectors, as shown by the fusion rules (2.10). Therefore, in this case, the third anyon doesn't add new states to the Hilbert space. After the fusion of the fourth one, instead, there is again a double possibility: the total charge of 4σ can be either 1 or ε and, therefore, a system with 4 Ising anyons is described by 4 states. For each pair of anyons, the number of states in the Hilbert space is doubled since their total charge can be either 1 or σ.

The Brattelli digram in Fig. 2.2 illustrates the doubling of the number of states at each even anyon. Every point of the diagram represents the total charge of the system, $1, \varepsilon$ or σ, as a function of the number of non-Abelian anyons considered and

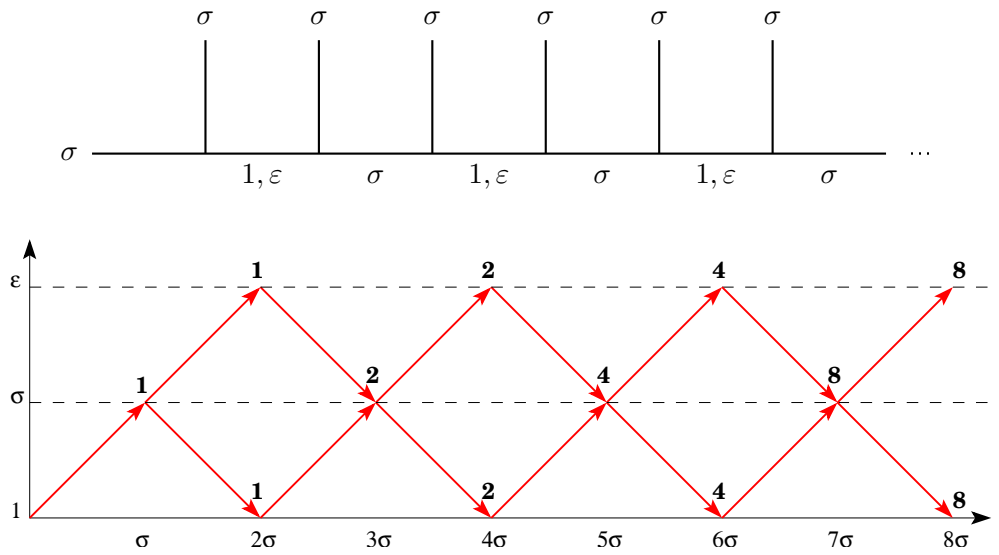

Figure 2.2: Fusion graph and Brattelli diagram corresponding to a chain of non-Abelian Ising anyons. The chain is composed by σ anyons and the possible fusion outcomes are indicated. Depending on the parity of the anyons considered, their total charge is given by σ (odd number of anyons) or by the two possible charges 1 and ε (even number of anyons). In the Brattelli diagram the number of independent states at each fusion is shown: they correspond to the different paths along the diagram.

it is labelled by the number of orthogonal states characterized by the corresponding charge. These states can be visualized as the different paths on the Brattelli diagram and their number grows as $2^{\frac{n}{2}}$ where n is the number of Ising anyons considered.

The fusion rules of anyon models can be related to several physical processes; in particular they allow to describe the amplitudes of scattering processes among anyons since the probability $p(ab \to c)$ that the total charge of the anyons a and b is c is given by [52]:

$$P\left(ab \to c\right) = \frac{N_{ab}^{c} d_c}{d_a d_b}. \tag{2.13}$$

In particular, if a is self-dual, one obtains that the quantum dimension d_a is linked to the probability that two equal anyons annihilate: $p(aa \to 1) = d_a^{-2}$. Finally, considering the steady state distribution of an hypothetical anyonic gas, the anyons with charge a appear with a probability [52]:

$$p_a = \frac{d_a^2}{\mathcal{D}^2}. \tag{2.14}$$

Therefore, if anyons are created through a random process, those with a charge associated to a larger quantum dimension are more likely to be produced.

As we previously mentioned, anyon models can be strictly related to conformal models; under this point of view the fusion rules of topological superselection sectors can be considered as the operator product expansions of primary fields:

$$\phi_a(z_1)\phi_b(z_2) = \sum_c N_{ab}^c \frac{\phi_c(z_2)}{(z_1 - z_2)^{\Delta_a+\Delta_b-\Delta_c}} \tag{2.15}$$

where z_1 and z_2 are the positions in complex coordinates of the anyons a and b, and Δ_i is the conformal dimension of the field ϕ_i in the holomorphic sector. This is the key relation to map conformal models into anyon models and, as we will see in the next sections, the conformal weights play an important role in defining the monodromy matrices, and thus the braiding rules, characterizing anyon models.

2.2 Associativity rules and F-matrices

The fusion of topological sectors is associative:

$$(a \times b) \times c = a \times (b \times c)\,. \tag{2.16}$$

This simple mathematical requirement corresponds to the fact that the total topological charge of three anyons is an intrinsic property of the particles and must not depend on the fusion path one chooses to evaluate the final outcome. The associativity of the fusion rules implies, at the level of the fusion matrices N, the equation (2.3) which represents the fusion of three particles $(abc) \to d$; an analogous relation can be written for the fusion space V_{abc}^d defined by equation (2.5):

$$V_{abc}^d = \bigoplus_x V_{ab}^x \otimes V_{xc}^d = \bigoplus_y V_{ay}^d \otimes V_{bc}^y, \tag{2.17}$$

where the two expressions correspond to different fusion decompositions as shown in Fig. (2.3).

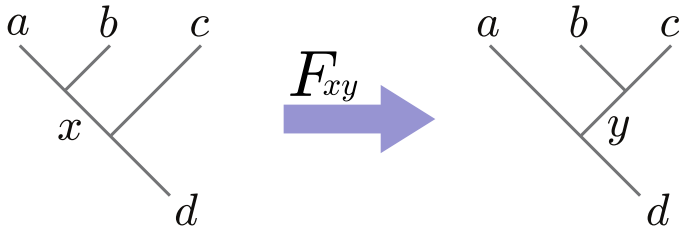

Figure 2.3: The F-matrix describes a change of basis between two equivalent representations of the same fusion space V_{abc}^d (see eq.(2.18)).

Since there are two equivalent decompositions of the fusion space V_{abc}^d, it is natural to consider the isomorphism between the two spaces in equation (2.17). This isomorphism is usually called an F-move and corresponds to the following change of basis:

$$|ab \to x\rangle \otimes |xc \to d\rangle = \sum_y \left(F_d^{abc}\right)_{xy} |ay \to d\rangle \otimes |bc \to y\rangle \tag{2.18}$$

where the states on the left-hand side are elements of $V_{ab}^{x} \otimes V_{xc}^{d}$ and the ones on the right-hand side correspond to $V_{ay}^{d} \otimes V_{bc}^{y}$. The matrix $\left(F_{d}^{abc}\right)_{xy}$ depends on the charges a, b, c and d involved in the fusion process and its indices x and y run, in general, over all the possible sectors of the model. In the most common cases the F matrix is a unitary matrix $\left(F_{d}^{abc}\right)^{-1} = \left(F_{d}^{abc}\right)^{\dagger}$ and the F-moves can be thought as a generalization of the $6j$-symbols arising in the tensor product of the group representations; however, starting from non-unitary conformal models, it is possible to build anyon models characterized by non-unitary F-matrices [66] and it is interesting to notice that systems having the same topological sectors and fusion rules may differ for the F matrices.

In order to generalize the F-moves for every number of anyons, one must enforce a consistency relation which assures that the isomorphism obtained as a change of basis of the fusion spaces depends only on the initial and final decomposition of the space, and not by the particular sequence of moves from which the isomorphism is constructed. This consistency condition is called *pentagon equation* and it is represented in Fig. 2.4.

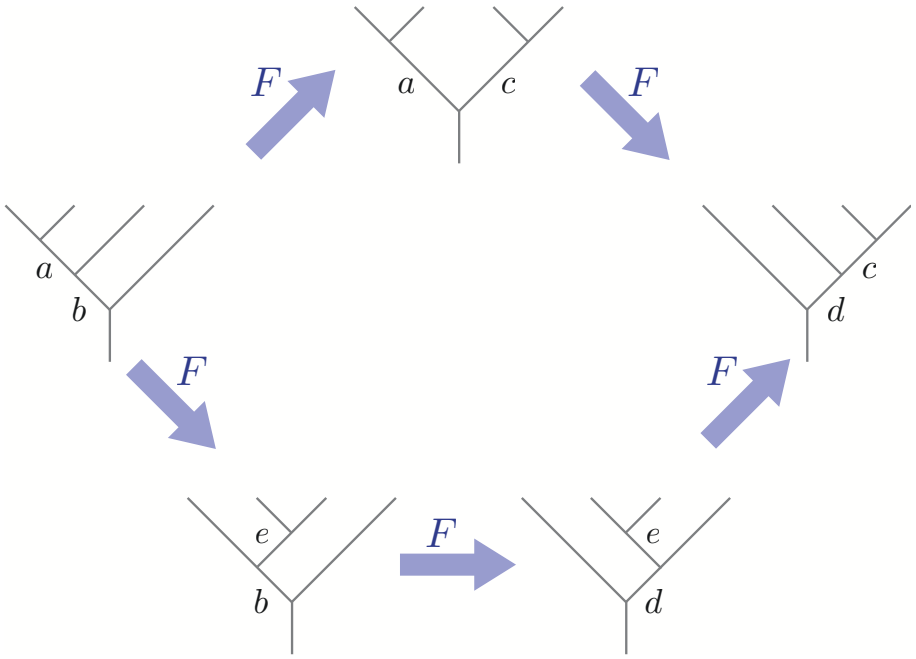

Figure 2.4: The same decomposition of the fusion space of four anyons can be obtained through different sequences of F-moves. The pentagon equation (2.19) assures the consistency of the two sequences of decompositions illustrated. (Taken from [63]).

In particular the pentagon equation relates two different sequences of F-moves for the fusion of four anyons, from the 'left-ordered basis' to the 'right-ordered basis' as shown in Fig. 2.4. If we label with α, β, γ and δ the four anyons and we

assume that their total charge is τ, the pentagon equation reads:

$$\sum_e \left(F_d^{\beta\gamma\delta}\right)_{ec} (F_\tau^{\alpha e\gamma})_{bd} \left(F_b^{\alpha\beta\gamma}\right)_{ae} = \left(F_\tau^{\alpha\beta c}\right)_{ad} \left(F_\tau^{a\gamma\delta}\right)_{bc} \tag{2.19}$$

This equation involves only four anyons, however a well-known result in tensor category theory, the MacLane coherence theorem, assures that this consistency equation is sufficient to enforce the consistency of all the possible sequences of F-moves for every number of anyons (see [12] and references therein). Besides the pentagon equation provides a first constraint to explicitly determine the expression for the F matrices; as we will see in the next section, the other main constraint is the hexagon equation, involving the braidings matrices and the Yang-Baxter relations. Moreover, in general, the unitary F-matrices are also linked to the quantum dimensions of the anyons by the following relation:

$$(F_a^{aaa})_{11} = \frac{1}{d_a} \tag{2.20}$$

which is related to the possibility of describing anyon models in terms of loop or string-net models (see, for example, [30, 19]) and of calculating their partition function.

The physical meaning of the F-moves can be related to an elastic scattering process (see Fig. 2.5) and to the corresponding crossing symmetry. Let us consider a system of four anyons, a, b, c and d, whose total topological charge is trivial. This neutrality constraint imposes the relation $a \times b = c \times d$ but also $a \times d = b \times c$ (under the hypothesis of self-duality); thus the fusion of the four anyons can be described in two different ways that correspond to the s and t channels of an elastic scattering process of two particles.

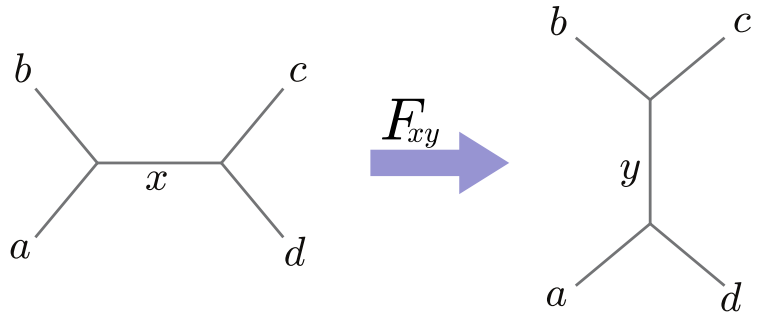

Figure 2.5: The F-moves allow to describe the crossing symmetry of the fusion of four anyons. The graph in this figure is topologically equivalent to the one in Fig. 2.3.

The F-moves allow to relate the s and t channels and define the change of basis between the two fusion spaces. We can consider the example of four Ising anyons ($a = b = c = d = \sigma$). Knowing that the total charge of the Ising anyons a and b is

ε the probability of the fusion outcome between the anyons b and c is given by:

$$P(\sigma\sigma \to 1) = |(F_\sigma^{\sigma\sigma\sigma})_{\varepsilon\,1}|^2 = \frac{1}{2} \tag{2.21}$$

$$P(\sigma\sigma \to \varepsilon) = |(F_\sigma^{\sigma\sigma\sigma})_{\varepsilon\,\varepsilon}|^2 = \frac{1}{2} \tag{2.22}$$

since the F matrix of the Ising model reads (see, for example, [12, 58]):

$$F_\sigma^{\sigma\sigma\sigma} = \frac{1}{\sqrt{2}} \begin{pmatrix} 1 & 1 \\ 1 & -1 \end{pmatrix} \tag{2.23}$$

Under the point of view of conformal field theory, the F-matrices describe the crossing transformation of the four-point correlation functions [26]; they can be interpreted as a change of basis of the conformal blocks. Adopting the Dotsenko and Fateev approach [67], the four-point function of a primary field in a minimal model can be expressed in two equivalent forms:

$$\langle\phi(0)\phi(1)\phi(z)\phi(\infty)\rangle = \alpha I_1(z) + \beta I_2(z) = \alpha' I_1'(1-z) + \beta' I_2'(1-z) \tag{2.24}$$

where the I_i are hypergeometric functions [26, 65, 67]. The two expressions correspond to different decompositions in conformal blocks: in the first case the two-point function of the fields in z and in 0 is considered, in the second one, instead, the correlation between the fields in z and 1 is calculated. Once the hypergeometric functions I_i are properly normalized, the F-matrix allows to express $I_i(z)$ as a linear combination of $I_1'(1-z)$ and $I_2'(1-z)$ which correspond to a different integration contour in the expression of the four-point correlation function (see [26, 67] for more detail). The F-matrix can be therefore calculated by evaluating this change of basis between the conformal blocks and by imposing the unitarity constraint or other conditions.

2.3 Braiding rules

The exchange of two anyons on the plane does not affect their total charge $c = a \times b$. Therefore their counterclockwise braiding defines an isomorphism R_{ab}^c between the fusion spaces V_{ab}^c and V_{ba}^c. Since we are considering only models where the dimension of the fusion spaces V_{ab}^c is 1, R_{ab}^c is simply determined by a phase and its inverse $(R_{ab}^c)^{-1}$ corresponds to a clockwise exchange of the anyons a and b. Starting from all the possible outcomes of the fusion $a \times b$ it is possible to build the *braiding operator* $R_{ab} = \bigoplus_c R_{ab}^c$, also known as R-move (see Fig. 2.6).

Applying twice the braiding operator R we obtain the *monodromy operator*:

$$R_{ab}^2 : V_{ab}^c \to V_{ab}^c = \bigoplus_c (R_{ab}^c)^2 \tag{2.25}$$

This unitary operator corresponds to winding counterclockwise one anyon around the other and, similarly to R_{ab}, can be expressed in the basis given by the possible total charges c. The monodromy operator R^2 can be easily derived from the

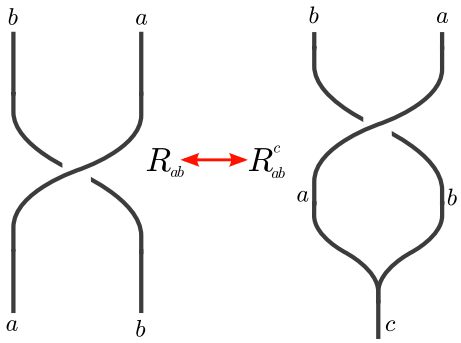

Figure 2.6: The counterclockwise exchange of two anyons leaves invariant their total charge. Therefore the operator R_{ab} can be decomposed in its projections R^c_{ab} on the fusion spaces V^c_{ab} characterized by a definite total charge c.

conformal field theory underlying the anyon model: let us consider the pair of anyons $a \times b$ which obey a fusion rule related to the operator product expansion in equation (2.15); from this equation it is evident that the monodromy operator corresponds to:

$$(R^c_{ab})^2 = e^{-2\pi i(\Delta_a+\Delta_b-\Delta_c)} \tag{2.26}$$

where Δ_j is the conformal weight in the holomorphic sector of the primary field ϕ_j, corresponding to the topological charge j. Therefore the mapping between anyon and conformal models allows us to determine the unitary operator R_{ab} up to the signs of the phases R^c_{ab}. Usually the phases $2\pi\Delta_j$ in (2.26) are also called *topological spins* of the corresponding anyons j and it can be shown that these phases are related to the following braiding [12, 52]:

$$R^1_{aa} = e^{-i\theta_a}. \tag{2.27}$$

Therefore the topological spin describes both the rotation of 2π of a single anyon, meant as a charge-flux composite, and the exchange process of a pair of equal anyons that annihilate [12, 52]. Moreover, the expression (2.26) shows that the monodromy operator $(R^c_{ab})^2$, expressed as a function of the topological spins, can be interpreted as a rotation of c by 2π while rotating a and b by -2π.

The conformal weights (or the topological spins) that appear in (2.26) are not enough to fully determine the braiding operators R_{ab}. However, such operators must provide a representation of the braid group, and, therefore, are constrained to fulfill other conditions, such as the Yang-Baxter equations (1.2). In particular, similarly to the F-moves, also the R-moves must satisfy a consistency relation that guarantees that the isomorphism between equivalent fusion spaces obtained by a sequence of F and R-moves depends only on the initial and final decomposition of the space. This constraint is the *hexagon equation* (see Fig. 2.7):

$$R^c_{\gamma\beta}\left(F^{\alpha\gamma\beta}_{\delta}\right)_{ac} R^a_{\alpha\gamma} = \left(F^{\alpha\beta\gamma}_{\delta}\right)_{bc} R^{\delta}_{\gamma b}\left(F^{\gamma\alpha\beta}_{\delta}\right)_{ab} \tag{2.28}$$

The hexagon equation describes two equivalent sequences of F and R-matrices involving the fusion of three anyons α, β and γ giving a total charge δ. The

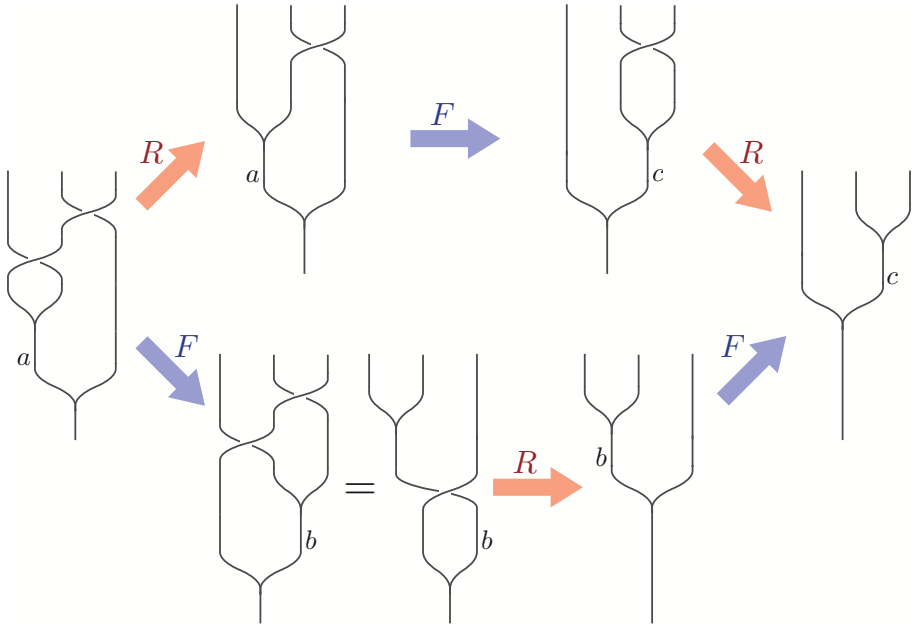

Figure 2.7: The F-moves and the R-moves must obey the hexagon equation (2.28). This constraint enforces the consistency of two different sequences of braidings and fusions for three anyons and guarantees that the isomorphism between two different fusion bases depends only on the bases and not by the moves applied to obtain them. The hexagon equation implies also that the Yang-Baxter equations (1.2) are fulfilled. (Taken from [63].)

equation (2.28) imposes, essentially, the property that a worldline may be passed over or under the fusion vertices, which, in the language of knot theory, constitutes one of the Reidemeister move (see, for example, [17]) and it is equivalent to the Yang-Baxter relations (1.2). Therefore braidings and fusions must commute, as shown in the second step of the lower path in Fig. 2.7.

The pentagon (2.19) and hexagon (2.28) equations, sometimes called Moore-Seiberg polynomial equations, together with the unitarity of the F-matrices, completely specify an anyon model; a fundamental result in tensor category theory, the MacLane theorem, assures that no further consistency relations are required beyond these equations (see [12, 58] and references therein for further detail).

Let us consider now a system of many anyons: as previously seen, the corresponding Hilbert space can be represented as a direct sum (2.5) where the sequences of the total charges of the first k anyons, b_k, label every possible state. In the basis described by the sequences of b_k, usually called the standard basis, the charge of two subsequent anyons $a_i \times a_{i+1}$ is not a diagonal observable, therefore also the generic braiding $R_{a_i a_{i+1}}$ has not a diagonal expression. Thus, to represent the braid group generators σ_i, one has to express the braidings R in the standard basis through appropriate F-moves (see Fig. 2.8). Hence, the generators σ can be

expressed in the following form:

$$(\sigma_i)_{b_i b_i'} = \left(F^{b_{i-1}a_i a_{i+1}}_{b_{i+1}}\right)^{-1}_{c_i b_i'} R^{a_i a_{i+1}}_{c_i} \left(F^{b_{i-1}a_i a_{i+1}}_{b_{i+1}}\right)_{b_i c_i} \tag{2.29}$$

Figure 2.8: The generators σ of the braid group can be represented in the standard basis $\{b_k\}$ by transforming the matrices R with appropriate F-moves.

The F-matrices are therefore essential in defining proper representations of the braid group. The matrices σ_i obtained in this way are the building blocks for topological quantum computation and, under certain hypothesis, can be considered as a computational basis to obtain single-qubit gates. Let us consider, for example, the Hilbert space constituted by four Ising anyons, $\sigma_a, \sigma_b, \sigma_c$ and σ_d having a trivial total charge. There are two possible states corresponding to the fusion outcomes:

$$|0\rangle : \quad \sigma_a \times \sigma_b = \sigma_c \times \sigma_d = 1, \tag{2.30}$$

$$|1\rangle : \quad \sigma_a \times \sigma_b = \sigma_c \times \sigma_d = \varepsilon; \tag{2.31}$$

these states are represented in Fig. 2.9. In the figure the Ising anyons are depicted as green dots: the red ellipses correspond to the fusion outcome of the first and second pair of anyons: $\sigma \times \sigma = 1 + \varepsilon$. The fusion outcomes must be equal for the two pairs since the total charge of the system (blue ellipse) is trivial, and they are 1 for the state $|0\rangle$ and ε for the state $|1\rangle$.

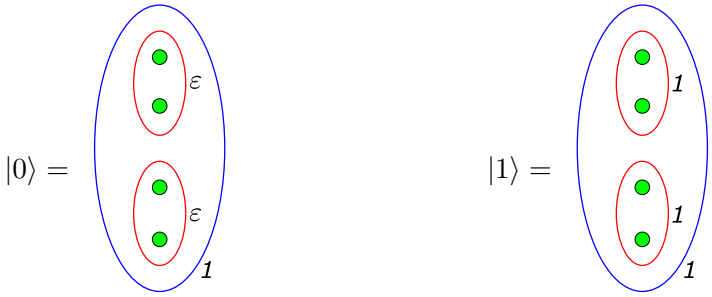

Figure 2.9: A system of four Ising anyons with a trivial total charge is characterized by two possible states. Each pair of anyons must have the same total charge. Depending on the charge of the pairs, the states are labelled as $|0\rangle$ or $|1\rangle$

The braiding matrix $R_{\sigma\sigma}$ of a pair of Ising anyons in the basis $(1, \varepsilon)$ reads:

$$R_{\sigma\sigma} = \begin{pmatrix} e^{-i\frac{\pi}{8}} & 0 \\ 0 & e^{i\frac{3\pi}{8}} \end{pmatrix} \tag{2.32}$$

according to the conformal weights $\Delta_\sigma = 1/16$ and $\Delta_\varepsilon = 1/2$. The system of four Ising anyons shown in Fig. 2.9 presents three possible braid generators representing

the exchanges of subsequent anyons. To calculate the corresponding matrices one has to consider the associativity matrix (2.23) $F_\sigma^{\sigma\sigma\sigma} = (F_\sigma^{\sigma\sigma\sigma})^{-1}$:

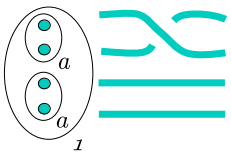

$$\sigma_1 = R_{\sigma\sigma} = e^{-i\frac{\pi}{8}} \begin{pmatrix} 1 & 0 \\ 0 & i \end{pmatrix} \tag{2.33}$$

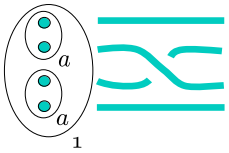

$$\sigma_2 = F_\sigma^{\sigma\sigma\sigma} R_{\sigma\sigma} F_\sigma^{\sigma\sigma\sigma} = \frac{e^{i\frac{\pi}{8}}}{\sqrt{2}} \begin{pmatrix} 1 & -i \\ -i & 1 \end{pmatrix} \tag{2.34}$$

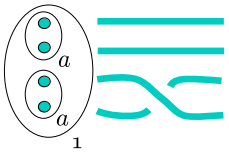

$$\sigma_3 = R_{\sigma\sigma} = e^{-i\frac{\pi}{8}} \begin{pmatrix} 1 & 0 \\ 0 & i \end{pmatrix} \tag{2.35}$$

The generators σ_1 and σ_3 involve anyons in the same pair, therefore they are diagonal in the chosen basis, which depends only on the pairs total charge, and they both correspond to the matrix $R_{\sigma\sigma}$. The braiding σ_2, instead, represents the exchange of two anyons in different pairs and thus it presents also off-diagonal terms which allow the transition from a state to the other. As we will see in the next chapter, these braidings generate only a finite subgroup of SU(2), therefore Ising anyons are not suitable to implement a universal topological quantum computation. In the next section we will analyze another non-Abelian model, the Fibonacci anyons, whose braiding rules allow, on the contrary, to cover in a dense way the whole SU(2) space.

2.4 Fibonacci anyons

The simplest example of non-Abelian anyon model is the one of Fibonacci anyons; this model is characterized by only two topological charges: the vacuum sector 1 and the topological sector corresponding to the presence of a single Fibonacci anyon, hereafter labelled as τ. These two charges are related by the following fusion rules

$$1 \times \tau = \tau\,, \tag{2.36}$$
$$\tau \times \tau = 1 + \tau\,; \tag{2.37}$$

which highlight that τ is a non-Abelian anyon since the fusion of two of them can result either in an annihilation or in the presence of a single anyon.

Despite the simplicity of this model, Fibonacci anyons provide the main example of a universal topological quantum computation [33, 34] and they show

intriguing connections with CFTs and RSOS models. The purpose of this section is to describe the main characteristics of Fibonacci anyons that are useful for quantum computation and to provide an example of the non-Abelian anyon models described above. Therefore we will deal only with the case of non-interacting anyons, even if Fibonacci anyons are also a natural playground to study the effects of ferromagnetic of antiferromagnetic interactions between non-Abelian anyons, through the so-called *golden chain* model [68, 69]. Further details on the general theory of Fibonacci anyons can be found in [39, 63] and references therein.

From an abstract point of view, the Fibonacci model corresponds to the $SU(2)_3$ algebra (and the related Chern-Simons theory), up to Abelian phases that are irrelevant to the purpose of quantum computation. Its fusion and braiding rules characterize several quantum Hall states that are supposed to describe different quantum Hall plateaux, in particular the $SU(2)_3$ Read-Rezayi state [70] and the $SU(3)_2$ non-Abelian spin-singlet state at $\nu = 4/7$ [71].

The Read-Rezayi states are a family of wavefunctions which generalize the Moore-Read Pfaffian state [25, 72] to the $SU(2)_k$ algebras and correspond to the correlation functions of $\mathbb{Z}_k$ parafermions in CFT [73]. In particular the $SU(2)_3$ Read-Rezayi wavefunction describes a quantum Hall state with filling factor $\nu = 3/5$ whose particle-hole conjugate is the main candidate description for the observed $\nu = 12/5$ plateau [74] that, therefore, could be suitable to have Fibonacci anyons as gapped excitations. Moreover, explicit quasihole wavefunctions have been worked out for the $k = 3$ Read-Rezayi state using quantum group techniques, with results consistent with the predicted $SU(2)_3$ braiding properties [75].

The non-Abelian spin-singlet states [71, 76] are instead a generalization of the Abelian Halperin wavefunctions [77] which extend the non-Abelian statistics to multi-component quantum Hall liquids considering also the spin degree of freedom of the electrons.

For a review of all the mentioned wavefunctions and their role in topological quantum computation see [78].

In order to better analyze the Hilbert space characterizing systems of Fibonacci anyons it is useful to introduce the Brattelli diagrams as seen in section 2.1:

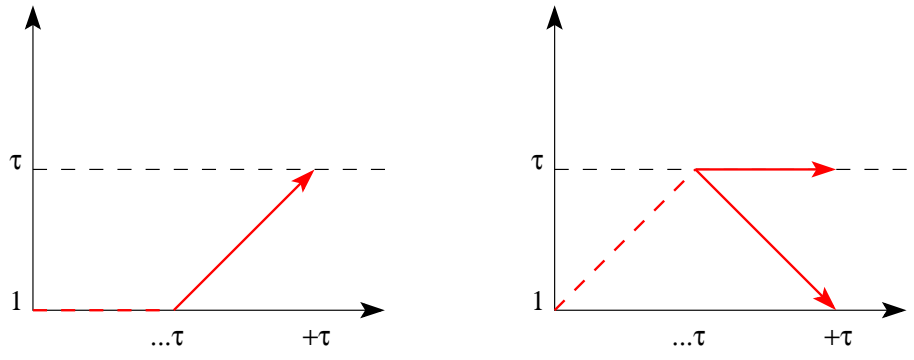

$1 \times \tau = \tau$ $\qquad$ $\tau \times \tau = 1 + \tau$

Figure 2.10: Brattelli diagrams for the fusion rules of the non-Abelian Fibonacci anyons (2.36,2.37).

From the fusion rule (2.37) one can easily obtain that the quantum dimension associated with a Fibonacci anyons is the well-known golden ration $d_\tau = \varphi = \frac{1}{2}\left(\sqrt{5}+1\right) \simeq 1.618$. To understand the meaning of this particular value (and to understand why the Fibonacci anyons are named after an Italian mathematician of the XIII century) we must consider a chain composed of n Fibonacci anyons (see Fig. 2.11).

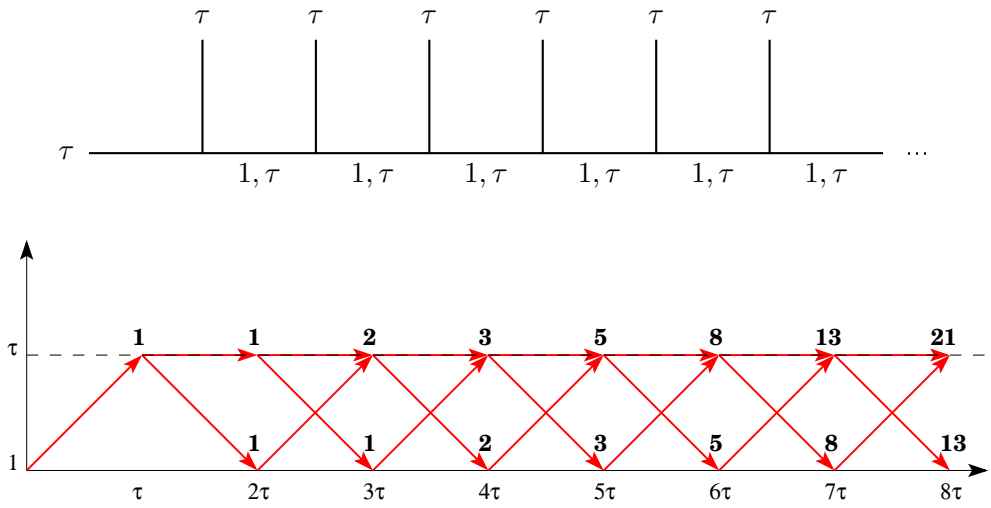

Figure 2.11: Fusion graph and Brattelli diagram corresponding to a chain of non-Abelian Fibonacci anyons. The Fibonacci numbers determine the number of orthogonal states for a system of k Fibonacci anyons at a given topological charge.

As we already saw, the states in the fusion space of n anyons can be identified by the sequence of the intermediate charges b_k. After the fusion of the first two anyons, the intermediate charge b_k of the first k Fibonacci anyons may assume both the values 1 and τ. However, since $1 \times \tau = \tau$, there is one constraint: if $b_{k-1} = 1$ then $b_k = \tau$ and therefore, a charge 1 cannot be followed by another intermediate charge 1. This condition implies that the quantum dimension of a chain can be calculated by recursion. If the total charge of n Fibonacci anyons is $c = \tau$, then the first $n-1$ anyons can fuse giving either the vacuum or τ, and there is a one to one correspondence of the states of $n-1$ anyons and the states with n anyons but fixed total charge τ; therefore $D_n^{c=\tau} = D_{n-1}$. Otherwise, if the total charge of n Fibonacci anyons is $c = 1$, then the first $n-1$ anyons must fuse in τ and one has $D_n^{c=1} = D_{n-1}^{c=\tau} = D_{n-2}$. Therefore the total dimension of the fusion space of n Fibonacci anyons is given by:

$$D_n = D_n^{c=\tau} + D_n^{c=1} = D_{n-1} + D_{n-2}; \tag{2.38}$$

this recursion relation generates the Fibonacci numbers F_n, thus the quantum dimension of a system of n Fibonacci anyons is the Fibonacci number F_{n+1}. Since these numbers grow asymptotically as a power of the golden ratio φ^n, one recovers the quantum dimension $d_\tau = \varphi$.

So far we considered only the fusion rules (2.36,2.37) of the model. It is interesting to notice that such fusion rules characterize both the non-unitary Yang-Lee conformal model (the minimal model $\mathcal{M}_{5,2}$) and the $\mathbb{Z}_3$ parafermions related to the $SU(2)_3$ algebra. To understand the difference between the two conformal theories one must consider the associativity matrices of Fibonacci anyons. In particular the Fibonacci model has only one nontrivial matrix, $F_\tau^{\tau\tau\tau} \equiv F$ (we drop the τ indices for the sake of simplicity), whereas all the other F-matrices, involving at least one vacuum, are trivially the identity. To find the F matrix one must consider the pentagon equation (2.19). Such equation imposes several conditions and, in particular, one finds:

$$F_{1,\tau}F_{\tau,1} = F_{11}\,, \qquad \text{for} \quad b=c=1\,; \tag{2.39}$$

$$F_{11} + (F_{\tau\tau})^2 = 1\,, \qquad \text{for} \quad c=b=d=\tau \quad \text{and} \quad a=1 \tag{2.40}$$

Imposing also the unitarity of the F-matrix, the only possible solution, up to arbitrary phases of the off-diagonal terms, is [52, 69]:

$$F_F = \begin{pmatrix} \varphi^{-1} & \varphi^{-1/2} \\ \varphi^{-1/2} & -\varphi^{-1} \end{pmatrix} \tag{2.41}$$

where φ is the golden ratio. One can notice that the unitary matrix F_F has determinant -1 and $F_F^{-1} = F_F$. This associativity matrix corresponds to the unitary theory $SU(2)_3$ (or $SO(3)_3$ to be more precise [39]) and it will be used in the following to build a basis for universal quantum computation. It is possible, however, to relax the unitarity condition [66]; in this case there is another solution to the pentagon and hexagon equation that implies the following non-unitary F-matrix:

$$F_{YL} = \begin{pmatrix} -\varphi & -i\varphi^{1/2} \\ -i\varphi^{1/2} & \varphi \end{pmatrix}. \tag{2.42}$$

Such matrix corresponds to the Yang-Lee conformal model which brings to a non-unitary dynamics.

To find the only nontrivial braiding matrix $R_{\tau\tau}$ one has to solve the hexagon equation (or similarly the Yang-Baxter equations). The resulting R matrix reads (in the basis $1, \tau$) [52, 69]:

$$R_{\tau\tau} = \begin{pmatrix} e^{-i\frac{4}{5}\pi} & 0 \\ 0 & -e^{-i\frac{2}{5}\pi} \end{pmatrix} \tag{2.43}$$

and the only other solution is its complex conjugate which corresponds to exchange clockwise and counterclockwise braidings. One can observe that $R_{\tau\tau}$ is compatible with the conformal weight $\Delta_\tau = -\frac{1}{5}$ of the Yang-Lee model [26] that defines the monodromy matrix $R_{\tau\tau}^2$.

Once we stated the fundamental characteristics of Fibonacci anyons, we can analyze a system of four anyons to find a suitable basis to encode the logical qubit [37, 39]. To this purpose it is conventional to use a notation which is slightly different from the one we adopted so far: since in the Fibonacci model only one nontrivial sector is present, we can label the topological charge of a set of anyons

in terms of the corresponding number of Fibonacci anyons; therefore, the vacuum sector which topologically corresponds to the absence of a charge is labelled with 0, whereas the τ sector is labelled with a unitary charge 1.

To encode a single qubit we can consider the two-state system composed by four Fibonacci anyons with a trivial total charge. Similarly to the previously discussed case of Ising anyons (2.30,2.31), there are only two possible states characterized by a null total charge (see Fig. 2.12 (a)): in the state $|0\rangle$ both the first and second pair of anyons (represented by the small ellipses) show a total charge 0, whereas the state $|1\rangle$ is characterized by having both pair with total charge 1. The logical qubit can be encoded also in a system with three Fibonacci anyons (Fig. 2.12 (b)) with a total charge 1, which is ideally obtained from the previous case by removing one anyon. In this case the fusion outcome of the first pair, depicted as the smaller ellipse, determines the logical value of the qubit, whereas the total charge is constrainted to be 1; finally the third possible state of the system, $|NC\rangle$, characterized by a trivial total charge, is a non-computational state [37, 39] which cannot be obtained by simple braids of the three anyons once the system is initialized in the two logical states.

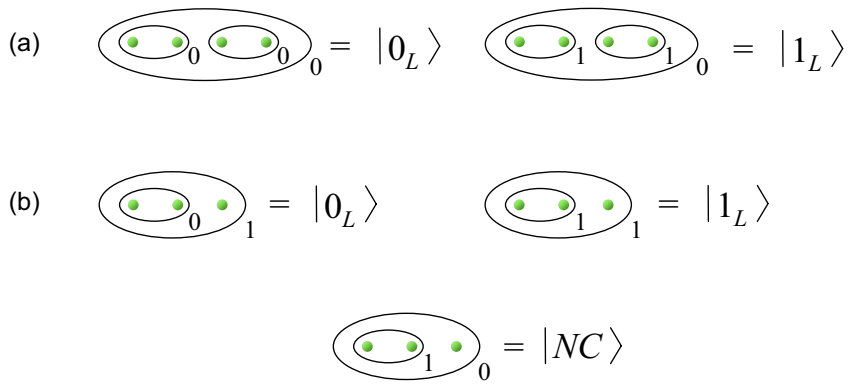

Figure 2.12: The logical qubit states $|0_L\rangle$ and $|1_L\rangle$ can be encoded either in a system with four Fibonacci anyons with a trivial topological charge (a) or in a system with three Fibonacci anyons and a total charge 1 (b). The state $|NC\rangle$ in (b) represents the only state with a charge 0 and constitutes a non-computational state. (Taken from [39]).

Having defined the logical basis to encode a qubit, we can now describe the effect of braidings on the four-anyon system represented in Fig. 2.12 (a). Like the case of Ising anyons, the exchanges of two Fibonacci anyons in the same pair, σ_1 and σ_3, are diagonal in the basis $|0\rangle, |1\rangle$ and they are represented by the same matrix $R_{\tau\tau}$ (2.43). Therefore, to the purpose of quantum computation, we will use only the braidings σ_1 and σ_1^{-1}. The braiding σ_2, which involves anyons of different pairs, is instead non-diagonal in the logical basis and must be obtained through the application of the F-matrix (2.41):

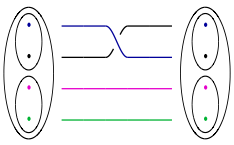

$$\sigma_1 = R_{\tau\tau} = \begin{pmatrix} e^{-i\frac{4}{5}\pi} & 0 \\ 0 & -e^{-i\frac{2}{5}\pi} \end{pmatrix} \tag{2.44}$$

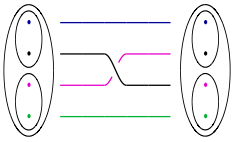

$$\sigma_2 = F_F R_{\tau\tau} F_F = \begin{pmatrix} -\varphi^{-1}e^{-i\pi/5} & -\sqrt{\varphi^{-1}}e^{i2\pi/5} \\ -\sqrt{\varphi^{-1}}e^{i2\pi/5} & -\varphi^{-1} \end{pmatrix} \tag{2.45}$$

where $\varphi = \frac{1}{2}\left(1+\sqrt{5}\right)$ is the the golden mean. One can verify that the above braidings fulfill the Yang-Baxter equation; besides, the Fibonacci braidings are characterized by the relation $\sigma_1^{10} = \sigma_2^{10} = 1$ since they can be considered as rotations of $\frac{7}{5}\pi$ with respect to the representations (3.5) of unitary operators.

The main property of the representation of the braid group provided by Fibonacci anyons is that σ_1, σ_2 and their inverses generate a dense group in SU(2), which brings to the possibility of approximating with a braid of Fibonacci anyons every single-qubit gate. As we will see in the next chapter this is a nontrivial task and we will analyze the main strategies offered by Fibonacci anyons to solve the problem of quantum compiling.

Chapter 3

Quantum Hashing with the Icosahedral Group

The eventual physical implementation of quantum computation would open new scenarios in the future technological development. This justifies the intensive efforts made by the scientific community to develop theoretical approaches suitable for effectively building a quantum computer and, at the same time, to reduce all the sources of errors that would spoil the achievement of quantum computation.

To implement quantum computation one needs to realize, through physical operations over the qubits, arbitrary unitary operators in the Hilbert space that describes the system. This task can be achieved by using a finite number of elementary gates that constitutes a basis. A small set of gates is said to be *universal* for quantum computation if it allows to approximate, at any given accuracy, every unitary operator in terms of a quantum circuit made of only those gates [79]. It can be shown that a basis able to reproduce every SU(2) operator and one entangling gate (as CNOT) for every pair of qubits is indeed universal [80]; therefore the problem of finding an approximation of unitary operators in SU(N) can be reduced to searching an efficient representation, in terms of the elements of the basis, of single-qubit gates in SU(2) and of the two-qubit gate CNOT.

For SU(2) it is possible to find a universal set of single-qubit operators involving just two elementary gates, which we will label as σ_1 and σ_2, and their inverses, σ_1^{-1} and σ_2^{-2}. This means that every single-qubit gate can be efficiently approximated by a string of these four elementary elements. In the scheme of topological quantum computation, these fundamental gates are realized by the elementary braid operation on the anyons that we analyzed in the previous chapter. In order to be universal, the group obtained by multiplying the four σ gates must be dense in SU(2): it is therefore sufficient that σ_1 and σ_2 do not belong to the same finite subgroup of SU(2). For what concerns controlled gates in SU(4) as CNOT, their approximation can be usually reduced to the case of operators in SU(2), as described in Refs. [39] and [42] in the context of topological quantum computation, the main subject of our following considerations.

The simplest way to obtain an approximation of a given target gate $T \in \mathrm{SU}(2)$ using only four elementary gates $\sigma_{1,2}^{\pm 1}$ is to search, among all the ordered products

of N of such operators, the one which best represents T minimizing its distance to it (the rigorous definition of distance is given in section 3.1). This operation is called the *brute-force* procedure [39]. The number of all the possible products of this kind grows exponentially in N as α^N (where $\alpha \approx 3$ since an element σ cannot be followed by its inverse and other constraints can be present) and, because of the three-dimensional nature of SU(2), one can show that, for a suitable choice of the universal basis, the average error obtained with different targets decreases approximately as $e^{-\frac{N}{3}\ln\alpha}$ (in section 3.1.2 we will describe in more detail the brute-force search for Fibonacci anyons).

This approach, consisting of a search algorithm over all the possible ordered product up to a certain length, has an extremely clear representation if one encodes qubits using non-Abelian anyons. In this case, the computational basis for the quantum gate is the set of the elementary braidings between every pair of anyons, and their products are represented by the braids describing the world lines of these anyonic quasiparticles. Starting from this kind of universal basis, the search among all the possible products of N elements gives, of course, the optimal result, but the search time is exponential in N and therefore it is impractical to reach sufficiently small error for arbitrary gates.

There are, however, other possible approaches that allow to reach an arbitrary small error in a faster way, even if they do not obtain the best possible result in terms of the number N of elementary gates involved. The textbook example is the Solovay-Kitaev algorithm [79, 81, 82]. This algorithm provides a powerful tool to obtain an approximation of arbitrary target gates in SU(2) at any given accuracy starting from an ϵ-net, i.e. a finite covering of SU(2) such that for every single-qubit operator T there is at least one gate inside the ϵ-net that has a distance from T smaller than ϵ. The Solovay-Kitaev algorithm is based on the decomposition of small rotations with elements of the ϵ-net and both the runtime and the length of the final product of elementary gates scale poly-logarithmically with the final error ε. The exponents depend on the detailed construction of the algorithm: the simplest realization of the algorithm, as provided in [39] in the context of topological quantum computation, is characterized by the following scaling:

$$N \sim (\ln(1/\varepsilon))^c \qquad \text{with} \quad c = \frac{\ln 5}{\ln(3/2)} \approx 3.97 \tag{3.1}$$

$$T \sim (\ln(1/\varepsilon))^d \qquad \text{with} \quad d = \frac{\ln 3}{\ln(3/2)} \approx 2.71 \tag{3.2}$$

As discussed in the Appendix 3 of [79] and in [82], a more sophisticated implementation of the Solovay-Kitaev algorithm realizes

$$N \sim (\ln(1/\varepsilon))^2 \ln(\ln(1/\varepsilon)) \tag{3.3}$$

$$T \sim (\ln(1/\varepsilon))^2 \ln(\ln(1/\varepsilon)) \,. \tag{3.4}$$

The hashing algorithm, which was proposed in Ref. [1, 2], has the aim of obtaining a more efficient approximation of a target operator than the Solovay-Kitaev algorithm in a practical regime, with a better time scaling and without the necessity of building an ϵ-net covering the whole target space of unitary operators. Our

main strategy will be to create a dense mesh $\mathcal{S}$ of fine rotations with a certain average distance from the identity and to reduce the search of the target approximation to the search among this finite set of operators that, in a certain way, play the role of the ϵ-net in a neighborhood of the identity. This set will be built exploiting the composition property of a finite subgroup (the icosahedral group) of the target space SU(2) and exploiting also the almost random errors generated by a brute-force approach to approximate at a given precision the elements of this subgroup. Therefore the algorithm allows us to associate a finite set of approximations to the target gate and each of them is constituted by an ordered product of the elementary gates chosen in a universal quantum computation basis. Since our braid lookup task is similar to finding items in a database given its search key, we borrow the computer science terminology to name the procedure *hashing*.

With this algorithm we successfully limit our search within a small number of elements instead of an exponentially growing one as in the case of the brute-force search; this significantly reduces the runtime of the hashing algorithm. Furthermore, we can easily iterate the procedure in the same spirit of the renormalization group scheme, based on the possibility of restricting the set S in a smaller neighborhood of the identity at each iteration, obtaining in this way a correction to the previous result through a denser mesh.

Topological quantum computation is the natural playground for the implementation of the hashing procedure, therefore we adopt Fibonacci anyons to encode qubits, as already shown in Sec. 2.4. Their braidings, defined in equations (2.44,2.45), constitute the universal basis for quantum computation we will exploit to approximate single-qubit gates. In the following section we introduce the basic ideas of the icosahedral group and its braid representations, which are pseudogroups. We describe in detail the iterative hashing algorithm in Sec. 3.2 and analyze the performance of its iteration scheme in Sec. 3.3. Moreover, in Appendix A we derive the distribution of the best approximation in a given set of braids, which can be used to estimate the performance of, e.g., the brute-force search.

3.1 SU(2), subgroups and pseudogroups

3.1.1 Single-qubit gates and distances in SU(2)

The main purpose of this chapter is to describe a new procedure, the quantum hashing [1, 2], to approximate every target single-qubit gate in terms of an ordered sequence of the elementary quantum gate composing a universal basis. In particular the universal basis we will refer to is the one obtained through the braidings of Fibonacci anyons that allow to encode quantum information exploiting the topological properties of anyons that we discussed in Chapter 2. As we already saw, the peculiarity of physical systems presenting a non-Abelian topological order is that a collection of non-Abelian anyonic excitations with fixed positions spans a multi-dimensional Hilbert space and, in such a space, the quantum evolution of the multi-component wavefunction of the anyons is realized by braiding them.

Therefore, it is natural to consider the unitary matrices representing the exchange of two anyons as the elementary gates for a quantum computation scheme.

In this way the universal basis for the quantum computation acquires an immediate physical meaning and its elements are implemented in a fault-tolerant way; therefore the problem of approximating a target unitary gate is translated in finding the best "braid" of anyons that represents the given operator up to a certain length of ordered anyons exchanges [39].

The hashing algorithm allows to approximate every target single-qubit gate in SU(2) exploiting the composition rules of one of its subgroups, as the icosahedral one; therefore it is useful to consider the standard homomorphism from the group of rotations in $\mathbb{R}^3$, $SO(3)$, and the group of single-qubit gates, that permits to write every operator $U \in \mathrm{SU}(2)$ as

$$\begin{aligned} U(\hat{m},\phi) &= e^{i\hat{m}\cdot\vec{\sigma}(\phi/2)} = \\ &= \begin{pmatrix} \cos(\phi/2) + im_z \sin(\phi/2) & m_y \sin(\phi/2) + im_x \sin(\phi/2) \\ -m_y \sin(\phi/2) + im_x \sin(\phi/2) & \cos(\phi/2) - im_z \sin(\phi/2) \end{pmatrix}. \end{aligned} \tag{3.5}$$

$U(\hat{m},\phi)$ represents a rotation, in SO(3), of an angle ϕ around the axes identified by the unitary vector $\hat{m}$. Therefore, if we exclude an overall phase, which is unimportant to the purpose of single-qubit gates, SU(2) can be mapped on a sphere of radius π: a point in the sphere defined by a radius $0 \leq \phi \leq \pi$ in the direction $\hat{m}$ corresponds to the rotation $U(\hat{m},\phi)$. In the following we will often address the elements of SU(2) not only as single qubit gates but also as rotations, implicitly referring to this homomorphism.

The distance d (also referred to as error) between two gates (or their matrix representations) U and V is defined as the operator norm distance

$$d(U,V) \equiv \|U - V\| = \sup_{\|\psi\|=1} \|(U-V)\,\psi\|. \tag{3.6}$$

Thus, if we consider two operators $U = U(\hat{m},\phi)$ and $V = U(\hat{n},\theta)$ the distance between them is

$$d(U,V) = \sqrt{2 - 2\cos\frac{\phi}{2}\cos\frac{\theta}{2} - 2\,\hat{m}\cdot\hat{n}\,\sin\frac{\phi}{2}\sin\frac{\theta}{2}}, \tag{3.7}$$

which is bound above by $\sqrt{2}$. We notice that the distance of a rotation $U(\hat{m},\phi)$ from the identity operator is $d = 2\sin(\phi/4)$.

3.1.2 Brute-force search with Fibonacci anyons

The matrices σ_1 and σ_2 defined in the equations (2.44, 2.45) and their inverses, σ_1^{-1} and σ_2^{-1}, are the universal quantum basis that we adopt to generate operators in SU(2). Considering the representation (3.5), σ_1 and σ_2 correspond to rotations of $\frac{3}{5}\pi$ whose axes differ for an angle $\theta = \arccos\left(\sqrt{5}-2\right)$ as a result of the change of basis F in (2.41). Such rotations do not belong to any finite subgroup of SO(3), therefore the group generated by σ_1 and σ_2 must be dense in SU(2) [34].

In particular this matrix representation of the braidings generates the four-strand braid group B_4, corresponding to the four-anyon qubit in Fig. 2.12 (a), or an equivalent three-strand braid group B_3, related to the three-anyon qubit in Fig.

2.12 (b): these are infinite dimensional groups consisting of all possible sequences of length L of the generators σ_i and σ_i^{-1} and, with increasing L, the whole set of braidings generates a dense cover of the SU(2) single-qubit rotations.

Besides, Simon *et al.* [38] demonstrated that, in order to achieve universal quantum computation, it is sufficient to move a single Fibonacci anyon around the others at fixed position. Thanks to this result, one can study an infinite subgroup of the braid group B which is the group of *weaves*, braids characterized by the movement of only one quasiparticle around the others. From a practical point of view it seems simpler to realize and control a system of this kind, therefore we will consider only weaves in the following. There is also another advantage in doing so: the elementary gates to cover SU(2) become σ_1^2, σ_2^2 and their inverses; therefore the weaves avoid the equivalence between two braids caused by the Yang-Baxter relations (1.2), so that it is more immediate to find the set of independent weaves up to a certain length. In fact, the only relations remaining for Fibonacci anyons that give rise to different but equivalent weaves are the relations $\sigma_1^{10} = \sigma_2^{10} = 1$, because they imply that $\sigma_i^6 = \sigma_i^{-4}$ and one can always reduce weaves with terms of the kind $\sigma_i^{\pm 6}$ to shorter but equivalent ones.

In order to calculate the efficiency in approximating a target gate through the brute-force search, which gives the optimal result up to a certain length, it will be useful calculating here the number of independent weaves of Fibonacci anyons; in general a weave of length L can be written as

$$\sigma_{p_1}^{q_1}\sigma_{p_2}^{q_2}\cdots\sigma_{p_s}^{q_s}, \tag{3.8}$$

where $p_i \in \{1,2\}$, $p_i \neq p_{i\pm1}$, and $\sum_i |q_i| = L$. As mentioned above, to ensure that this braid is not equivalent to a shorter braid, one must have $q_i = \pm 2$ or ± 4.

Let us assume the number of length-L weaves is $N(L)$, consisting of $N_4(L)$ weaves ending with $\sigma_p^{\pm 4}$ and $N_2(L)$ weaves ending with $\sigma_p^{\pm 2}$. To form a weave of length $L+2$, the sequence must be appended by σ_r^2 or σ_r^{-2}. For sequences ending with σ_p^2 (or σ_p^{-2}), we can append σ_p^2 (or σ_p^{-2}), σ_{3-p}^2, or σ_{3-p}^{-2}. However, for sequences ending with σ_p^4 (or σ_p^{-4}), we can only append σ_{3-p}^2 or σ_{3-p}^{-2}. Therefore, we have the recurrence relations:

$$N(L) = N_4(L) + N_2(L), \tag{3.9}$$

$$N(L+2) = 2N_4(L) + 3N_2(L), \tag{3.10}$$

$$N_4(L+2) = N_2(L). \tag{3.11}$$

With an ansatz $N(L) \sim \alpha^{L/2}$ [and so are $N_4(L)$ and $N_2(L)$], we find $\alpha = 1 \pm \sqrt{3}$. Therefore the exact number of weaves of length L is

$$N(L) = \left(1 - \frac{1}{\sqrt{3}}\right)\left(1 - \sqrt{3}\right)^{L/2} + \left(1 + \frac{1}{\sqrt{3}}\right)\left(1 + \sqrt{3}\right)^{L/2}, \tag{3.12}$$

which grows as $(1+\sqrt{3})^{L/2}$ asymptotically.

To find a weave whose matrix representation efficiently approximates a particular desired single-qubit operator, the brute-force search is the most straightforward approach [37, 39]. This procedure consists in a direct search among all the possible

sequences $\{q_i\}$, characterizing all the weaves (3.8), up to the length L, in order to find the braid which is closest to the target gate (with respect to the distance (3.7)). As an example we can consider the target gate:

$$iZ = \begin{pmatrix} i & 0 \\ 0 & -i \end{pmatrix}. \tag{3.13}$$

The brute-force search up to $L = 8$ gives the following result:

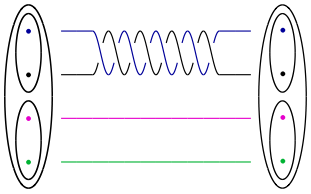

$$\tilde{Z}_8 \cong \begin{pmatrix} 0.31 + 0.95i & 0 \\ 0 & 0.31 - 0.95i \end{pmatrix}$$

with an error $\varepsilon_8 = 0.31$ which is too high to the purpose of quantum computation. However increasing L one obtains more precise representations of iZ (see Fig. 3.1). In particular, for $L = 24$ and $L = 40$, the errors respectively decrease to $\varepsilon_{24} = 0.024$ and $\varepsilon_{40} = 0.001$.

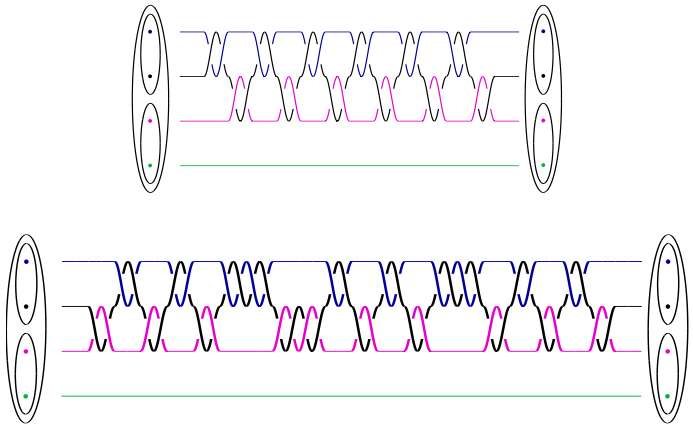

Figure 3.1: Braid representations of the gate iZ characterized by $L = 24$ and $L = 40$. The corresponding errors are $\varepsilon_{24} = 0.024$ and $\varepsilon_{40} = 0.001$.

From the number of weaves $N(L)$ in equation (3.12), we can estimate the general efficiency for the brute-force search algorithm through the probability distribution of the error of any weave of length L from a given target gate in SU(2). We assume that the collection of the $N(L)$ nontrivial weaves of length L are uniformly distributed on the sphere of SU(2). Representing the elements of SU(2) on the surface of the four-dimensional sphere (since an element in SU(2) can be parametrized by two complex numbers whose norms sum to 1), we find the distribution $p_{BF}(d)$ of their distance from the identity operator to be

$$p_{BF}(d) = \frac{4}{\pi} d^2 \sqrt{1 - (d/2)^2} \tag{3.14}$$

where $d = 2 \sin(\phi/4)$ (see Fig. 3.6).

Given this distribution, we obtain the average error for the brute-force search to be

$$\bar{d}(L) = \frac{\pi^{1/3}\Gamma\left(\frac{1}{3}\right)}{6^{2/3}[N(L)]^{1/3}} \approx 1.021 e^{-L/5.970} \tag{3.15}$$

asymptotically (see Appendix A for more detail).

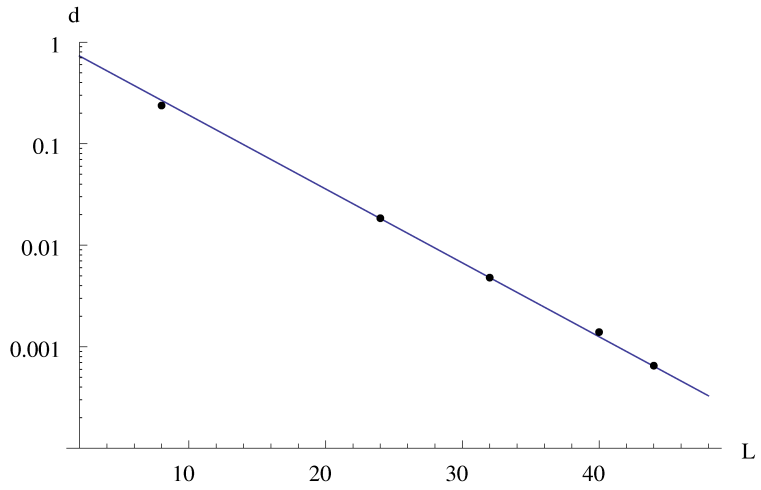

Figure 3.2: The average errors (dots) of the approximations to the 60 rotations of the icosahedral group with the brute-force search as a function of the length of the weaves used. These errors characterize the pseudogroups used in the hashing algorithm for the lengths $L = 8$, 24, 32, 40, and 44. The results are in very good agreement with the prediction in Eq. (3.15) (solid line).

The brute-force approach can be improved using several techniques, such as a bidirectional search, which can be applied to perform deeper searches resulting in longer and more accurate weaves. In particular, it has been shown that the introduction of a geometric redundancy through the decomposition of the target gate in three rotations can lead to errors of about 4×10^{-10} for braids of length $L \sim 300$ [42]. Nevertheless the exponential growth in the number of weaves $N(L)$ makes any brute-force approach unfeasible to reach high accuracies. Therefore one has to find more practical alternatives to reach small errors in a runtime not increasing as a power of the precision required.

3.1.3 The Icosahedral group

The hashing procedure relies on the possibility of exploiting the group structure of a finite subgroup of the target space to build sets $\mathcal{S}(L)$ of fine rotations, distributed with smaller and smaller mean distances from the identity, that can be used to progressively correct a first approximation of a target gate T. Therefore, it is fundamental to search, for every target space of unitary operators, a suitable subgroup to build the sets $\mathcal{S}$. Among the different finite subgroups of SU(2) we considered the $SO(3)$ subgroups corresponding to the symmetry group of the icosahedron and of the cube, which have order 60 and 24, respectively. However, for

practical purposes, we will refer in the following mainly to the icosahedral group because its implementation of the hashing algorithm, as we will describe below, is more efficient in terms of the final braid length.

The icosahedral rotation group $\mathcal{I}$ is the largest polyhedral subgroup of SU(2), excluding reflection. For this reason, it has been often used to replace the full SU(2) group for practical purposes, as for example in earlier Monte Carlo studies of SU(2) lattice gauge theories [83, 84, 85], and its structure can be exploited to build meshes that cover the whole SU(2) [86].

$\mathcal{I}$ is composed by 60 rotations around the axes of symmetry of the icosahedron (platonic solid with twenty triangular faces) or of its dual polyhedron, the dodecahedron (regular solid with twelve pentagonal faces); there are six axes of the fifth order (corresponding to rotations with fixed vertices), ten of the third (corresponding to the triangular faces) and fifteen of the second (corresponding to the edges). Moreover $\mathcal{I}$ is isomorphic to the $\mathcal{A}_5$ group of the even permutations of five elements. Let us for convenience write $\mathcal{I} = \{g_0, g_1, ..., g_{59}\}$, where $g_0 = e$ is the identity element. In figure 3.3**a** the elements of the icosahedral group are represented inside the SU(2) sphere.

Because of the group structure, given any product of n elements of a subgroup $g_{i_1} g_{i_2} \cdots g_{i_n}$ there always exists a group element $g_{i_{n+1}} = g_{i_n}^{-1} \cdots g_{i_2}^{-1} g_{i_1}^{-1}$ that is its inverse. In this way $g_{i_1} g_{i_2} \cdots g_{i_n} g_{i_{n+1}} = e$ and one can find O^n different ways of obtaining the identity element, where O is the order of the group (60 in the case of the icosahedral one). This is the key property we will use in order to create a dense mesh $\mathcal{S}$ of fine rotations distributed around the identity operator in the target space. To achieve this goal, however, we need to break the exact group structure and to exploit the errors given by a brute-force search approximation of the elements of the chosen subgroup.

3.1.4 Pseudogroups

The main idea in the realization of the mesh $\mathcal{S}$ is that, representing the 60 elements of the subgroup $\mathcal{I}$ with weaves of a given length L, we can control, due to the relation (3.15), the average distance (or error) between the exact rotations in $\mathcal{I}$ and their braid representations that constitute the set $\tilde{\mathcal{I}}(L)$ which we will refer to as a *pseudogroup*.

Thanks to the homomorphism between SU(2) and $SO(3)$ we associate to every rotation $g \in \mathcal{I}$ a 2×2 matrix (3.5). Then we apply a brute-force search of length L to approximate the 60 elements in $\mathcal{I}$; in this way we obtain 60 braids that give rise to the pseudogroup $\tilde{\mathcal{I}}(L) = \{\tilde{g}_0(L), \tilde{g}_1(L), \ldots, \tilde{g}_{59}(L)\}$. These braids are characterized by an average distance $\epsilon(L)$ with their corresponding elements $g_i \in \mathcal{I}$ given by Eq. (3.15) (see Table 3.1). We notice from Fig. 3.3 that the large errors for $L = 8$ completely spoil the symmetry of the group (and we will exploit this characteristic in the preprocessor of the hashing algorithm); however, increasing the length L, one obtains pseudogroups with smaller and smaller errors. Choosing, for instance, a fixed braid length of $L = 24$, the error of each braid representation to its corresponding exact matrix representation varies from 0.003 to 0.094 with a mean distance of 0.018. Figure 3.4 shows the example provided by the rotation of

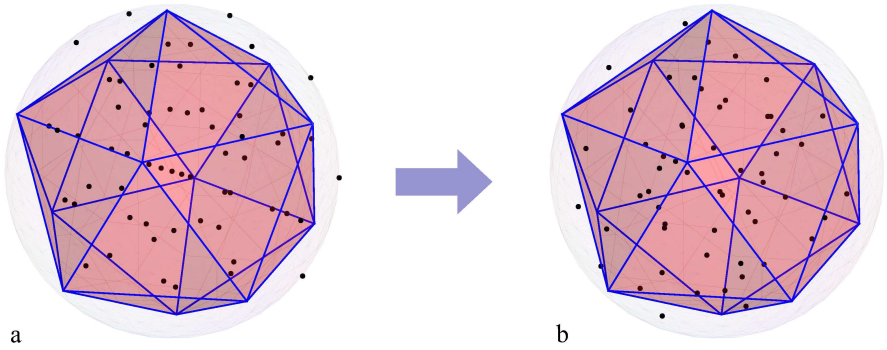

Figure 3.3: **a**: The icosahedral group representation inside the SU(2) sphere. **b**: the pseudogroup representation $\tilde{\mathcal{I}}(8)$ used in the preprocessor. Due to the large errors (~ 0.24) the elements of $\tilde{\mathcal{I}}(8)$ seem to span the SU(2) sphere randomly.

π around the x-axis, which is an element of $\mathcal{I}$: this rotation, corresponding to the quantum gate $-iX$, is represented by a braid of length $L = 24$ belonging to the pseudogroup $\tilde{\mathcal{I}}(24)$.

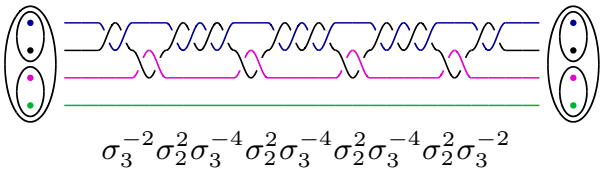

Figure 3.4: Approximation to the $-iX$ gate (an element of the icosahedral group) in terms of braids of the Fibonacci anyons of length $L = 24$ in the graphic representation. In this example the error is 0.0031.

One of the key elements of the hashing procedure is that the braid representations of the icosahedral group with different lengths are obtained by a brute-force search once and for all. The so obtained braids are then stored for future utilizations and this is the only step in which we apply, preliminarily, a brute-force search. Due to limiting computing resources, we construct the pseudogroups representations for the 60 rotations up to the length $L = 68$, which, as we will describe below, is sufficient to implement three iterations of the hashing algorithm. In principle one could calculate the brute-force approximation of the group elements to larger lengths once and for all, in order to use them for a greater number of iterations. The average errors characterizing the main pseudogroups we use in the iterations are shown in Fig. 3.2 and in Table 3.1; they agree well with Eq. (3.15), with the exception of the $L = 68$ pseudogroup which was obtained through an incomplete

implementation of the brute-force search algorithm for technical reasons.

Length	Pseudogroup average error
8	0.2374
24	0.01845
32	4.794×10^{-3}
40	1.394×10^{-3}
44	6.513×10^{-4}
68	2.424×10^{-5}

Table 3.1: Average errors of the pseudogroups obtained approximating with a brute-force search the icosahedral group. These results are represented in Fig. 3.2 and they agree with the predicted behaviour in (3.15). The pseudogroup with $L = 68$ was obtained through an incomplete implementation of the brute-force search algorithm, therefore its mean error is higher than the one expected.

Let us stress that that the 60 elements of $\tilde{\mathcal{I}}(L)$ (for any finite L) do not close any longer the composition laws of the icosahedral group; in fact a pseudogroup $\tilde{\mathcal{G}}(L)$ becomes isomorphic to its corresponding group $\mathcal{G}$ only in the limit $L \to \infty$. If the composition law $g_i g_j = g_k$ holds in $\mathcal{I}$, the product of the corresponding elements $\tilde{g}_i(L)$ and $\tilde{g}_j(L)$ is not $\tilde{g}_k(L)$, although it can be very close to it for large enough L. Interestingly, the distance between the product $\tilde{g}_i(L)\,\tilde{g}_j(L)$ and the corresponding element g_k of $\mathcal{I}$ can be linked to the Wigner-Dyson distribution (see Sec. 3.2.2).

Using the pseudogroup structure of $\tilde{\mathcal{I}}(L)$, it is easy to generate a mesh $\mathcal{S}(L)$ made of a large number of braids only in the vicinity of the identity matrix: this is a simple consequence of the original group algebra, in which the composition laws allow us to obtain the identity group element in various ways. The set $\mathcal{S}$ is instrumental to achieve an important goal, i.e. to search among the elements of $\mathcal{S}$ the best correction to apply to a previous approximation of the target single-qubit gate T we want to hash.

It is important to notice that, changing the length L of the pseudogroup representation, we can control the average distance of the fine rotations in $\mathcal{S}$ from the identity. To correct an approximation of T with an error ε, we need a mesh $\mathcal{S}$ characterized by roughly the same average error in order to reach an optimal density of possible corrections and so increase the efficiency of the algorithm. Therefore, knowing the average error of the distribution of the approximations we want to improve, we can choose a suitable L to generate a mesh. As represented in Fig. 3.5, this allows us to define a series of denser and denser meshes to iterate the hashing algorithm in order to correct at each step the expected mean error, which we have determined by analyzing the distributions of errors of 10000 random targets after the corresponding iteration.

To create the mesh of fine rotations, labelled by $\mathcal{S}(L, n)$, we consider all the possible ordered products $\tilde{g}_{i_1}(L)\tilde{g}_{i_2}(L)\ldots\tilde{g}_{i_n}(L)$ of a fixed number $n \geq 2$ of elements of $\tilde{\mathcal{I}}(L)$ of length L, and multiply them by the matrix $\tilde{g}_{i_{n+1}}(L) \in \tilde{\mathcal{I}}(L)$ such that $g_{i_{n+1}} = g_{i_n}^{-1} \ldots g_{i_2}^{-1} g_{i_1}^{-1}$. In this way we generate all the possible combinations of $n+1$ elements of $\mathcal{I}$ that produce the identity, but, thanks to the errors that

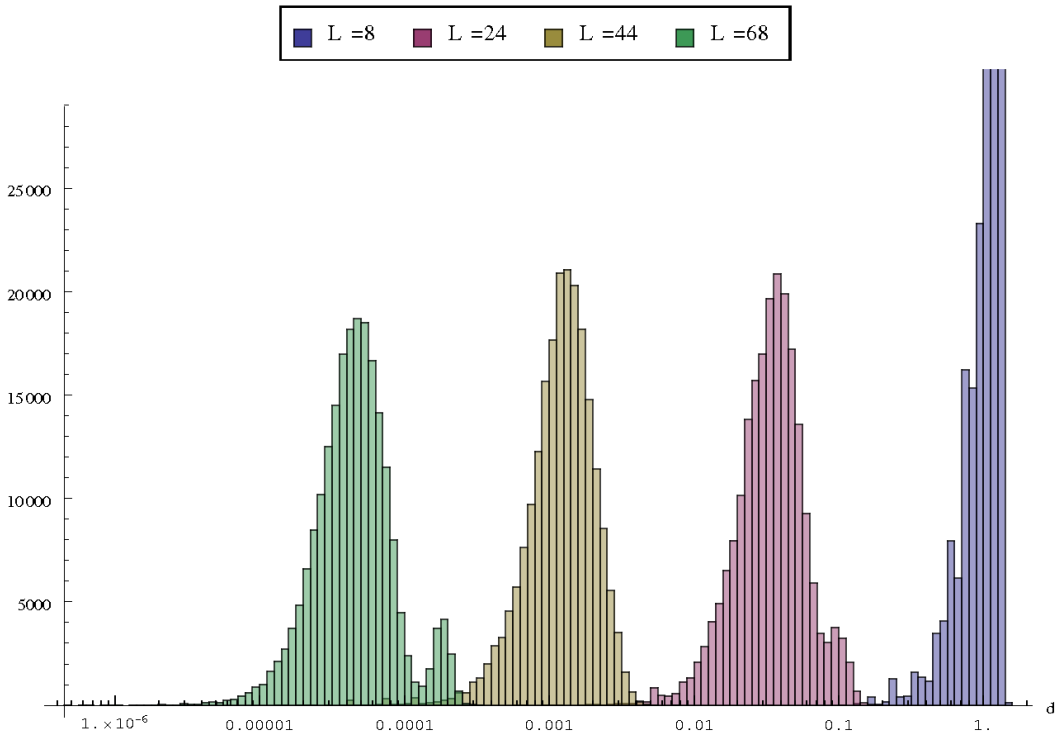

Figure 3.5: Distribution of the meshes $\mathcal{S}(L,3)$ used by the renormalization scheme of the hashing algorithm. The distance d from the identity is represented in logarithmic scale. The mesh with $L=8$ comprehends every possible product of three elements in $\tilde{\mathcal{I}}(8)$ and, therefore, it spans the whole SU(2) space up to the distance $\sqrt{2}$. The meshes $\mathcal{S}(24,3)$, $\mathcal{S}(44,3)$ and $\mathcal{S}(68,3)$, instead, are the product of four braids whose corresponding rotations are combined to approximate the identity. $\mathcal{S}(24,3)$ and $\mathcal{S}(44,3)$ follow the Wigner-Dyson distribution while $\mathcal{S}(68,3)$ exhibits a second local maximum due to the incomplete brute-force search we used to obtain $\tilde{\mathcal{I}}(68)$.

characterize the braid representation $\tilde{\mathcal{I}}$, we obtain 60^n small rotations in SU(2), corresponding to braids of length $(n+1)L$. In Sec. 3.2.2 we will describe their distribution around the identity with the help of random matrices.

The meshes $\mathcal{S}(L,n)$ obtained through this procedure are spread around the identity with an average distance related to the accuracy obtained by the brute-force algorithm in generating the pseudogroups $\tilde{\mathcal{I}}(L)$ (see Table 3.1). The high density around the identity of these sets of braids is exploited in the quantum hashing algorithm and constitutes one of the main advantages with respect to other algorithm. In particular, in the brute-force search, the whole SU(2) sphere is sampled with the same density of braids, therefore the most probable ones are generated with the largest distance to the target gate; as we will see in the next section, the hashing procedure employs instead only braids in a neighbourhood of the desired gate. See Fig. 3.6 for a comparison between the distribution of the meshes used in the different algorithms.

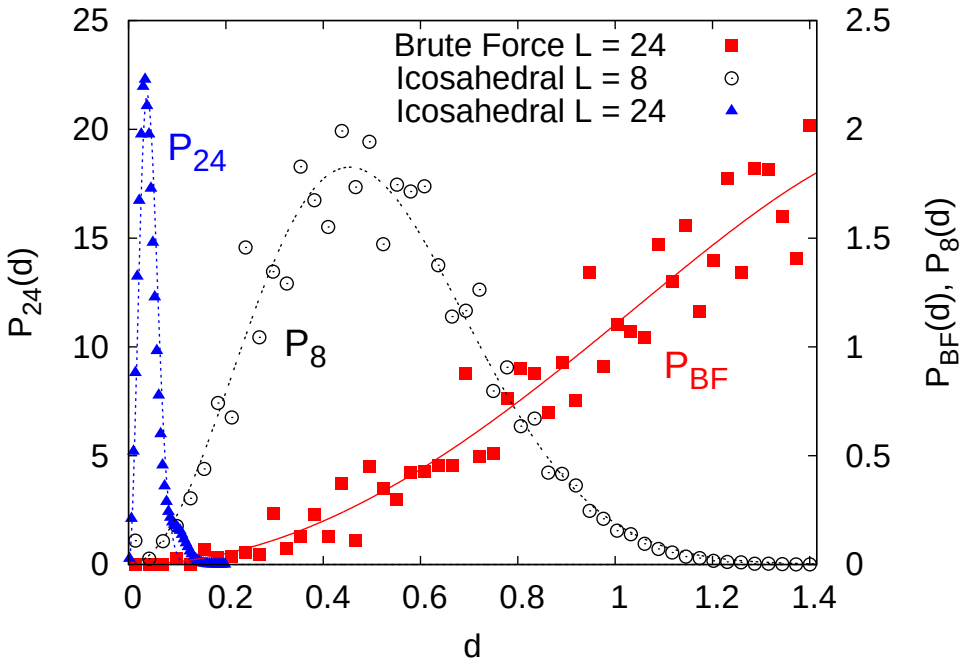

Figure 3.6: Probability distribution of the distance d to the identity matrix in the set of nontrivial braids that one samples in different algorithms. $P_{BF}(d)$ of the brute-force search (red solid squares) roughly follows Eq. (3.14), reflecting the four-dimensional spherical nature of the unitary matrix space (three independent parameters apart from an unimportant phase). In the pseudo icosahedral group approach ($n = 4$), distributions for $L = 8$ (P_8, black empty circles) and $L = 24$ (P_{24}, blue solid triangles) agree very well with the energy-level-spacing distribution of the unitary Wigner-Dyson ensemble of random matrices, $P_L(d) = (\frac{32}{\pi^2})(d^2/d_L^3)e^{-(4/\pi)(d/d_L)^2}$. $P_L(d)$ differ only by their corresponding average d_L (not a fitting parameter), which decays exponentially as L increases. Note $P_{24}(d)$ is roughly ten-times sharper and narrower than $P_8(d)$.

3.2 Iterative pseudogroup hashing in SU(2)

3.2.1 The iterative pseudogroup hashing algorithm

The hashing algorithm [87] is based on the possibility of finding progressive corrections to minimize the error between the target gate $T \in SU(2)$ and the braids that represent it. These corrections are chosen among the meshes $\mathcal{S}(L_i, 3)$ whose distribution around the identity operator is shown in Fig. 3.5.

The algorithm consists of a first building block, called *preprocessor*, whose aim is to give an initial approximation $\tilde{T}_0$ of T, and a *main processor* composed of a series of iterations of the hashing procedure that, at each step, extend the previous representation by a braid in $\mathcal{S}(L_i, 3)$. The final braid has the form

$$\tilde{T}_3 = \underbrace{\tilde{g}_{j_1}(L_0)\cdots\tilde{g}_{j_3}(L_0)}_{\text{Preprocessor}}\underbrace{\tilde{g}_{p_1}(L_1)\cdots\tilde{g}_{p_4}(L_1)}_{\text{1st Iteration}}\underbrace{\tilde{g}_{q_1}(L_2)\cdots\tilde{g}_{q_4}(L_2)}_{\text{2nd Iteration}}\underbrace{\tilde{g}_{r_1}(L_3)\cdots\tilde{g}_{r_4}(L_3)}_{\text{3rd Iteration}} \tag{3.16}$$

Each $\tilde{g}_j(L_i)$ is an element of the pseudogroup $\tilde{\mathcal{I}}(L_i)$ and, as explained in the previous section, the braid segment in each main iteration is constrained by $g_{k_4} = g_{k_3}^{-1} g_{k_2}^{-1} g_{k_1}^{-1}$, $k = p$, q, or r.

Each iteration starts from an input approximation $\tilde{T}_{i-1}$ with a distance ε_{i-1} from the target T. We exploit the elements of the mesh $\mathcal{S}(L_i, n)$ to generate a new braid $\tilde{T}_i$ with a smaller distance ε_i. The lengths L_i in Eq. (3.16), which characterize the pseudogroups used in the main processor, control the density of the corresponding meshes and are chosen among the sets of stored pseudogroups in order to correct the residual error in an efficient way (see Sec. 3.3).

Let us analyze now the details of each step in the hashing algorithm. The preprocessor is a fast procedure to generate a rough approximation of the target gate $T \in SU(2)$ and, in general, it associates to every T a braid which is an element of $[\tilde{\mathcal{I}}(L_0)]^m$ (of length mL_0). Therefore, the preprocessor approximates T with the ordered product of elements in the icosahedral pseudogroup $\tilde{\mathcal{I}}(L_0)$ that best represents it, minimizing their distance. Thus we obtain a starting braid

$$\tilde{T}_0^{L_0,m} = \tilde{g}_{j_1}(L_0)\,\tilde{g}_{j_2}(L_0)\ldots\tilde{g}_{j_m}(L_0) \tag{3.17}$$

with an initial error to reduce. The preprocessor procedure relies on the fact that, choosing a small L_0, we obtain a substantial discrepancy between the elements g_i of the icosahedral group and their representatives $\tilde{g}_i$, as shown in Fig. 3.3. Because of these seemingly random errors, the set $[\tilde{\mathcal{I}}(L_0)]^m$ of all the products $\tilde{g}_{j_1}\tilde{g}_{j_2}\ldots\tilde{g}_{j_m}$ is well spread all over SU(2) and can be thought as a random discretization of the group. In particular we find that the pseudogroup $\tilde{\mathcal{I}}(8)$ has an average error of about 0.24 and it is sufficient to take $m = 3$ [as we did in Eq. (3.16)] to cover the whole SU(2) in an efficient way with 60^3 operators. The average error for an arbitrary single-qubit gate with its nearest element $\tilde{T}_0^{8,3} \in [\tilde{\mathcal{I}}(8)]^3$ is about 0.027.

One can then apply the main processor to the first approximation $\tilde{T}_0$ of the target gate. Each subsequent iteration improves the previous braid representation of T by adding a finer rotation to correct the discrepancy with the target and generate a new braid. In the first iteration we use the mesh $\mathcal{S}(L_1, n)$ to efficiently

reduce the error in $\tilde{T}_0^{l,m}$. Multiplying $\tilde{T}_0^{l,m}$ by all the elements of $\mathcal{S}(L_1, n)$, we generate 60^n (O^n if we use a subgroup of order O) possible braid representations of T :

$$\tilde{T}_0^{l,m}\tilde{g}_{i_1}\tilde{g}_{i_2}\ldots\tilde{g}_{i_n}\tilde{g}_{i_{n+1}} \tag{3.18}$$

Among these braids of length $(n+1)L_1+mL_0$, we search the one with the shortest distance to the target gate T. This braid, $\tilde{T}_1\,(L_0, m, L_1, n)$, is the result of the first iteration in the main processor. Fig. 3.7 shows the distribution of the errors after this first step for 10,000 randomly selected target gates obtained with a preprocessor with $L_0 = 8$ and $m = 3$ and the first iteration of the hashing procedure with $L_1 = 24$ and $n = 3$.

The choice of $L = 24$ for the first step is dictated by the analysis of the mean error of the preprocessor (~ 0.03) that requires, as we will see in the following section, a pseudogroup with compatible error for an efficient correction.

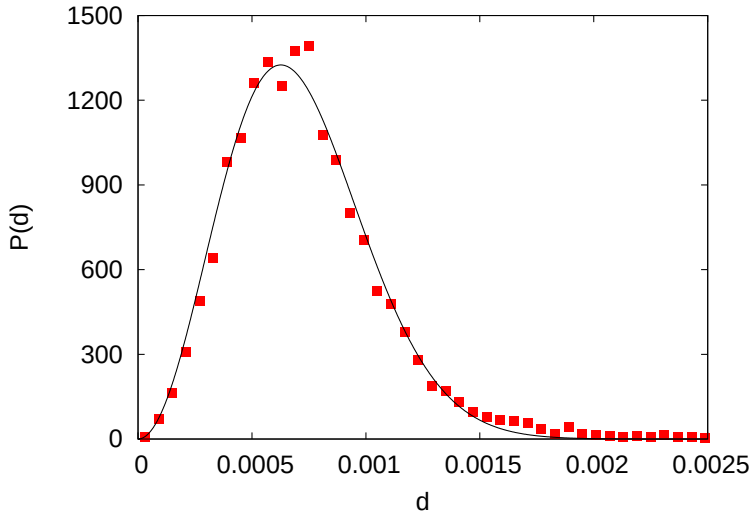

Figure 3.7: Probability distribution of d in 10,000 random tests using the icosahedral group approach with a preprocessor of $L_0 = 8$ and $m = 3$ and a first iteration of the hashing with $L_1 = 24$ and $n = 3$. The total length of the braids (neglecting accidental cancellations when component braids connect) is 120. The trend agrees with the unitary Wigner-Dyson distribution (solid line) with an average error 7.1×10^{-4}.

With $\tilde{T}_1$ we can then apply the second and third iterations of the main processor to obtain an output braid of the form in Eq. (3.16). These iterations further reduce the residual discrepancy in decreasing error scales. Each step in the main processor requires the same runtime, during which a search within 60^n braids selects the one with the shortest distance to T. One must choose appropriate pseudogroups with longer braid lengths L_2 and L_3 to generate finer meshes. As for L_1, we choose L_2 and L_3 to match the error of the corresponding pseudogroup to the respective mean residual error. In practice, we choose $L_2 = 44$ and $L_3 = 68$. The final output assumes the form in Eq. (3.16) and the average distance to the target braid

(in 10000 random tests) is 2.29×10^{-5} after the second iteration and 8.24×10^{-7} after the third (see Figures 3.8 and 3.9 for the distribution of the results after the second and third iteration). These average values do not take into account the necessary corrections of the braids in the tails of the distributions that we will discuss in the next sections; therefore the trend describing their distribution must be based on the lower average errors reported in Table 3.2 which are more effective to define the final probability density of the errors. Besides, we can notice that, without reductions, the final length of the resulting braids is 568; however, due to shortenings at the junctions where different braid segments meet, the practical final length of the weave is usually smaller.

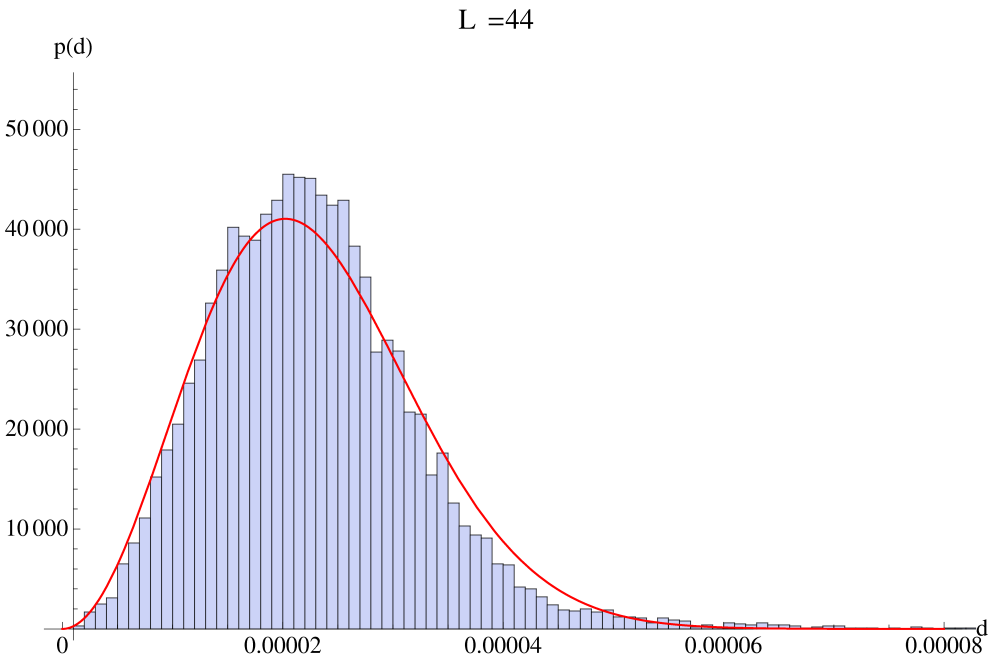

Figure 3.8: Probability density of the distance d from the target of 10000 random tests after the second ($L = 44$) iteration of the hashing procedure. The trend agrees with the unitary Wigner-Dyson distribution with average error 2.28×10^{-5}.

To illustrate better the functioning of the two building blocks (preprocessor and main processor) of the hashing algorithm, it is useful to consider a concrete example: suppose we want to find the best braid representation of the target gate

$$T = iZ = \begin{pmatrix} i & 0 \\ 0 & -i \end{pmatrix} \tag{3.19}$$

Out of all combinations in $[\tilde{\mathcal{I}}(8)]^3$, the preprocessor selects a $\tilde{T}_0^{8,3} = \tilde{g}_{p_1}(8)\tilde{g}_{p_2}(8)\tilde{g}_{p_3}(8)$, which minimizes the distance to T to 0.038. Applying now the first iteration in the main processor, the best rotation in $\mathcal{S}(24,3)$ that corrects $\tilde{T}_0^{8,3}$ is given by $\tilde{g}_{q_1}(24)\tilde{g}_{q_2}(24)\tilde{g}_{q_3}(24)\tilde{g}_{q_4}(24)$, where $g_{q_4} = g_{q_3}^{-1} g_{q_2}^{-1} g_{q_1}^{-1}$. The

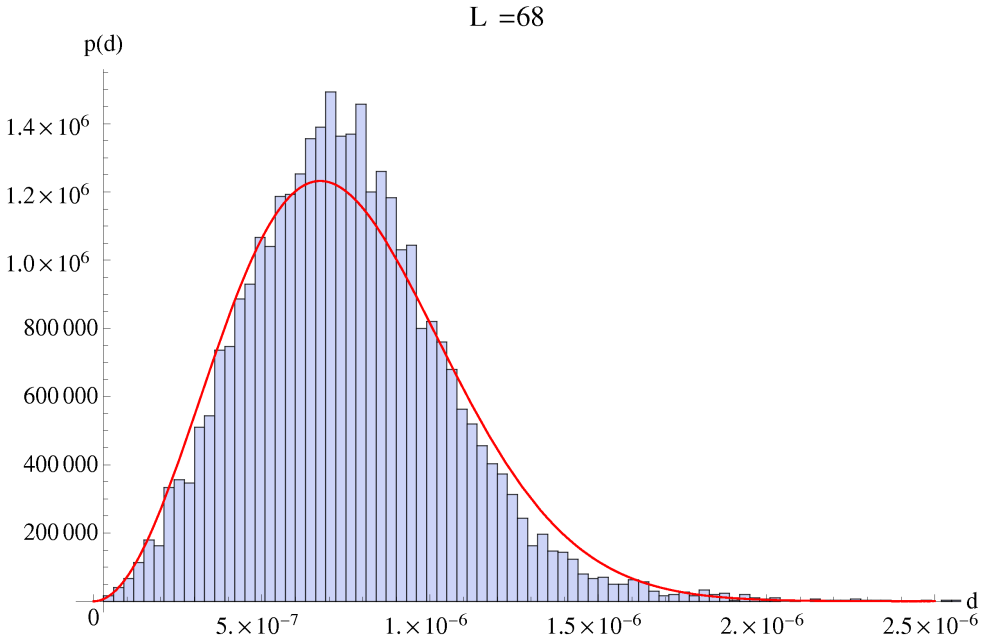

Figure 3.9: Probability density of the distance d from the target of 10000 random tests after the third ($L = 68$) iteration of the hashing procedure. The trend agrees with the unitary Wigner-Dyson distribution with average errors 7.60×10^{-7}, where we applied the tail correction to obtain the right value of the average (see Sec. 3.2.4).

resulting braid [87] is then represented by

$$\tilde{T}_1 = \tilde{g}_{p_1}(8)\tilde{g}_{p_2}(8)\tilde{g}_{p_3}(8)\tilde{g}_{q_1}(24)\tilde{g}_{q_2}(24)\tilde{g}_{q_3}(24)\tilde{g}_{q_4}(24) = \\ = \begin{pmatrix} -0.00040 + 1.00000i & -0.00073 - 0.00054i \\ 0.00073 - 0.00054i & -0.00040 - 1.00000i \end{pmatrix} e^{\frac{4}{5}\pi i}$$

for the special set of p's and q's and, apart from an overall phase, the final distance is reduced to 0.00099 (Fig. 3.10).

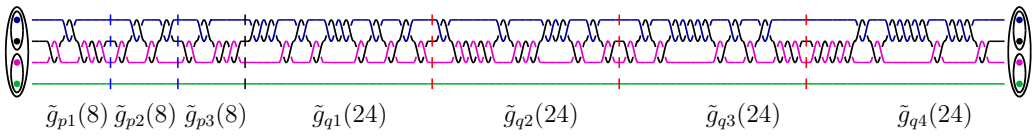

Figure 3.10: The graphic representation of the braid approximating the target gate iZ in the icosahedral group approach after a preprocessor of $L_0 = 8$ and $m = 3$ and the first iteration with $L_1 = 24$ and $n = 3$. To emphasize the structure, we mark the segments belonging to the pseudogroups, among which $\tilde{g}_{p1}\tilde{g}_{p2}\tilde{g}_{p3} \approx iZ$ and $\tilde{g}_{q1}\tilde{g}_{q2}\tilde{g}_{q3} \approx \tilde{g}_{q4}^{-1}$ up to a phase. The braid (with a reduced length of 98 due to accidental cancellations where the component braids connect) has an error of 0.00099 [87].

After the first iteration, the second and third ones are applied in the same way with $L_2 = 44$ and $L_3 = 68$. The final output assumes the form (3.16) and the distance to the target braid iZ is reduced to $1.88 \cdot 10^{-5}$ after the second iteration and $1.04 \cdot 10^{-6}$ after the third one. In principle the final length obtained is 568, however there are simplifications that occur fusing different braids of the pseudogroups and the final length of the weave is reduced to 498.

3.2.2 Connection with random matrix theory and reduction factor for the main processor

To analyze the efficiency of the main processor we must study the random nature of the meshes $\mathcal{S}(L, n)$. The distribution of the distance between the identity and their elements has an intriguing connection to the Gaussian unitary ensemble of random matrices, which helps us to understand how close we can approach the identity in this way, and therefore what the optimal choice of the lengths of the pseudogroups is for each iteration of the main processor.

Let us analyze the group property deviation for the pseudogroup $\tilde{\mathcal{I}}(L)$ for braids of length L. One can write $\tilde{g}_i = g_i e^{i\Delta_i}$, where Δ_i is a Hermitian matrix, indicating the small deviation of the finite braid representation to the corresponding SU(2) representation for an individual element. For a product of $\tilde{g}_i$ that approximate $g_i g_j \cdots g_{n+1} = e$, one has

$$\tilde{g}_i \tilde{g}_j \cdots \tilde{g}_{n+1} = g_i e^{i\Delta_i} g_j e^{j\Delta_j} \cdots g_{n+1} e^{i\Delta_{n+1}} = e^{iH_n}, \tag{3.20}$$

where H_n, related to the accumulated deviation, is

$$H_n = g_i \Delta_i g_i^{-1} + g_i g_j \Delta_j g_j^{-1} g_i^{-1} + \cdots + g_i g_j \cdots g_n \Delta_n g_n^{-1} \cdots g_j^{-1} g_i^{-1} + \Delta_{n+1} + O(\Delta^2). \tag{3.21}$$

The natural conjecture is that, for a long enough sequence of matrix product, the Hermitian matrix H_n tends to a random matrix corresponding to the Gaussian unitary ensemble. This is plausible as H_n is a Hermitian matrix that is the sum of random initial deviation matrices with random unitary transformations. A direct consequence is that the distribution of the eigenvalue spacing s obeys the Wigner-Dyson form [88],

$$P(s) = \frac{32}{\pi^2 s_0} \left(\frac{s}{s_0} \right)^2 e^{-(4/\pi)(s/s_0)^2}, \tag{3.22}$$

where s_0 is the mean level spacing. For small enough deviations, the distance of H_n to the identity, $d\left(1, e^{iH_n}\right) = \|H_n\| + O\left(\|H_n\|^3\right)$, is proportional to the eigenvalue spacing of H and, therefore, should obey the same Wigner-Dyson distribution. The conjecture above is indeed well supported by our numerical analysis, even for n as small as 3 or 4: the distances characterizing the meshes with $L = 24$ and $L = 48$ obtained from the corresponding pseudogroups (Figures 3.5 and 3.6) follow the unitary Wigner-Dyson distribution.

From the figures 3.7, 3.8 and 3.9, one can see that also the distances from the target of the output braids of the algorithm at each iteration of the quantum hashing roughly follow the Wigner-Dyson distribution.

The elements of the meshes $\mathcal{S}(L,n)$ are of the form in Eq. (3.20) and this implies that, once we choose a pseudogroup $\tilde{\mathcal{I}}(L)$ whose average error $\bar{d}(L)$ is given by Eq. (3.15), the mean distance s_0 in (3.22) of the corresponding mesh from the identity is $s_0(L) \approx \sqrt{n+1}\,\bar{d}(L)$ as resulting from the sum of $n+1$ Gaussian terms.

At each iteration of the main processor, we increase the braid by $(n+1) = 4$ braid segments with length L_i. By doing that, we create 60^n braids and the main processor search, among them, the best approximation of the target. Therefore, the runtime is linear in the dimension of the meshes used and in the number of iterations. The unitary random matrix distribution implies that the mean deviation of the 4-segment braids from the identity (or any other in its vicinity) is a factor of $\sqrt{n+1}$ times larger than that of an individual segment. Considering the 3-dimensional nature of the unitary matrix space, we find that at each iteration the error (of the final braid to the target gate) is reduced, on average, by a factor of $f \sim 60^{n/3}/\sqrt{n+1} = 30$, where 60 is the number of elements in the icosahedral group. This has been confirmed in the numerical implementation and can be understood by evaluating the distribution obtained inserting the Wigner-Dyson probability density (3.2.2) in the equation (A.6), which approximates the probability distribution of the error of the best braid in the mesh considered (see Appendix A).

3.2.3 Hashing with the cubic group

For comparison, we also implemented the hashing procedure with the smaller cubic group. In this case the rotations in the group of the cube are 24; thus we choose $n = 4$ to generate a comparable number of elements in each mesh $\mathcal{S}(L,n)$. Our implementation of the hashing with the cubic group uses a preprocessor with $L_0 = 8$ and $m = 4$ and a single main processor with $L_1 = 24$ and $n = 4$. Approximating over 10000 random targets, we obtained an average error 7.09×10^{-4} after the main processor, comparable to 7.24×10^{-4} after the first iteration in the previous icosahedral group implementation. This result is consistent with the new reduction factor $f_{\text{cube}} = 24^{4/3}/\sqrt{5} \approx 30.96$. However we note that the cubic hashing is less efficient both in terms of the braid length (because it requires $n = 4$ instead of $n = 3$) and in terms of the runtime (because the time required for the searching algorithm is linear in the elements of $\mathcal{S}$ and $24^4 > 60^3$).

The comparison between the error distributions of the final braids for the icosahedral and cubic group is shown in Fig. 3.11. In particular one can notice that the standard deviation of the results is smaller for the cubic group, probably because of the smaller number of elements in the corresponding pseudogroups. The distribution for the icosahedral group is broader and presents a higher average error.

3.2.4 Tail correction

The choice of the proper L_i is important. We determine them by the average error before each iteration. If a certain L_i is too large, it generates a mesh around the

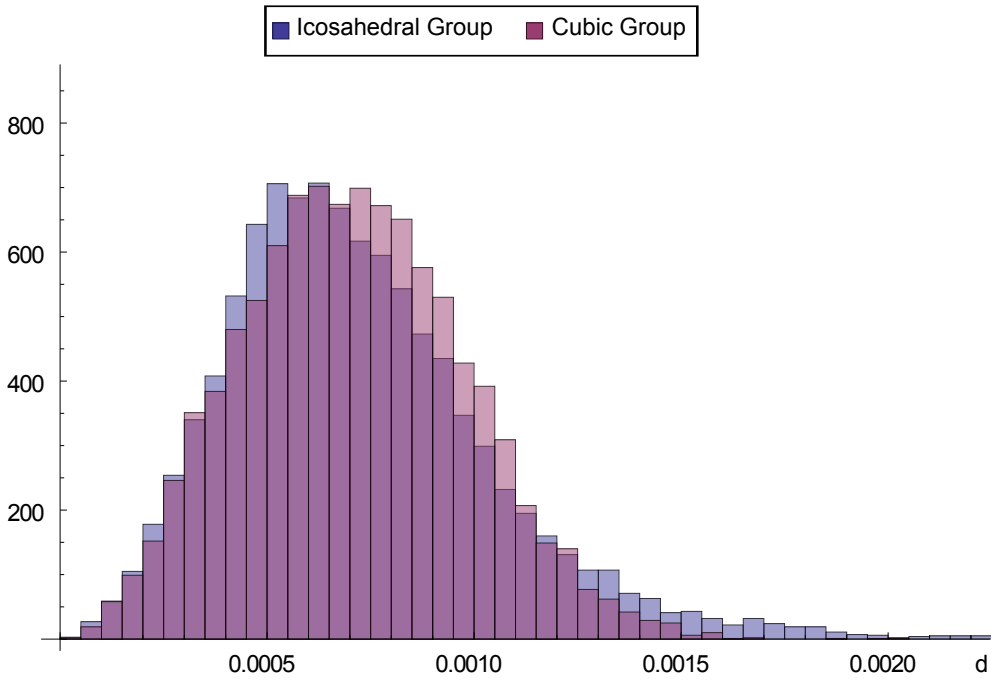

Figure 3.11: The results obtained with the first iteration of the main processor are illustrated for the icosahedral and cubic group and presents average errors of 7.24×10^{-4} and 7.09×10^{-4} respectively. The histograms are obtained with 10000 random targets and show that the error distribution for the icosahedral group is broader with a standard deviation of 3.36×10^{-4} to be compared with 2.69×10^{-4} for the cubic group.

identity that may be too small to correct the error relatively far from the identity, where the mesh is very fine. On the other hand, if L_i is too small, the mesh may be too sparse to correct efficiently. The former situation occurs exactly when we treat the braids with errors significantly larger than the average; they correspond to the rare events in the tail of the distributions as shown in Fig. 3.8 and 3.9. Such an already large error is then amplified with the fixed selection of $L_i = 24$, 44, and 68. To avoid this, one can correct the "rare" braids $\tilde{T}_{i-1}$, whose error is higher than a certain threshold, with a broader mesh [e.g., $\mathcal{S}(L_i - 4, n)$].

The tail correction is very efficient. If we correct for the 0.6% of the targets with the largest errors in the second iteration with $\mathcal{S}(40, 3)$ instead of $\mathcal{S}(44, 3)$, we reduce the average error by about 8% after the third iteration (see Table 3.2). The drastic improvement is due to the fact that once a braid is not properly corrected in the second iteration, the third one becomes ineffective. We can illustrate this situation with the example of the operator iY (where Y is the Pauli matrix): without tail correction it is approximated in the first iteration with an error of 0.0039, which is more than 5 times the average error expected. After the second iteration, we obtain an error of 4.3×10^{-4} (almost 20 times higher than the average value) and after the third the error becomes 2.0×10^{-4} (more than 200 times the

	Without tail correction		With tail correction	
10000 trials	Average Error	σ	Average Error	σ
Preprocessor*	0.027	0.010	0.027	0.010
Main, 1st iteration*	7.24×10^{-4}	3.36×10^{-4}	7.24×10^{-4}	3.36×10^{-4}
Main, 2nd iteration	2.29×10^{-5}	1.3×10^{-5}	2.28×10^{-5}	9.79×10^{-6}
Main, 3rd iteration	8.24×10^{-7}	5.6×10^{-6}	7.60×10^{-7}	3.27×10^{-7}

Table 3.2: Average error and standard deviation for the hashing algorithm after the preprocessor and the three iterations of the main processor. The outputs in absence or presence of a tail correction for the second and third iterations are shown (the asterisk indicates that the preprocessor and the first iteration are not affected by the tail correction). This correction is based on the pseudogroups with length 40 and 64 instead of the standard ones, 44 and 68. Only about the 0.6% of the targets used the tail correction in the second iteration, but one notice that the results, both in terms of average error and in terms of standard deviation σ, are extremely affected by these rare events.

mean value). If we use $\mathcal{S}(40,3)$ instead of $\mathcal{S}(44,3)$ in the second iteration we obtain an error 4.46×10^{-5}, with a shorter braid than before, and a final error of 1.31×10^{-6} which is less than twice the average error.

3.3 General efficiency of the algorithm

To evaluate the efficiency of the hashing algorithm it is useful to calculate the behaviour of the maximum length of the braids and of the runtime with respect to the average error obtained. We compare the results with those of the brute-force search (which gives the optimal braid length) and of the Solovay-Kitaev algorithm.

As described in Sec. 3.2.2, we reduce the average error at the i^{th} iteration to

$$\varepsilon_i \sim \varepsilon_{i-1}/f \qquad \text{with} \quad f \approx 30. \tag{3.23}$$

The total number of iterations (or *depth*) to achieve a final error of ε is then

$$M \sim \frac{\ln(1/\varepsilon)}{\ln f}, \tag{3.24}$$

so the expected error after each iteration is

$$\ln(1/\varepsilon_i) \sim i \ln f. \tag{3.25}$$

For efficient optimization, we choose the length L_i of the braid segments at the ith iteration to approximate the corresponding icosahedral group elements with an average error of ε_{i-1} (see discussions in Sec. 3.2.4). So we have, from Eq. (3.15),

$$L_i \sim \mathcal{L} \ln(1/\varepsilon_{i-1}) \tag{3.26}$$

with $\mathcal{L} \approx 6$ (see Eq. (3.15)) and the length of the braid we construct increases by $(n+1)L_i = 4L_i$ at the i-th iteration, i.e.,

$$L_i - L_{i-1} = 4\mathcal{L} \ln(1/\varepsilon_{i-1}) \sim 4\mathcal{L}(i-1) \ln f. \tag{3.27}$$

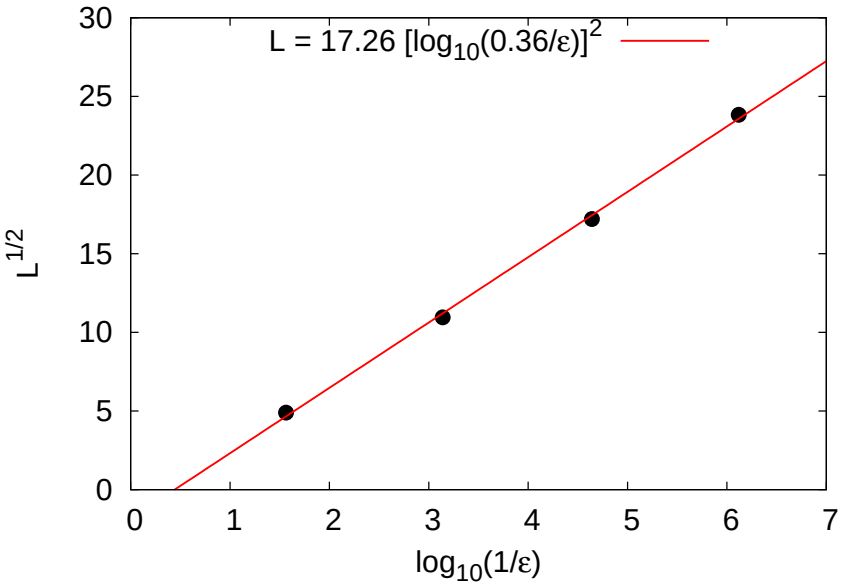

Figure 3.12: The scaling performance of the hashing algorithm in terms of the square root of the maximum length versus the logarithm of the inverse error. The error is the average error in approximating 10000 random targets after the preprocessor and the three iterations in the main processor. The results agree with the expected behaviour (Eqs. (3.29) and (3.30)).

Thus the total length of the braid with an error of ε is

$$L_M \sim \sum_{i=1}^{M} 4\mathcal{L}(i-1)\ln f \sim M^2. \tag{3.28}$$

The final results for the hashing algorithm are, therefore,

$$L_{\text{qh}} \sim \left(\ln\left(1/\varepsilon\right)\right)^2, \tag{3.29}$$

$$T_{\text{qh}} \sim M \sim \ln\left(1/\varepsilon\right). \tag{3.30}$$

We have explicitly confirmed that we can realize the perfect length-error scaling as shown in Fig. 3.12 up to three iterations in the main processor.

We can conclude that while no method beats the brute-force search in length, we achieve a respectable gain in time. Comparing these results with the length of the braids obtained by the Solovay-Kitaev algorithm in Eq. (3.3) and with its runtime in Eq. (3.4), the hashing algorithm gives results that are better than the Solovay-Kitaev results in terms of length and significantly better in terms of time.

3.4 Two-qubit gates and quantum hashing

So far we discussed only the case of single-qubit operators in SU(2), however such operators are essential also to define gates in SU(4) and, in particular, to decompose

the so-called controlled operators which are fundamental to generate entanglement in systems of two qubits.

There are several way to encode two qubits in a set of Fibonacci anyons and, in particular, six Fibonacci anyons with a trivial total topological charge span a Hilbert space of dimension five and are therefore enough to encode the four states of a pair of qubits. The most straightforward implementation of two qubits is, however, to simply double the single-qubit system used so far, adopting two quartets of Fibonacci anyons of the kind in Fig. 2.12 (a).

Among the different strategies studied to approximate two-qubit gates using braids of Fibonacci anyons [37, 39, 41], we are mainly interested in the decomposition of a controlled rotation in single-qubit blocks [42] which is naturally offered by topological quantum computation. In the usual logical basis, a controlled-gate assumes the form:

$$CR = e^{i\theta} \left[\begin{array}{cc|cc} 1 & 0 & 0 & 0 \\ 0 & 1 & 0 & 0 \\ \hline 0 & 0 & \multicolumn{2}{c}{\multirow{2}{*}{R}} \\ 0 & 0 & & \end{array}\right], \tag{3.31}$$

where θ is a general phase which has no role to our purpose and $R \in \mathrm{U}(2)$ is a single-qubit gate on the second qubit (the target qubit) which is applied only if the logic value of the first qubit (the control qubit) is 1. In topological quantum computation it is very intuitive to create a controlled-gate since the codification of the qubits we chose imply that moving one of the pairs of the control qubit (the control pair) around the pairs of anyons of the target qubit has a nontrivial effect only if the control qubit is in the state $|1\rangle$ so that the chosen pair has a nontrivial topological charge. Otherwise, if the control qubit is in the state $|0\rangle$, the control pair is in the vacuum sector and its braidings have no neat effect [37]. This procedure allows, essentially, to map two-qubit controlled-gate, in single-qubit phase shifts as shown in Fig. 3.13; in fact the weaves of the control pair A_2 around the pairs A_3 and A_4 in the target qubit result in the following controlled-phase gate:

$$CP = e^{i\theta} \left(\begin{array}{cc|cc} 1 & 0 & 0 & 0 \\ 0 & 1 & 0 & 0 \\ \hline 0 & 0 & 1 & 0 \\ 0 & 0 & 0 & e^{i(\alpha+\beta)} \end{array}\right) \tag{3.32}$$

since the only nontrivial effect is obtained when both the control pair and the pairs in the target qubit have a nontrivial topological charge. In this case all the pairs of the two qubits have charge 1 and thus, the system of eight anyons can be mapped in a single qubit of four anyons in the state $|0\rangle$ (Fig. 3.13 (a)). Therefore the operator CP can be implemented by a weave moving the whole control pair A_2 around the target pairs A_3 and A_4 (Fig. 3.13(b)), such that the corresponding single-qubit braid assumes the form:

$$P = e^{i\alpha} \begin{pmatrix} e^{i\beta} & 0 \\ 0 & e^{-i\beta} \end{pmatrix} \tag{3.33}$$

where $P \in \mathrm{U}(2)$ and its overall phase α plays an important role in the definition of the two-qubit gate CP [42].

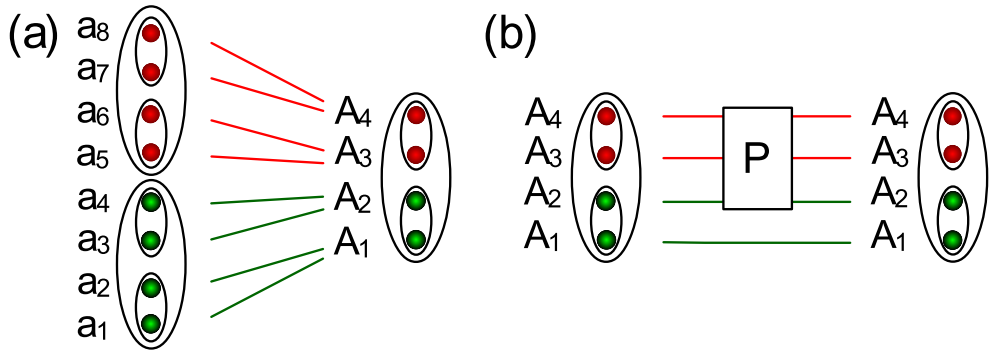

Figure 3.13: (a) Mapping two qubits (a_1-a_4 and a_5-a_8) into one qubit consisting of four composite anyons A_1-A_4. (b) Braid P of the composite anyons A_1 to A_4. As explained in the text the two-qubit controlled phase-shift CP can be built as a weave P of the control composite anyon A_2 around the target composite anyons A_3 and A_4. (Taken from [42]).

Let us consider now the two-qubit operator CR in (3.31). The corresponding single-qubit block R can be decomposed in the following form:

$$R = G \begin{pmatrix} 1 & 0 \\ 0 & e^{i\gamma} \end{pmatrix} G^{-1} e^{i\phi} \tag{3.34}$$

where $G = e^{i\theta_G}\hat{G}$ is a generic unitary operator in U(2) which can be decomposed into the single-qubit operator $\hat{G} \in \mathrm{SU}(2)$ with the form (3.5) and the phase θ_G which doesn't affect the two-qubit gate since it simplifies in the multiplication of G and G^{-1}. Therefore, to approximate a generic controlled rotation of the kind CR, one has to apply first the braid operator corresponding to G^{-1} to the target qubit, then one must weave the control pair around the target pairs following a braid that approximates the operator P in (3.33) with $\gamma = \alpha + \beta$, then the operator G must be applied to the target gate, and finally the control qubit must be braided in order to obtain a new phase operator P_1 such that:

$$P_1 = e^{i\theta_P} \begin{pmatrix} e^{-i\frac{\phi}{2}} & 0 \\ 0 & e^{i\frac{\phi}{2}} \end{pmatrix} \tag{3.35}$$

The total two-qubit gate obtained is:

$$CR = e^{i\left(\theta_P - \frac{\phi}{2}\right)} \left(\begin{array}{c|c} GG^{-1} = 1 & 0 \\ \hline 0 & R \end{array}\right) \tag{3.36}$$

which has the required form (3.31) up to an overall phase [42].

From Fig. 3.14 it is easy to see that the operator CR has been decomposed in the building blocks P, P_1, G and G^{-1}. Among these building blocks, P_1, G and G^{-1} are single-qubit gate whose overall phase is unimportant to the purpose of the final two-qubit computation, whereas the operator P acts on the effective single

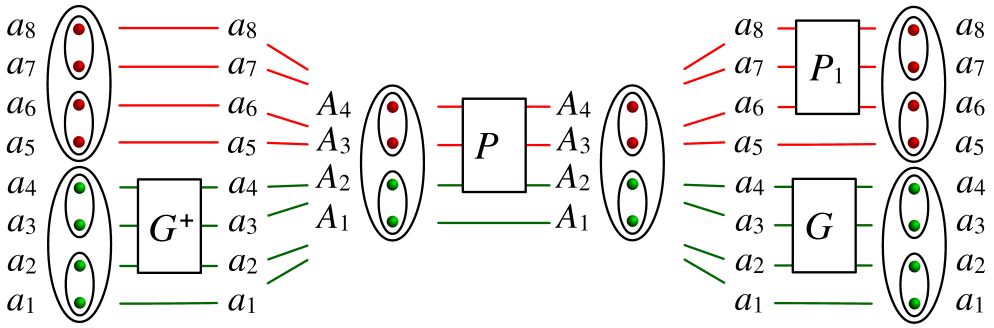

Figure 3.14: A scheme to realize a generic controlled-rotation gate in the Fibonacci anyon model. We consider two qubits composed of a_1-a_8. P, which realizes a two-qubit controlled-phase gate, is a braid acting on the effective single qubit formed by composite anyons A_1-A_4. G and P_1 are braids of single-qubit gates that modify the controlled-phase gate to a generic controlled-rotation gate. (Taken from [42]).

qubit formed by the pairs of the system qubits and its phase plays a determinant role.

Therefore the operators P_1, G and G^{-1} can be efficiently approximated by braids with the quantum hashing algorithm, since only their SU(2) component is important. The operator P in (3.33), instead, cannot be in general built through the quantum hashing. Considering also the overall phase associate to the single-qubit phase-gate P, in fact, the output weaves of the kind (3.8) obtained by the quantum hashing assume the form:

$$\tilde{P} = e^{in\frac{\pi}{5}}\hat{P}\,, \qquad \text{with} \quad \hat{P} \sim \begin{pmatrix} e^{i\gamma'} & 0 \\ 0 & e^{-i\gamma'} \end{pmatrix} \in \mathrm{SU}(2) \tag{3.37}$$

where n is the winding number of the weave of Fibonacci anyons, $n = \frac{1}{2}\sum_i q_i$, depending on the exponents q_i in (3.8). Therefore the direct application of the icosahedral quantum hashing is, in general, not sufficient to build controlled rotations, however it can be integrated with other techniques, such as the geometric decomposition of U(2) operators [42], to approximate with high accuracy controlled-gates with braids of Fibonacci anyons.

Nevertheless it is possible to think about other implementations of the hashing algorithm to approximate controlled operators: it could be possible to restrict the final output to braids having only the desired winding number in order to obtain the correct phase γ in (3.34) or it could be possible to completely change the approach and generalize the hashing procedure to the whole SU(4) space. To achieve this goal we should involve larger subgroups and pseudogroups to build meshes of braids that are effective in the two-qubit gate space. Even if the order of the subgroups required should be larger to build dense meshes in SU(4), the general structure of the algorithm doesn't change and can be applied also to the case of two qubits.

3.5 Concluding remarks

In this chapter we have demonstrated, for a generic universal topological quantum computer, that the iterative pseudogroup hashing algorithm allows an efficient search for a braid sequence that approximates an arbitrary given single-qubit gate. This can be generalized to the search for two-qubit gates as well. The algorithm applies to the quantum gate construction in a conventional quantum computer given a small universal gate set, or any other problems that involve realizing an arbitrary unitary rotation approximately by a sequence of "elementary" rotations.

The algorithm uses a set of pseudogroups based on the icosahedral group or other finite subgroups of SU(2), whose multiplication tables help generate, in a controllable fashion, smaller and smaller unitary rotations, which gradually (exponentially) reduce the distance between the result and the target. The iteration is in the same spirit as a generic renormalization group approach, which guarantees that the runtime of the algorithm is proportional to the logarithm of the inverse average final error $1/\varepsilon$; the total length of the braid is instead quadratic in $\ln(1/\varepsilon)$, and both the results are better than the Solovay-Kitaev algorithm introduced in textbooks.

We have explicitly demonstrated that the result from the performance analysis is in excellent agreement with that from our computer simulation. We also showed that the residual error distributes according to the Wigner-Dyson unitary ensemble of random matrices. The connection of the error distribution to random matrix theory ensures that we can efficiently carry out the algorithm and improve the rare cases in the distribution tail.

The overhead of the algorithm is that we need to prepare several sets of braid representations of the finite subgroup elements. Obtaining the longer representation can be time-consuming; but fortunately, we only need to compute them once and use the same sets of representations for all future searches.

Finally we considered the decomposition of SU(4) operators in terms of effective single-qubit gates which is possible in the topological quantum computation with Fibonacci anyons. The quantum hashing can improve the efficiency of the known decomposition schemes by obtaining accurate approximations of the SU(2) operators involved; however the hashing procedure cannot be directly applied to a target U(2) single-qubit gate if the corresponding overall phase cannot be neglected. Therefore an efficient extension of the quantum hashing to SU(4) gates is an open problem which, in principle, could be addressed by considering suitable subgroups of SU(4).

Chapter 4

Cold Atoms in non-Abelian Gauge Potentials

In the previous chapters we investigated problems involving the mathematical description of the anyons and their application to the field of quantum computation and information. Even if the presence of quantum Hall quasiparticles with non-Abelian braiding statistics has been predicted for a long time, so far, there is only a little experimental evidence of their existence and it is exclusively related to the Ising anyonic model [62].

The two most promising routes for the experimental studies of non-Abelian anyons seem to be the interferometric analysis of the $\nu = 5/2$ quantum Hall plateau and the new research field of quasi one-dimensional topological nanotubes, characterized by a strong intrinsic spin-orbit interaction, a proximity-induced s-wave pairing and an external magnetic field (see, for example, [50, 51]).

The quantum Hall setup, in principle, could offer the possibility of revealing different kinds of non-Abelian anyons exploring different plateaux. To exploit such excitations to the purpose of topologically protected quantum computation, however, there are some main issues that must be addressed. The first one is the problem of interaction among the quasiparticles and between quasiparticles and edges: from the first interferometric observations of non-Abelian anyons at $\nu = 5/2$, there are hints suggesting that such interactions cannot be neglected and lift the topological degeneracy of the ground states. If the topological states encoding the logical values of the qubits present different energies, they suffer from thermal decoherence and an eventual computation result to be spoiled. The second problem is the extreme difficulty in manipulating the position of quasiholes and quasiparticles, which are usually linked to impurities in the sample, resulting in an overwhelming complication in the realization of the braidings.

The study of topological semiconductor-superconductor heterostructures seems to be very promising for the detection of Majorana fermions and, therefore, Ising anyons. However they are limited to this non-universal anyonic model and it seems very difficult to engineer other kinds of non-Abelian anyons in these environments.

Given the extreme difficulty in the detection and, especially, in the control of non-Abelian anyons that characterize such systems, a significant issue, comple-

mentary with their study, consists in finding other experimental setups suitable to simulate the quantum Hall physics and realize non-Abelian anyons. With this respect, ultracold atomic systems provide a natural candidate [89], due to the possibility of using them as simulators of many-body systems [90]. Two essential (but in general not sufficient) ingredients are available in ultracold atomic systems.

First, one can simulate artificial magnetic fields by using rotating traps [44] or spatially dependent optical couplings between internal states of the atoms [91]; correspondingly, the possibility to have Laughlin states (with Abelian excitations) using strongly interacting, rapidly rotating two-dimensional ultracold Bose gases has been discussed in the literature, and it has been shown as well that incompressible vortex liquid states obtained for rotating ultracold bosons can be described by the Moore-Read wavefunction [92] (see the review [44]). Moreover a first experimental evidence of these strongly-correlated states has been produced for a set of a few ($N < 10$) atoms of ^{87}Rb loaded in time-modulated optical lattices [93].

The second ingredient, useful in the perspective to have ground states with non-Abelian excitations, is given by the possibility of trapping, both for ultracold bosons and fermions, two (or more) hyperfine levels of the same atomic species.

Combining the two ingredients, one may think to realize a system with two hyperfine levels, coupled between them and each one feeling a different artificial effective magnetic field. Several possible schemes have already been proposed in the literature to realize such *non-Abelian* gauge potentials, acting on the two (or more) components of an ultracold atomic gas (see the review [94]): in [64] laser fields couple three internal states with a fourth (the so-called tripod scheme), in such a way that for two degenerate dark states one can have a truly non-Abelian gauge potential. The extension of this scheme to the tetrapod setup has been recently discussed [95]. Another proposed scheme is based on laser assisted tunneling depending on the hyperfine levels to obtain U(2) vector potentials acting on ultracold atoms in optical lattices [96], while effective non-Abelian gauge potentials in cavity QED models have been recently addressed in [97]. Moreover these setups can be further generalized to obtain atoms with arbitrary pseudospins [98] subjected to SU(N) potentials. Several properties of ultracold atoms in artificial non-Abelian gauge potentials, including Landau levels and dynamical regimes, have been recently studied considering lattice systems [99, 100, 101, 102, 103, 104], free space [105, 106, 107, 108, 109, 3, 4], ring [110] or spherical geometry [111].

It is important to notice that translationally invariant SU(2) gauge potentials of the kind we will mainly consider in the following are equivalent to effective spin-orbit couplings between the orbital and pseudospin degrees of freedom of the atoms. In solid state physics such interaction is usually an intrinsic property of the material considered and it is crucial in the realization of topological insulators and superconductors. Recently there have been several studies to implement a spin-orbit coupling also in ultracold atomic gases: these systems may indeed provide the possibility to easily tune the spin-orbit coupling at different values and to allow new studies on topological phases of matter depending on this interaction. In particular it was experimentally shown that such interaction can be achieved in ^{87}Rb Bose-Einstein condensates where a pair of Raman lasers create a momentum-sensitive coupling between two internal atomic states [112, 113] which corresponds

to a U(1)×U(1) gauge potential; these experiments can be considered as a first step towards the realization of an artificial non-Abelian gauge potential.

Motivated by these experiments and theoretical proposals, the natural question is whether one can find non-Abelian anyons in such cold atom gases. Generally a non-Abelian gauge potential in the presence of strong interactions does not guarantee the non-Abelianity of the excitations; rather, deformed Laughlin states (characterized by Abelian quasiholes) appear. Recently, different kinds of anomalous quantum Hall effect for ultracold atomic gases in artificial gauge potential have been addressed [101, 102, 109, 103, 3]: in particular, in [102] it has been shown that a ultracold Fermi gas in a lattice subjected to a non-Abelian gauge field can present non-chiral and anomalous quantum Hall effects.

In the following section I will introduce the algebra of a single particle with a pseudospin 1/2 in a constant magnetic field in order to analyze the general feature of its spectrum in the presence of a non-Abelian SU(2) gauge potential independent of position, thus characterized by a constant Wilson loop [101]. We will show that there are only three classes of quadratic Hamiltonians, describing an atom in such effective U(2) gauge potential, that give rise to an analytically defined Landau level structure, where the eigenstates are expressed as a finite linear combination of the eigenstates of a particle in a magnetic field. The first class corresponds to an Abelian U(1)×U(1) gauge potential and it refers to uncoupled spin states, whereas the other two are characterized by a truly non-Abelian U(2) gauge potential and correspond to different kinds of Jaynes-Cummings models.

Section 4.2 will be devoted to the analysis of a U(2) gauge potential, characterized by both the presence of a fictitious magnetic field B, which breaks the time reversal symmetry, and a translationally invariant SU(2) potential which mixes the two inner states similarly to a spin-orbit coupling. Such potential can be engineered in a rotating gas of tripod atoms following the technique described in [64, 106, 107] and we will determine the parameters characterizing the Rabi frequencies necessary to obtain the correct dark states and potentials.

In Sec. 4.3 the single-particle problem will be mapped to the Jaynes-Cummings Hamiltonian following [3] and its spectrum, characterized by deformed Landau levels, will be determined. The problem will be further generalized to different gauge potentials.

Exploiting the mapping to the usual quantum Hall setup, in Sections 4.4, 4.5, 4.6 the strongly correlated states arising in the case of either bosonic gases subjected to strong intra-species interactions or free fermions are investigated in the non-degenerate regime, whereas in 4.7 the two-species quantum Hall states arising at the degeneracy points of the deformed Landau levels are studied [4]. Section 4.8 will be devoted to the analysis of the highest density state in the first degeneracy point and its anyonic excitations will be described.

Finally in Sec. 4.9 we will calculate the Haldane pseudopotentials related to the considered U(2) gauge potential, which are an essential tool for the study of more general interactions, and the example of weak inter-species contact repulsion will be shown in Sec. 4.10.

4.1 Single particle Hamiltonian and Landau levels

4.1.1 U(1) gauge potential

Let us first analyze the trivial case of a spinless atom moving on a plane and subjected to a fictitious magnetic field. This case corresponds to a U(1) gauge potential and will be useful to fix the notation used in the following. The minimal coupling Hamiltonian reads

$$H = (p_x + A_x)^2 + (p_y + A_y)^2 \tag{4.1}$$

where we chose units such that $\hbar = 1$ and $m = 1/2$. The effective charge of the atom is 1 and we can conveniently describe the vector potential $\vec{A}$ in the symmetric gauge in terms of the artificial magnetic field B perpendicular to the plane:

$$A_x = -\frac{B}{2}y\,, \qquad A_y = \frac{B}{2}x. \tag{4.2}$$

To analyze this system it is helpful to introduce the complex coordinate $z \equiv x - iy$ which allows us to easily define the following single-particle operators:

$$D = \frac{1}{2\sqrt{2B}}\left(Bz + 4\partial_{\bar{z}}\right), \qquad D^\dagger = \frac{1}{2\sqrt{2B}}\left(B\bar{z} - 4\partial_z\right) \tag{4.3}$$

$$L = \frac{1}{2\sqrt{2B}}\left(Bz - 4\partial_{\bar{z}}\right), \qquad L^\dagger = \frac{1}{2\sqrt{2B}}\left(B\bar{z} + 4\partial_z\right). \tag{4.4}$$

These operators generate the observable algebra of the system and are characterized by the commutation rules:

$$\left[D, D^\dagger\right] = 1\,, \qquad \left[L^\dagger, L\right] = 1\,, \qquad \left[L^\sharp, D^\natural\right] = 0. \tag{4.5}$$

where $L^\sharp$ labels either L or $L^\dagger$ and $D^\natural$ labels either D or $D^\dagger$. D and $D^\dagger$ can be considered as ladder operators and allow us to express the Hamiltonian in the form of a harmonic oscillator $H = 2B\left(D^\dagger D + 1/2\right)$. The operators L and $L^\dagger$ enter the definition of the angular momentum of the particle:

$$L_z = D^\dagger D - LL^\dagger \tag{4.6}$$

such that L and $L^\dagger$ respectively decrease and increase L_z.

Since the Hamiltonian commutes both with L and $L^\dagger$, each energy eigenstate is degenerate with respect to the angular momentum; therefore, it is possible to define the usual Landau levels characterized by the index $n = D^\dagger D$. In particular the existence of the Landau levels and their angular momentum degeneracy play a crucial role in the definition of all the quantum Hall states characterizing systems of interacting spinless atoms (see [44] for a review).

In order to maintain the angular momentum degeneracy of the eigenstates, a generic Hamiltonian H for a spinless atom must be independent of the operators L and $L^\dagger$. Imposing this Hamiltonian to be at most quadratic in momentum we obtain that H can be written as a function of the operators D and $D^\dagger$:

$$\frac{H}{E'} = D^\dagger D + aD^\dagger + a^* D + bD^{\dagger 2} + b^* D^2 + \mathcal{K}' \tag{4.7}$$

where E' is an overall energy scale, $\mathcal{K}'$ is a real parameter, and a and b are complex coefficients. It is easy to show that the Hamiltonian (4.7) can be recast in the following form:

$$H = E\,\Gamma^\dagger\Gamma + \mathcal{K}, \tag{4.8}$$

where the operators Γ and $\Gamma^\dagger$ are defined as

$$\Gamma = \frac{1}{2}\left(\alpha + \frac{1}{\alpha^*}\right) D + \frac{1}{2}\left(\alpha - \frac{1}{\alpha^*}\right) D^\dagger + \beta \tag{4.9}$$

$$\Gamma^\dagger = \frac{1}{2}\left(\alpha^* + \frac{1}{\alpha}\right) D^\dagger + \frac{1}{2}\left(\alpha^* - \frac{1}{\alpha}\right) D + \beta^* \tag{4.10}$$

in order to satisfy the commutation relation $\left[\Gamma, \Gamma^\dagger\right] = 1$, with the complex parameters α and β related to the coefficients in (4.7). The operators $\Gamma, \Gamma^\dagger$ allow us to redefine the algebra to express the Hamiltonian in the simple quadratic form (4.8), which highlights the Landau level structure of the single-particle problem. It is interesting to notice that the mapping from $D, D^\dagger$ to $\Gamma, \Gamma^\dagger$ corresponds to an affine transformation of the space coordinates of the kind:

$$z \to z' = \alpha x - \frac{i}{\alpha^*} y + \sqrt{\frac{8}{B}}\beta = \frac{1}{2}\left(\alpha + \frac{1}{\alpha^*}\right) z + \frac{1}{2}\left(\alpha - \frac{1}{\alpha^*}\right) \bar{z} + \sqrt{\frac{8}{B}}\beta. \tag{4.11}$$

4.1.2 U(1) × U(1) gauge potential

The main purpose of this chapter is to study systems of atoms characterized by a pseudospin degree of freedom (hereafter denoted simply as spin) that can assume the eigenstates $|\uparrow\rangle$ and $|\downarrow\rangle$ on the $\hat{z}$ direction. Therefore, in the above description of the single particle system, it is necessary to introduce also the Pauli matrices $\vec{\sigma}$ to complete the observable algebra generated by $D, D^\dagger, L$ and $L^\dagger$. The Pauli matrices σ_x and σ_y couple the two spin components, whereas σ_z and the 2×2 identity matrix $\mathbb{I}$ allow us to describe particles whose states $|\uparrow\rangle$ and $|\downarrow\rangle$ are decoupled. More generally, to describe a system characterized by a U(1)×U(1) symmetry corresponding to two decoupled states in the same magnetic field B, the Hamiltonian must be a function of the operators $D, D^\dagger, \mathbb{I}$ and a single linear combination of Pauli matrices, $\hat{k} \cdot \vec{\sigma}$, that we can relabel as σ_z without loss of generality.

This generic problem is defined by the Hamiltonian:

$$\begin{aligned} H = {} & (a_z\sigma_z + a_0)\, D^\dagger + (a_z^*\sigma_z + a_0^*)\, D + \\ & + (b_z\sigma_z + b_0)\, D^{\dagger 2} + (b_z^*\sigma + b_0^*)\, D^2 + \left(h_z'\sigma_z + h_0'\right) D^\dagger D + \mathcal{M}'\sigma_z + \mathcal{K}'. \end{aligned} \tag{4.12}$$

Such a Hamiltonian describes a particle in the uniform magnetic field B and is the most general one which is quadratic in momentum, fulfills the U(1)×U(1) gauge symmetry and is independent of angular momentum. It constitutes a simple generalization of the Hamiltonian (4.7) to two non-interacting spin components; thus, it can be solved by implementing two different coordinate transformations of the kind (4.11) for the two inner states.

It is helpful to notice that a unitary transformation of the kind:

$$U\psi = e^{-i\sigma_z(i\alpha\bar{z}-i\alpha^* z)}\psi \tag{4.13}$$

modifies the operators D and $D^\dagger$ in the following form:

$$D \to U^\dagger D U = D + \sqrt{\frac{2}{B}}\,\alpha\sigma_z\,, \qquad D^\dagger \to U^\dagger D^\dagger U = D^\dagger + \sqrt{\frac{2}{B}}\,\alpha^*\sigma_z. \tag{4.14}$$

This unitary transformation, combined with the real-space affine transformations (4.11), allows us to define the operators:

$$\Gamma = (\alpha_0 + \alpha_1\sigma_z)\,D + (\beta_0 + \beta_1\sigma_z)\,D^\dagger + \gamma_0 + \gamma_1\sigma_z \tag{4.15}$$

$$\Gamma^\dagger = (\alpha_0^* + \alpha_1^*\sigma_z)\,D^\dagger + (\beta_0^* + \beta_1^*\sigma_z)\,D + \gamma_0^* + \gamma_1^*\sigma_z \tag{4.16}$$

with the parameters chosen in order to satisfy the commutation relation $[\Gamma, \Gamma^\dagger] = 1$. With an adequate choice of the operators Γ and $\Gamma^\dagger$, the Hamiltonian (4.12) can be rewritten in the form:

$$H_a = \Gamma^\dagger\Gamma\,(h_0\mathbb{I} + h_z\sigma_z) + \mathcal{M}\sigma_z + \mathcal{K}, \tag{4.17}$$

with $h_0, h_z, \mathcal{M}$ and $\mathcal{K}$ being real parameters. Therefore every single particle Hamiltonian of the kind (4.12) can be recast in the form (4.17) with suitable transformations. H_a highlights the existence of a quantum number $n = \Gamma^\dagger\Gamma$, which defines the Landau level structure.

For an atom described by H_a, both the spin σ_z and the angular momentum L_z are proper quantum numbers and $\mathcal{M}$ constitutes a Zeeman term. Thus, the spectrum of the Hamiltonian is characterized by the presence of Landau levels, degenerate with respect to L_z and labeled by both σ_z and $n = \Gamma^\dagger\Gamma$. However, it is important to notice that the form of the operator n is not so trivial starting from the original operators D and $D^\dagger$. Finally, if h_z and $\mathcal{M}$ go to zero, all the Landau levels also become degenerate with respect to spin.

The main characteristic of the Hamiltonian H_a is the fact that it does not depend on σ_x and σ_y, therefore it corresponds to a gauge symmetry U(1)×U(1) and we will refer to this case as the Abelian limit.

4.1.3 U(2) gauge potential

The aim of this work is to describe systems of two-component cold atoms suitable to simulate the quantum Hall physics and some of the corresponding many-particle states. To reach this goal we will deal in the following with atoms subjected both to an artificial magnetic field and to an effective uniform SU(2) non-Abelian gauge potential simulating a spin-orbit coupling. Even if in the next section we will analyze a particular case of such potentials, here we want to show that the Hamiltonian we will study is representative of a much more general class of physical single-particle systems that are characterized by the following properties:

$\mathcal{P}1$: Their energy spectrum presents a genuine Landau level structure;

$\mathcal{P}2$: Every Landau level is degenerate with respect to the angular momentum L_z;

$\mathcal{P}3$: In the Abelian limit, the Landau levels become degenerate with respect of the spin degree of freedom.

These conditions guarantee the existence of proper Landau levels, although they can be deformed by spin-orbit interactions and, in general, by the couplings between the pseudospin eigenstates; therefore we want to identify what are the Hamiltonians that fulfill these conditions which are necessary to the realization of quantum Hall states. However, as we will discuss in 4.1.4, these properties could result quite restrictive for the description of particular phenomena such as the quantum spin Hall effect [114]; nevertheless, they provide a solid base for the description of the quantum Hall states we will address in this chapter.

To obtain the most general Hamiltonians satisfying the conditions $\mathcal{P}1$ - $\mathcal{P}3$ let us analyze them in the light of the single-particle algebra previously defined. Condition $\mathcal{P}2$ implies that the spectrum of the Hamiltonian must be degenerate with respect to the angular momentum L_z. Therefore one obtains $[H, L] = \left[H, L^\dagger\right] = 0$ and the Hamiltonian shall not depend on L and $L^\dagger$ but only on $D, D^\dagger, \vec{\sigma}$.

Condition $\mathcal{P}1$ about the existence of the Landau levels is quite general: it is indeed known that, for a broad class of spin-orbit interactions, the spectrum of the single-particle Hamiltonian is composed by eigenstates expressed as infinite series [115]. Instead, in this work, we would like to deal with analytically determined Landau levels such that the corresponding wavefunctions can be expressed as a finite sum of terms; this restriction corresponds, as we later discuss, to looking for an integral of motion that corresponds to the Landau level index and satisfies suitable commutation relations, as illustrated by the equations (4.20) given below.

As in the previous case (4.12), spin-orbit couplings can give rise, in general, to terms in the Hamiltonian that are not proportional to $D^\dagger D$. Therefore it is necessary to introduce a wider class of ladder operators Γ and $\Gamma^\dagger$ that generalize the operators D and $D^\dagger$ previously introduced (see [115] for an accurate description based on the Landau gauge). Condition $\mathcal{P}1$ can be rephrased in terms of these generalized ladder operators imposing that there must exist an integral of motion n characterized by:

$$[H, n] = 0 \tag{4.18}$$

$$\left[n, \Gamma^\dagger\right] = \Gamma^\dagger \tag{4.19}$$

$$[n, \Gamma] = -\Gamma \tag{4.20}$$

where Γ and $\Gamma^\dagger$ fulfill the following commutation properties

$$\left[\Gamma, \Gamma^\dagger\right] = 1 \qquad \left[L^\sharp, \Gamma^\natural\right] = 0 \tag{4.21}$$

and such that there exists an eigenstate Ψ_0 of Γ with eigenvalue 0: $\Gamma\Psi_0 = 0$. Γ and $\Gamma^\dagger$ are defined as linear combination of D and $D^\dagger$ plus, eventually, some constant terms. For example we could consider the operator $\Gamma = D + \beta'$ corresponding to a translation $z \to z - \beta$. It can be easily shown that these operators give rise,

in general, to a Landau level structure starting from the coherent state $\Psi_{0,\zeta} = e^{-\frac{B}{4}(z+\beta)(\bar{z}+\bar{\zeta})}$ for every value of the parameter ζ. In particular, if we choose $\beta = \zeta$, this structure constitutes just a translation of the one obtained from D and $D^\dagger$ we will exploit in the next sections.

The role of the integral of motion n is to label the generalized Landau levels obtained from the couplings between the pseudospin states. To satisfy (4.19) and (4.20), n must be in the form:

$$n = \Gamma^\dagger \Gamma + \vec{c} \cdot \vec{\sigma} \tag{4.22}$$

where $\vec{c}$ is a real vector that we want to determine.

Unlike the previous ones, the condition $\mathcal{P}3$ is not strictly necessary to obtain a proper Landau level structure, however it is necessary to implement the U(2) gauge symmetry which characterizes the Hamiltonian we will investigate in the following sections. In general, terms such as the ones in h_z and $\mathcal{M}$ in (4.17) break this symmetry and do not satisfy the condition $\mathcal{P}3$. Nevertheless they do not spoil the main characteristics of the system we will study in section 4.3 and can easily be taken into account in the following analysis.

Let us define the most general single-particle hermitian Hamiltonian, satisfying the previous conditions, with the constraint that it can be at most quadratic in the momentum $\vec{p}$ and, therefore, in the operators D and $D^\dagger$. For the sake of simplicity we divide the Hamiltonian into two terms: the first one, H_a, corresponds to the previously described Abelian limit with gauge symmetry U(1)×U(1), which represents the case of uncoupled spin components:

$$H_a = (h_0 + h_z \sigma_z)\, D^\dagger D + \mathcal{M}_z \sigma_z + \mathcal{K} \tag{4.23}$$

The second term is instead the non-Abelian contribution H_{na}:

$$H_{na} = (\vec{a} \cdot \vec{\sigma} + a_0)\, D^\dagger + \left(\vec{a^*} \cdot \vec{\sigma} + a_0^*\right) D + \left(\vec{b} \cdot \vec{\sigma} + b_0\right) D^{\dagger 2} + \left(\vec{b^*} \cdot \vec{\sigma} + b_0^*\right) D^2 + \\ + (h_x \sigma_x + h_y \sigma_y)\, D^\dagger D + \mathcal{M}_x \sigma_x + \mathcal{M}_y \sigma_y \tag{4.24}$$

where $\vec{\mathcal{M}}$ is a real vector, $\mathcal{K}$ is real constant; h^μ is a real vector with spacial part $\vec{h}$; and a^μ and b^μ are complex vectors with spacial parts $\vec{a}$ and $\vec{b}$. The total Hamiltonian can be expressed as the sum $H = H_a + H_{na}$.

First of all we must observe that, if the following conditions are satisfied:

- $\vec{a} = e^{i\theta_a} \vec{a_R}$, with $\vec{a_R}$ a real vector and θ_a a real constant;
- $\vec{b} = e^{i\theta_b} \vec{b_R}$, with $\vec{b_R}$ a real vector and θ_b a real constant;
- all the vectors $\vec{\mathcal{M}}, \vec{h}, \vec{b_R}$ and $\vec{a_R}$ are parallel to each other along the direction $\hat{k}$;

then the Hamiltonian can be reduced to the U(1)×U(1) case (4.12) previously studied through proper transformations. In this case we have shown that there is a Landau level operator $n = \Gamma^\dagger \Gamma$ that commutes with the Hamiltonian. The

previous conditions imply that the system isn't characterized by a proper U(2) gauge potential since only one effective component of the spin, $\hat{k}\cdot\vec{\sigma}$, enters the Hamiltonian.

In the generic U(2) case with arbitrary vectors $\vec{a}$ and $\vec{b}$, instead, it is impossible to gauge away all the terms in $\vec{a}\cdot\vec{\sigma}$; therefore, in general, it is not possible to reduce the spin terms in the previous Hamiltonian to simpler ones and it is convenient to search for an integral of motion n defined in terms of the D operators as $n = D^\dagger D + \vec{c}\cdot\vec{\sigma}$; in order to satisfy the relation $[H, n] = 0$, we obtain from the commutation rules the following conditions:

$$\epsilon^{lmn} h_l c_m = \epsilon^{lmn} \mathcal{M}_l c_m = 0 \tag{4.25}$$

$$-a_n + 2i\epsilon^{lmn} a_l c_m = 0\,, \qquad a_n^* + 2i\epsilon^{lmn} a_l^* c_m = 0\,, \qquad a_0 = 0 \tag{4.26}$$

$$-2b_n + 2i\epsilon^{lmn} b_l c_m = 0\,, \qquad 2b_n^* + 2i\epsilon^{lmn} b_l^* c_m = 0\,, \qquad b_0 = 0 \tag{4.27}$$

Equation (4.25) requires that the vectors $\vec{h}, \vec{\mathcal{M}}$ and $\vec{c}$ must be parallel, therefore, without loss of generality, we can impose them to be in the $\hat{z}$ direction with an appropriate spin rotation, and $\vec{c}$ assumes the form $(0, 0, c_z)$. The equations (4.26) and (4.27) are not compatible in general, unless either $\vec{a}$ or $\vec{b}$ is zero. Let us consider the equation (4.26): after imposing $a_0 = 0$ and $b_0 = 0$ through transformations of the kind (4.9,4.10), (4.26) can be recast in the following form:

$$\Im\left(\vec{a}\right) = 2\Re\left(\vec{a}\right) \times \vec{c} \tag{4.28}$$

$$\Re\left(\vec{a}\right) = -2\Im\left(\vec{a}\right) \times \vec{c} \tag{4.29}$$

We have decomposed the complex $\vec{a}$ into its real and imaginary parts and the previous equations state that they must be orthogonal to each other and orthogonal to $\vec{c}$. Therefore the condition (4.18) implies, for the case $\vec{b} = 0$, that $\vec{a}$ must lie in the system plane and, moreover, that $|c_z| = 1/2$ in order to satisfy (4.28) and (4.29). Without loss of generality we can choose a proper spin basis and obtain:

$$\vec{a} = (iq/2, q/2, 0)\,, \qquad \vec{c} = (0, 0, 1/2) \tag{4.30}$$

Similarly one can consider the case in which $\vec{a} = 0$: to satisfy the equation (4.27), $\vec{b}$ must lie in the system plane and $\Re(\vec{b}) \perp \Im(\vec{b})$ with $|c_z| = 1$ (which is incompatible with the previous case).

So far we considered conditions $\mathcal{P}1$ and $\mathcal{P}2$ and we obtained, in the general U(2) case, that there are two possible Hamiltonian classes defined by $\vec{b} = 0$ and $\vec{a} = 0$; the transformations (4.9,4.10) required to obtain $a_0 = 0$ and $b_0 = 0$ imply that the Landau level operator n has the general form (4.22) in terms of certain operators Γ and $\Gamma^\dagger$. For the sake of simplicity, we hereafter restrict ourself to the case $\Gamma = D$ and $\Gamma^\dagger = D^\dagger$, since all the other cases can be studied through a change of the space coordinates (4.11); therefore we will deal with generalized Landau levels expressed as a finite sum of the eigenstates of $D^\dagger D$. In this case we are reducing the previous Hamiltonians to the following classes:

- The Jaynes-Cummings class, obtained by imposing $\vec{b} = 0$, whose Hamiltonian reads:

$$H = \left(E + h_z\sigma_z\right) D^\dagger D + \mathcal{M}_z\sigma_z + \mathcal{K} - iq\sigma_+ D + iq\sigma_- D^\dagger \tag{4.31}$$

where $\sigma_\pm = \sigma_x \pm i\sigma_y$. In the limit $h_z, \mathcal{M}_z \to 0$ this Hamiltonian satisfies also the condition $\mathcal{P}3$ and is characterized by a full U(2) gauge symmetry. Moreover, it can be shown that the Hamiltonian (4.31) is gauge equivalent to both a pure Rashba spin-orbit coupling and a pure Dresselhaus interaction. This case will be extensively discussed in the next sections, where we will show that it can be described in terms of a minimal coupling with a non-Abelian gauge potential.

- The two-photon Jaynes-Cummings class, obtained by imposing $\vec{a} = 0$, which corresponds to:

$$H = (E + h_z\sigma_z)\, D^\dagger D + \mathcal{M}_z\sigma_z + \mathcal{K} - iq\sigma_+ D^2 + iq\sigma_- D^{\dagger 2} \tag{4.32}$$

This Hamiltonian cannot be described by a quadratic minimal coupling with a non-Abelian gauge potential since it presents the product between quadratic terms in D and $D^\dagger$ and the σ matrices. However it can be exactly solved [116, 117], showing a Landau level structure. Also in this case the condition $\mathcal{P}3$ is satisfied in the limit $h_z, \mathcal{M}_z \to 0$.

To summarize, up to transformations of the spin basis, there are only three classes of Hamiltonians, quadratic in the momentum, that satisfy the conditions $\mathcal{P}1$ and $\mathcal{P}2$ and can be described by generic ladder operators Γ and $\Gamma^\dagger$. The first one is the Abelian class with a U(1)×U(1) gauge symmetry (4.17). The other two are characterized by a full U(2) gauge potential and correspond to different Jaynes-Cummings models. In particular we will restrict ourselves to the case in which Γ and $\Gamma^\dagger$ correspond to D and $D^\dagger$ and we will focus, in the following sections, on the class (4.31) in the limit of U(2) gauge symmetry, fulfilling also the condition $\mathcal{P}3$.

4.1.4 Constant magnetic field

So far we required that the analyzed system is characterized by both a uniform magnetic field B and a translationally invariant SU(2) gauge potential component. To understand the implications of the second hypothesis and its relation with the conditions $\mathcal{P}1$, $\mathcal{P}2$ and $\mathcal{P}3$, it is worth to investigate the properties of a generic U(2) gauge potential $\vec{A}$.

Let us consider the 2×2 minimal coupling Hamiltonian $H = \left(\vec{p}\mathbb{I} + \vec{A}\right)^2$, in the non-Abelian case the corresponding 2×2 magnetic field reads:

$$\vec{\mathcal{B}} = \vec{\nabla} \times \vec{A} + i\vec{A} \times \vec{A} \tag{4.33}$$

so that the magnetic field can arise in two different ways, corresponding to the two different terms in the right-hand side of the equation. From this observation Coleman first suggested that there are only two gauge-inequivalent classes of SU(2) gauge potentials producing a uniform magnetic field, as explained in [118] (see also the discussion in [111]):

1. A commuting field with linear potential $\vec{A} = \frac{1}{2}\vec{\mathcal{B}} \times \vec{r}$ where $\vec{\mathcal{B}}$ is the 2×2 uniform magnetic field and $\vec{r}$ is the position vector. This case can be considered Abelian in nature, since the components of $\vec{A}$ commute and correspond

to an effective U(1)×U(1) gauge; only the first term in (4.33) contributes to the field strength and, considering a magnetic field along $\hat{z}$, the potential $\vec{A}$ can be recast in the symmetric gauge:

$$\vec{A} = \frac{B}{2}\sigma_z\,(-y, x, 0) \;\Rightarrow\; \mathcal{B}_z = B\sigma_z \tag{4.34}$$

2. A uniform non-commuting potential of the kind $\vec{A} = q\,(\sigma_x, \sigma_y, 0)$ such that $\vec{\mathcal{B}} = i\vec{A}\times\vec{A} = -2q^2\sigma_z\hat{z}$. This corresponds to a truly SU(2) potential.

The first case of U(1)×U(1) potential linear in space, however, does not fulfill the condition $\mathcal{P}2$, since the coordinates x and y can be expressed as a linear combination of both the operators $D, D^\dagger$ and the operators $L, L^\dagger$. Therefore a Hamiltonian involving such space-dependent SU(2) gauge potential cannot be expressed neither as the Hamiltonian (4.12) nor as the Hamiltonian (4.23,4.24). Hence a potential of the kind (4.34) doesn't satisfy our definition of proper Landau levels corresponding to the condition $\mathcal{P}1$ and $\mathcal{P}2$. However such conditions can result too restrictive for a broad class of topological systems such as the quantum spin Hall effect [114]. This phenomenon is described by a Hamiltonian showing a potential equivalent to (4.34) which presents a double Landau level structure, corresponding to the two pseudospin states subjected to an opposite magnetic field. In this case, however, the Landau levels are generated by the operators D and $D^\dagger$ for $|\uparrow\rangle$ states and by the operators L and $L^\dagger$ for $|\downarrow\rangle$ states; so that, in general, the spectrum depends on the angular momentum and violates $\mathcal{P}2$.

In this work we will exclude the case of U(1)×U(1) potentials linear in the position and we will deal only with the second class of SU(2) potentials generating a uniform magnetic field. As we will see, this non-Abelian potential combined with a usual Abelian magnetic field, gives rise to systems in the universality class of the quantum Hall effect, that breaks the time reversal invariance. A generalization of this work in order to include the quantum spin Hall effect could be the base for future works.

4.2 Engineering the Non-Abelian Gauge Potential

It has been proved that a rich number of different physical systems can mimic the presence of an external and classical non–Abelian gauge field in a bidimensional ultracold gas. For instance, Lewenstein et al. established a method to obtain U(2) vector potentials acting on cold atoms in optical lattices with a laser assisted tunneling that depends on the hyperfine levels [96]; but it is possible to obtain similar effects also with atoms characterized by a tripod electronic structure [64, 106] subjected to optical couplings, in spin-orbit-coupled Bose-Einstein condensates [108] or in cavity QED models [97]. All these kinds of systems can be described in terms of a gas of particles with an internal degree of freedom (*spin*) subjected to an effective external non–Abelian vector potential that acts on the corresponding two–state Hilbert spaces (see [94] and references therein for more detail).

In [107] Santos et al. analyze with a first order perturbation theory the deformation of Landau levels of a gas in a potential described by a Landau–like

non-Abelian gauge; moreover, in the last years, different kinds of anomalous quantum Hall effect in cold atomic gases have been addressed: in [101] Goldman et al. investigate the fundamental properties of a ultracold Fermi gas trapped in an optical lattice with a non-Abelian gauge potential characterized by a constant Wilson loop whereas in [102] the authors study the features of a Fermi gas in a relativistic regime subjected to an anisotropic non–Abelian field.

In this chapter we analyze the behaviour of a bidimensional gas of ultracold atoms under a fictitious U(2) potential composed by both an effective magnetic term and a uniform optically induced non-Abelian component. In particular, we will study the following non-relativistic minimal coupling Hamiltonian (here and in the following we will choose units such that the atom mass is $m = 1/2$ and $\hbar = 1$):

$$H = (p_x + A_x)^2 + (p_y + A_y)^2 \tag{4.35}$$

where A_x and A_y are 2×2 matrices coupling the two pseudospin inner states:

$$A_x = q\sigma_x - \frac{B}{2} y \mathbb{I}\,, \qquad A_y = q\sigma_y + \frac{B}{2} x \mathbb{I}\,; \tag{4.36}$$

(the identity matrix $\mathbb{I}$ will be dropped in the following). The vector potential $\vec{A}$ is constituted by a SU(2) term proportional to the parameter q, which corresponds to the second class of SU(2) potentials mentioned in 4.1.4, and by a magnetic contribution (B represents a fictitious magnetic field orthogonal to the system). Therefore $\vec{A}$ describes a proper U(2) potential whose total effective magnetic field is

$$\mathcal{B} = \nabla \times \vec{A} + i\vec{A} \times \vec{A} = \begin{pmatrix} B - 2q^2 & 0 \\ 0 & B + 2q^2 \end{pmatrix} \tag{4.37}$$

where $\mathcal{B}$ is proportional to the commutator of the covariant derivatives. It is important to notice that $\mathcal{B}$ does not depend on the position and the system is characterized by a translationally invariant Wilson loop as in the cases analyzed in [101]. As we will see in the next section, the Hamiltonian (4.35) satisfies the three conditions in section 4.1.3 and it is representative of the first class (4.31) of Hamiltonians previously considered. Moreover the non-Abelian term of (4.36) mimics the effect of a spin-orbit coupling and it can be shown to be gauge equivalent both to the Dresselhaus and to the Rashba coupling.

It is well known that the effect of a constant magnetic field can be reproduced in a rotating frame thanks to the Coriolis force (see, for example, the review [44]); instead, the SU(2) contribution can be obtained through proper optical couplings in a system of atoms showing quasi-degenerate ground states as described in [64, 106, 94]. Therefore, to engineer the effective gauge potential $\vec{A}(q)$ (4.36), we will consider a rotating system of the so-called tripod atoms whose coupling is described in [64] and depends on the Rabi frequencies Ω_i:

$$\Omega_1 = \Omega \sin(\theta) \cos(\phi)\, e^{iS_1}\,, \quad \Omega_2 = \Omega \sin(\theta) \sin(\phi)\, e^{iS_2}\,, \quad \Omega_3 = \Omega \cos(\theta)\, e^{iS_3} \tag{4.38}$$

where S_1 and S_2 are functions of the position and of the parameter q whereas the angles ϕ and θ and S_3 are chosen constants. These frequencies describe the couplings of three quasi-degenerate ground states, constituted by different hyperfine

levels, with an excited state. This interaction gives rise to two different dark states whose dynamics is described by the effective Hamiltonian (4.35). Such dark states constitute the different pseudospin component coupled by the non-Abelian terms in H and will be identified hereafter as $|\uparrow\rangle$ and $|\downarrow\rangle$.

We observe that in deriving Equation (4.35), we are making the assumption that the dark states of the tripod scheme [64] are unaffected by the rotation: a more careful analysis would require us to consider the whole four-states space in the presence of rotation and to derive the effective Hamiltonian for the dark states in the rotating frame. A careful derivation of the effective Hamiltonian in a rotating tripod scheme is contained in [119].

In the following we will calculate the dependence of the Rabi frequencies Ω_i on q to obtain, through a proper gauge transformation, the Hamiltonian (4.35) for the atomic gas in a rotating frame.

Let us consider first a system of tripod atoms in an inertial frame of reference characterized by a non-Abelian gauge potential $\tilde{A}$, a scalar potential $V_{\rm rot} \equiv \Phi(\tilde{A}) + V$ as described in [64] and a harmonic confining potential $\omega r^2/4$. The corresponding Hamiltonian reads:

$$H_{\rm IF} = \left(\vec{p} + \vec{\tilde{A}}\right)^2 + \frac{1}{4}\omega^2 r^2 + V_{\rm rot} \tag{4.39}$$

Once the whole system is put in rotation with angular velocity Ω, the Hamiltonian in the rotating frame of reference reads [105]:

$$H_{\rm Rot} = \left(\vec{p} + \vec{\tilde{A}}\right)^2 + \frac{1}{4}\omega^2 r^2 + \Omega \mathbb{L}_z + V_{\rm rot} \tag{4.40}$$

where we introduced the gauge-invariant angular momentum

$$\mathbb{L} = \vec{r} \times \left(\vec{p} + \vec{\tilde{A}}\right), \tag{4.41}$$

and all the coordinates are now considered in the rotating frame. It is useful to rewrite $H_{\rm Rot}$ introducing the gauge potential:

$$A_x = \tilde{A}_x - \frac{B}{2} y\,, \qquad A_y = \tilde{A}_y + \frac{B}{2} x, \tag{4.42}$$

where we impose $B = \omega$. We obtain:

$$H_{\rm Rot} = \left(\vec{p} + \vec{A}\right)^2 - \Delta \mathbb{L}_z + V_{\rm rot}, \tag{4.43}$$

with $\Delta = \omega - \Omega$.

Our aim is to identify the correct family of Rabi frequencies, $V_{\rm rot}$ and gauge transformation such that the Hamiltonian $H_{\rm Rot}$ can be cast in the form:

$$H_L = \left(\vec{p} + \vec{A}\right)^2 - \Delta L_z, \tag{4.44}$$

with A given by (4.36) and $L_z = \vec{r} \times \vec{p}$ being the usual angular momentum in the rotating frame. As we will show in section 4.6, H_L can be exactly solved and, in

the limit $\Omega \to \omega$, becomes the Hamiltonian (4.35). In particular we need:

$$\vec{\tilde{A}} = (q\sigma_x, q\sigma_y) \tag{4.45}$$
$$V_{\text{rot}} = q\Delta(x\sigma_y - y\sigma_x) \tag{4.46}$$

In order to obtain, in the rotating frame, the potential A in (4.36) starting from the potential $\mathcal{A}$ given in [64] (the difference in sign with respect to [64] is related to the different convention chosen for the Hamiltonian)

$$\mathcal{A}_{11} = -\cos^2\phi\nabla S_{23} - \sin^2\phi\nabla S_{13} \tag{4.47}$$
$$\mathcal{A}_{22} = -\cos^2\theta\left(\cos^2\phi\nabla S_{13} + \sin^2\phi\nabla S_{23}\right) \tag{4.48}$$
$$\mathcal{A}_{12} = -\cos\theta\left(\frac{1}{2}\sin 2\phi\nabla S_{12} - i\nabla\phi\right) \tag{4.49}$$

we need a suitable unitary gauge transformation $O(\vec{r})$. In particular the field transforms as $\mathcal{A} \to O\mathcal{A}O^\dagger - iO\nabla O^\dagger$ and thus we must have

$$O\mathcal{A}O^\dagger - iO\nabla O^\dagger = \tilde{A} = (q\sigma_x, q\sigma_y) \tag{4.50}$$

From the definition of $\mathcal{A}$ it is evident that, choosing a constant ϕ, it is not possible to obtain $\mathcal{A}_y \propto \sigma_y$ but it is easy to check that we can obtain $\mathcal{A}_y = k\mathbb{I} - q\sigma_z$ and $\mathcal{A}_x = q\sigma_x$ for a suitable choice of the parameters as functions of q. Therefore the gauge transformation we apply is:

$$\Psi \to O\Psi\,, \qquad \text{with } O = e^{iky - i\frac{\pi}{4}\sigma_x} \tag{4.51}$$

with k to be defined in the following. In this way we obtain:

$$\mathcal{A}_x = q\sigma_x \xrightarrow{O} \tilde{A}_x = q\sigma_x\,, \qquad \mathcal{A}_y = k\mathbb{I} - q\sigma_z \xrightarrow{O} \tilde{A}_y = q\sigma_y \tag{4.52}$$

We also must consider that the scalar potential in [64] are affected by O as $O\left(V + \Phi\right)O^\dagger$, thus, in order to obtain (4.44) from (4.43) we must have:

$$O\left(V + \Phi\right)O^\dagger = V_{\text{rot}} = \Delta\vec{r} \times \tilde{A} \tag{4.53}$$

and then:

$$V + \Phi = -q\Delta\left(y\sigma_x + x\sigma_z\right) \tag{4.54}$$

Now we can find the suitable parameters to satisfy (4.52) and (4.54). First of all we impose $\phi = \pi/4$ and $S_3 = \text{const}$. Then, from the definition of $\mathcal{A}$ we obtain that:

$$\partial_x\left(S_1 + S_2\right) = 0 \tag{4.55}$$
$$-\cos\theta\partial_x\left(S_1 - S_2\right) = 2q \tag{4.56}$$
$$2k - 2q = -\partial_y\left(S_1 + S_2\right) \tag{4.57}$$
$$2q + 2k = -\cos^2\theta\partial_y\left(S_1 + S_2\right) \tag{4.58}$$

A possible solution is given by:

$$S_1 = \lambda(x+y) \tag{4.59}$$
$$S_2 = \lambda(-x+y) \tag{4.60}$$

with $\lambda = -q/\cos\theta$ in order to satisfy the first two equations; we obtain from the last two equations:

$$\cos^2\theta - 2\cos\theta - 1 = 0 \quad \Rightarrow \quad \cos\theta = 1 - \sqrt{2} \tag{4.61}$$

Therefore:

$$\lambda = -\frac{q}{\cos\theta} = \frac{q}{\sqrt{2}-1}\,, \qquad k = \frac{1+\cos^2\theta}{2\cos\theta}\,q = -\sqrt{2}q \tag{4.62}$$

The corresponding Rabi frequencies result

$$\Omega_1 = \Omega' e^{iq\frac{x+y}{\sqrt{2}-1}}\,, \quad \Omega_2 = \Omega' e^{iq\frac{-x+y}{\sqrt{2}-1}}\,, \quad \Omega_3 = -\Omega'\sqrt{\sqrt{2}-1}e^{iS_3} \simeq -0.64\Omega' e^{iS_3} \tag{4.63}$$

with Ω' and S_3 arbitrary, and guarantee to obtain the right $\tilde{A}$ after the gauge transformation. Let us consider now the scalar potentials; imposing $\phi = \pi/4$ and $\cos\theta = 1-\sqrt{2}$ we find the following from [64] and from (4.54):

$$V_{11} + \Phi_{11} = \frac{V_1+V_2}{2} + \lambda^2\sin^2\theta = -q\Delta x \tag{4.64}$$
$$V_{22} + \Phi_{22} = \frac{V_1+V_2}{2}\cos^2\theta + V_3\sin^2\theta + \lambda^2\cos^2\theta\sin^2\theta = q\Delta x \tag{4.65}$$
$$V_{12} + \Phi_{12} = \frac{V_1-V_2}{2}\cos\theta = -q\Delta y \tag{4.66}$$

The solution is given by:

$$V_1 = -q\Delta x - \lambda\Delta y - \lambda^2\sin^2\theta \tag{4.67}$$
$$V_2 = -q\Delta x + \lambda\Delta y - \lambda^2\sin^2\theta \tag{4.68}$$
$$V_3 = \sqrt{2}q\Delta x \tag{4.69}$$

with λ given by (4.62).

This choice for the scalar potentials V_i completes the set of parameters (4.63) needed to obtain the Hamiltonian (4.44) in the rotating frame. However we can notice that it is possible to modify the previous equations of the scalar potential in order to obtain a Zeeman splitting reproducing the term proportional to $\mathcal{M}_z$ in (4.31).

Finally we show that it is impossible to obtain the gauge potential $\vec{A}$ defined in Eq. (4.36) (or a gauge-equivalent version of it) using only the gauge potential $\vec{\mathcal{A}}$ (4.47,4.48,4.49) defined in [64] without introducing other physical elements such as the rotation of the system. Indeed, applying the gauge transformation $O^\dagger$ (4.51) we can express $\vec{A}$ as:

$$A_x = -\frac{B}{2}y + q\sigma_x\,, \qquad A_y = \frac{B}{2}x - q\sigma_z + k \tag{4.70}$$

This form of the potential $\vec{A}$ is real and does not depend on σ_y. Therefore, imposing $\vec{\mathcal{A}} = \vec{A}$ and considering Eq. (4.49), we obtain that the parameter ϕ entering in the definition of the Rabi frequencies (4.38) must be independent on the position, otherwise an imaginary term proportional to $\nabla\phi$ would appear. Let us consider now the term $\vec{\mathcal{A}}_{11}$: from the equation (4.47) one obtain that $\partial_y \mathcal{A}_{11,x} = \partial_x \mathcal{A}_{11,y}$; however, this is not the case for $A_{11,x}$ and $A_{11,y}$ in (4.70) unless $B = 0$. Therefore, to obtain the term proportional to the magnetic field B one needs an additional physical mechanism (the rotation in our analysis) besides the construction of the non-Abelian gauge potentials for tripod atoms described in [64].

4.3 Single-Particle Hamiltonian

For the sake of simplicity we will begin our analysis of the system by studying the single-particle Hamiltonian (4.35) that corresponds to the limit $\Omega \to \omega$ which is necessary to satisfy the condition $\mathcal{P}2$. In Section 4.6, instead, we will address the case in which a term linear in the angular momentum (4.44) is also present. These results are exploited in Sections 4.4 and 4.5 where we introduce two-body interactions and we study the many-particle problem and the corresponding quantum Hall states.

The Hamiltonian H (4.35) can be decomposed into two terms as we discussed in Sec. 4.1.3. The first one is the *Abelian Hamiltonian* H_a which corresponds to the case addressed in section 4.1.2 but is proportional to the spin identity in order to satisfy the condition $\mathcal{P}3$ (this constraint is not strictly necessary to the solution of the problem and can be removed by applying a Zeeman term). The other term is the off–diagonal component provided by the non–commutative contribution of $\vec{A}$, the *non–Abelian Hamiltonian* H_{na}. Using the previously introduced complex variables, $z = x - iy$ and $\bar{z} = x + iy$, we can rewrite H_a and H_{na} in a form corresponding to equation (4.31) with $h_z = \mathcal{M}_z = 0$:

$$H_a = 2q^2 + B + \frac{1}{4}\left(B\bar{z} - 4\partial_z\right)\left(Bz + 4\partial_{\bar{z}}\right) = 2q^2 + B + \frac{1}{4}d^\dagger d \tag{4.71}$$

$$H_{na} = q\begin{pmatrix} 0 & -iBz - 4i\partial_{\bar{z}} \\ iB\bar{z} - 4i\partial_z & 0 \end{pmatrix} = q\begin{pmatrix} 0 & -id \\ id^\dagger & 0 \end{pmatrix} \tag{4.72}$$

where we defined the operators:

$$d^\dagger = B\bar{z} - 4\partial_z = 2\sqrt{2B}D^\dagger\,, \qquad d = Bz + 4\partial_{\bar{z}} = 2\sqrt{2B}D \tag{4.73}$$

that are proportional to the previously defined D and $D^\dagger$ so that the following relations hold:

$$[d, z] = 0\,, \qquad \left[d, d^\dagger\right] = 8B \tag{4.74}$$

Introducing the standard Gaussian ground state wavefunction $\psi_0 = \sqrt{B/2\pi}e^{-\frac{Bz\bar{z}}{4}}$ one has $d\psi_0 = 0$ and $d^\dagger\psi_0 = 2B\bar{z}\psi_0$; thus, for H_a, we obtain the usual Landau level structure of the eigenstates, which are degenerate with respect to the angular momentum $n - m$:

$$\psi_{n,m} = \frac{i^n d^{\dagger\,n}\left(z^m\psi_0\right)}{(8B)^{\frac{n}{2}}\sqrt{n!m!}} \propto D^{\dagger\,n}L^m\psi_0. \tag{4.75}$$

The corresponding energy levels are:

$$E_n = 2q^2 + 2B\left(n + \frac{1}{2}\right) \tag{4.76}$$

Let us consider now the non–Abelian part of the Hamiltonian. The eigenvalues of H_{na} are $\lambda^{\pm} = \pm 2q\sqrt{2Bn}$ and the corresponding eigenstates $\varphi^{\pm}_{n,m}$ can be expressed in terms of the eigenstates of H_a:

$$\varphi^{\pm}_{n,m} = \psi_{n-1,m}\left|\uparrow\right\rangle \pm \psi_{n,m}\left|\downarrow\right\rangle \tag{4.77}$$

where the following relation holds for $n \geq 1$:

$$2\sqrt{2Bn}\psi_{n,m} = id^{\dagger}\psi_{n-1,m} \tag{4.78}$$

Thus, in general, the non–Abelian term mixes the $(n-1)^{\text{th}}$ and the n^{th} Landau levels; but there are also uncoupled eigenstates $\varphi_0 = \psi_{0,m}\left|\downarrow\right\rangle$ with eigenvalue $\lambda = 0$ for every $\psi_{0,m}$ in the lowest Landau level. The spectrum of H_{na} is similar to the one obtained in the relativistic case typical of graphene systems [120]; in particular, these results are analogous to the ones obtained in [102] starting from the Dirac equation in an anisotropic regime, and we can notice that H_{na} corresponds to the known Jaynes–Cummings model.

We can now diagonalize the whole Hamiltonian using as a basis the functions $\varphi^{\pm}_n$:

$$H\varphi^{\pm}_n = \left(2q^2 + 2Bn \pm 2q\sqrt{2Bn}\right)\varphi^{\pm}_n - B\varphi^{\mp}_n \tag{4.79}$$

so that, for $n \geq 1$, the Hamiltonian is splitted in blocks H_n of the form:

$$\begin{pmatrix} 2q^2 + 2Bn + 2q\sqrt{2Bn} & -B \\ -B & 2q^2 + 2Bn - 2q\sqrt{2Bn} \end{pmatrix} \tag{4.80}$$

whereas for the uncoupled states we have:

$$H\varphi_0 = \left(B + 2q^2\right)\varphi_0 \tag{4.81}$$

The eigenvalues of H are therefore:

$$\varepsilon^{\pm}_n = 2Bn + 2q^2 \pm \sqrt{B^2 + 8q^2Bn} \tag{4.82}$$

and its unnormalized eigenstates result:

$$\begin{aligned}\chi^{\pm}_{n,m} = &\left(B + 2q\sqrt{2Bn} \mp \sqrt{B^2 + 8q^2Bn}\right)\psi_{n-1,m}\left|\uparrow\right\rangle + \\ &+ \left(B - 2q\sqrt{2Bn} \pm \sqrt{B^2 + 8q^2Bn}\right)\psi_{n,m}\left|\downarrow\right\rangle,\end{aligned} \tag{4.83}$$

where we explicited the angular momentum degeneracy. We can notice that the angular momentum is not a good quantum number for these states unless we also introduce a spin-1/2 component defining a total angular momentum $J = L + S$. J commutes with both Hamiltonians (4.35) and (4.44) and

$J\chi^{\pm}_{n,m} = (n - m - 1/2)\,\chi^{\pm}_{n,m}$. Moreover the wavefunctions $\chi^{\pm}_{n,m}$ are eigenstates for the operator $n = D^{\dagger}D + \sigma_z/2$ defined in (4.22), thus they constitute deformed Landau levels.

Analyzing the spectrum, we can notice that there is a correspondence between the usual Landau levels and the states χ: every Landau level is splitted into two parts corresponding to the states χ^{+}_{n-1} and χ^{-}_{n} and, in the case $q \to 0$, their energy becomes approximately $E_{n-1} \pm 4q^2 n$. Therefore, for $q \to 0$ one recovers the usual Landau level structure characterized by the (double) spin degeneracy as prescribed by the condition $\mathcal{P}3$. The non-Abelian term of the Hamiltonian removes this degeneracy through the coupling between the $(n-1)^{\text{th}}$ level with spin up and the n^{th} with spin down. The energy spectrum (4.82) is plotted in Fig. 4.1 as a function of the non-Abelian intensity q^2, which seems a parameter easier to change in atomic gases, and in Fig. 4.2 as a function of the magnetic field B which instead is the usual situation in solid state physics where the spin-orbit coupling is very difficult to tune.

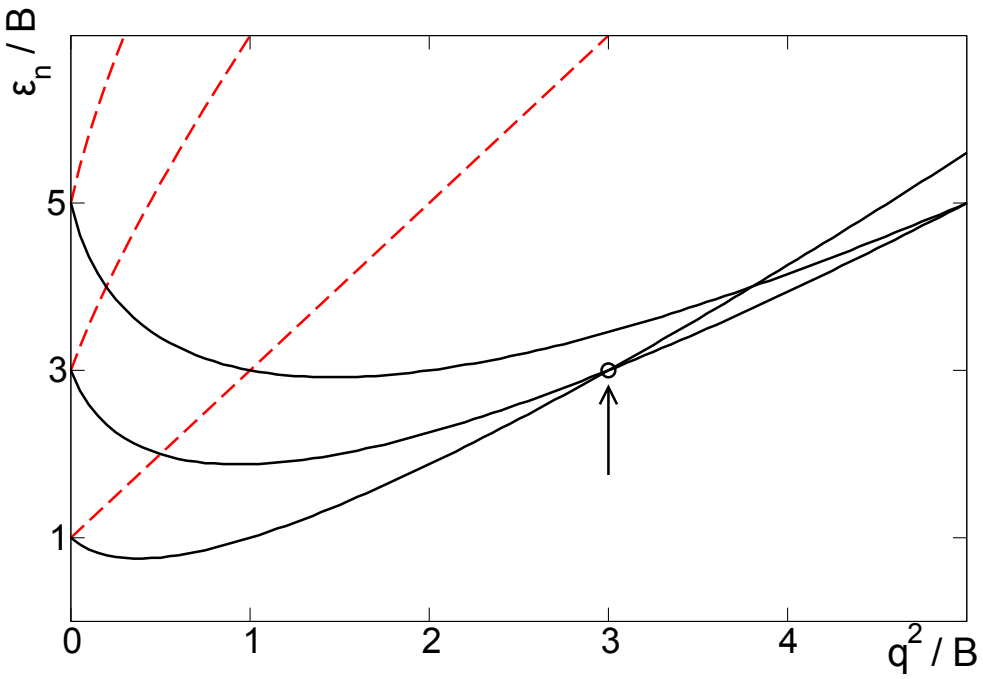

Figure 4.1: Energies of the first 6 eigenstates as a function of q^2/B. The n^{th} Landau level is split by the non-Abelian contribution of the external field in χ^{-}_{n+1} (black solid) and χ^{+}_{n} (red dashed); for $q = 0$ one recovers the usual Landau levels, whereas for $q^2/B = 3$ there is a degeneracy of the Landau levels (indicated by a circle). Here and in Fig. 4.3 the energy ε_n/B and the parameter q^2/B are dimensionless ratios and, in dimensional units, correspond respectively to $2m\varepsilon_n/\hbar B = \varepsilon_n/\hbar\omega$ and $q^2/\hbar B$, where $B = 2m\omega$ (in the text we used units such that $\hbar = 1$ and $2m = 1$).

Varying the value of the parameter q^2/B, which measures the ratio of the Abelian and non-Abelian contributions in the gauge field, the eigenvalues $\varepsilon^{\pm}_{n}$ show an interesting pattern of crossings (see Fig. 4.3): each pair of eigenstates of the

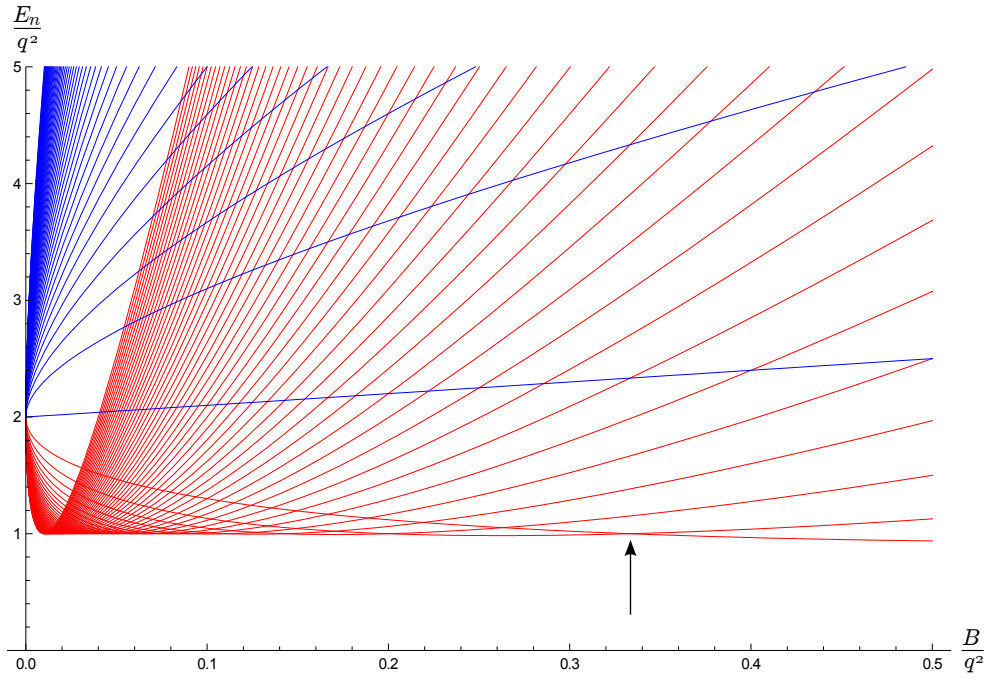

Figure 4.2: The first 50 energy levels ε_n^- (in red) and ε_n^+ (in blue) are shown as a function of B/q^2. The eigenvalues plotted correspond to the dimensionless ratio $2m\varepsilon_n/q^2$ (in the text the units are such that $2m = 1$). We can notice that for $B \to 0$ the distribution of the energy becomes continuous, corresponding to free particles with spin-orbit coupling. Moreover for this range of parameters $\left(2B < q^2\right)$ the energy of the alternating ground states χ^- is almost constant around q^2. The arrow identifies the crossing between χ_1^- and χ_2^- at $q^2 = 3B$.

kind χ_a^- and χ_b^- becomes degenerate for

$$\frac{q^2}{B} = \frac{1}{2}\left(a + b + \sqrt{1 + 4ab}\right) \tag{4.84}$$

and the energy of the crossing is $\varepsilon_c\,(a, b) = (a + b)\,B$. Instead, a pair of different eigenstates of the kind χ_a^+ and χ_b^- has a crossing only if $a < b$; in this case the degeneracy point is

$$\frac{q^2}{B} = \frac{1}{2}\left(a + b - \sqrt{1 + 4ab}\right) \tag{4.85}$$

and, also for these energy levels, the corresponding energy is $\varepsilon_c\,(a, b) = (a + b)\,B$. Therefore all the energy level crossings are characterized by an integer energy in units of B (see the inset in Fig 4.3).

As shown in Fig. 4.1, the uncoupled-state family (4.81), which corresponds to χ_0^+, is characterized by the energy level $\varepsilon_0^+ = B + 2q^2$, which is higher than the energy $\varepsilon_1^- = 2B + 2q^2 - \sqrt{B^2 + 8Bq^2}$ of χ_1^-. Therefore χ_1^- is the ground state family of the system for $q^2 < 3B$ (the general case with $q^2 \geq 3B$ is analyzed in

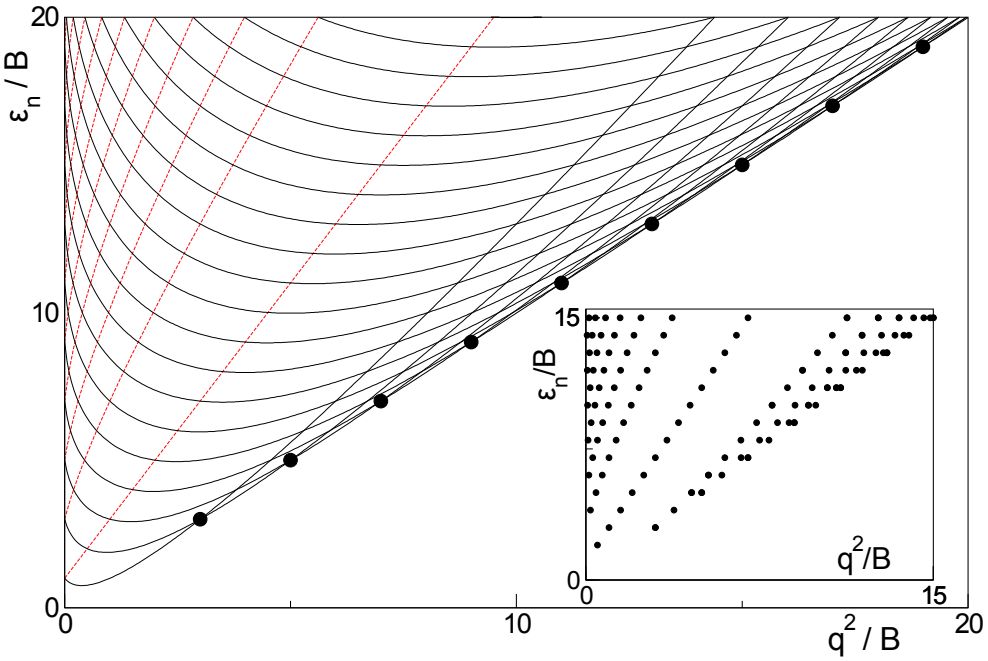

Figure 4.3: Energies of χ^-_{n+1} (black solid line) and χ^+_n (red dashed line) for $n = 0, \ldots, 10$ as a function of q^2/B. The crossings of the ground states happen in the degeneracy points $q^2/B = (1+2n)$, denoted by solid circles. Inset: Degeneracy points of Landau levels.

section 4.5). We can rewrite every state of the family χ^-_1 in the form:

$$\chi^-_1 = e^{-\frac{B}{4}|z|^2}\left(c_{\uparrow,1}P\left|\uparrow\right\rangle + 2c_{\downarrow,1}B\bar{z}P\left|\downarrow\right\rangle - 4c_{\downarrow,1}\partial_z P\left|\downarrow\right\rangle\right) \tag{4.86}$$

where P is a generic polynomial in z and we have defined the constants:

$$c_{\uparrow,n} = B + 2q\sqrt{2Bn} + \sqrt{B^2 + 8q^2Bn} \tag{4.87}$$

$$c_{\downarrow,n} = i\left(B - 2q\sqrt{2Bn} - \sqrt{B^2 + 8q^2Bn}\right)\left(2\sqrt{2Bn}\right)^{-1}. \tag{4.88}$$

Besides, it is useful to introduce the operator

$$\mathcal{G}_1 \equiv c_{\uparrow,1}\sigma_x + c_{\downarrow,1}d^\dagger \tag{4.89}$$

which allows us to map uncoupled states in χ^+_0 to states in χ^-_1. Thus, we can rewrite (4.86) using the operator $\mathcal{G}_1$:

$$\chi^-_1 = \mathcal{G}_1\left(P(z)e^{-\frac{B}{4}|z|^2}\left|\downarrow\right\rangle\right) \tag{4.90}$$

Thanks to the degeneracy of these ground states, we can build also wavefunctions minimizing supplementary terms in the Hamiltonian (4.35); for instance, we can introduce a repulsive potential for the spin up component of the form

$V_\uparrow(z,\zeta) = \delta(z-\zeta)\,|\uparrow\rangle\langle\uparrow|$, where ζ plays the role of the coordinates of a *quasihole* in the spin up wavefunction. The corresponding single-particle ground states are

$$\phi(z,\zeta) = \mathcal{G}_1\left((z-\zeta)\,Q(z)\,e^{-\frac{B}{4}|z|^2}\,|\downarrow\rangle\right) \tag{4.91}$$

where $Q(z)$ is a generic polynomial. We can notice that the wavefunction density for the spin up component in ϕ goes to zero for $z=\zeta$ whereas the spin down density, in general, doesn't, due to the derivative term in $d^\dagger$. We can consider also a repulsive potential not affected by the spin, $V(\zeta) = \delta(z-\zeta)$; in this case we obtain as a ground state the wavefunctions:

$$\Phi(z,\zeta) = \mathcal{G}_1\left((z-\zeta)^2\,Q(z)e^{-\frac{B}{4}|z|^2}\,|\downarrow\rangle\right) \tag{4.92}$$

that have a vanishing density in ζ both for the spin up and the spin down components. Besides, we must notice that it's impossible to create a wave function with a zero spin-down density in ζ but a nonvanishing spin up component, inside the space χ_1^-.

With respect to the Hamiltonian (4.35), these excitations are gapless; however they increase the total angular momentum of the system, and, as we will show in section 4.6, this implies an increment in energy once we consider the case $\Delta \neq 0$ in (4.44).

4.3.1 U(3) non-Abelian gauge potentials

As shown in [95, 98] it is possible to engineer gauge potentials involving a higher number of internal states. For instance, considering atoms with a tetrapod electronic structure, one can obtain three degenerate dark states, denoted as $|+\rangle$, $|0\rangle$ and $|-\rangle$, that corresponds to an effective spin 1 and allows us to mimic the effect of an external U(3) potential.

In particular we can generalize the construction of the previous section to the following potential:

$$A_x = -\frac{B}{2}y\,\mathbb{I} + \begin{pmatrix} 0 & \alpha & 0 \\ \alpha & 0 & \beta \\ 0 & \beta & 0 \end{pmatrix}, \qquad A_y = \frac{B}{2}x\,\mathbb{I} + \begin{pmatrix} 0 & -i\alpha & 0 \\ i\alpha & 0 & -i\beta \\ 0 & i\beta & 0 \end{pmatrix} \tag{4.93}$$

where $\mathbb{I}$ is the 3×3 identity matrix, B is the effective magnetic field and α and β are two arbitrary parameters that constitute the coefficients of different Gell-Mann matrices. A_x and A_y do not commute with each other and describe a particular family of effective uniform non-Abelian U(3) potentials whose corresponding non-Abelian magnetic field is

$$\mathcal{B} = \begin{pmatrix} B-2\alpha^2 & 0 & 0 \\ 0 & B+2\alpha^2-2\beta^2 & 0 \\ 0 & 0 & B+2\beta^2 \end{pmatrix} \tag{4.94}$$

which is translationally invariant as in eq. (4.37). These potentials are similar to the one chosen in [98] to simulate Weyl fermions through multi-component cold atoms on optical lattices.

Given the potential (4.93), the minimal coupling Hamiltonian (4.35) assumes the form:

$$H(\alpha,\beta) = B + \frac{1}{4}d^\dagger d + \begin{pmatrix} 2\alpha^2 & -i\alpha d & 0 \\ i\alpha d^\dagger & 2\alpha^2+2\beta^2 & -i\beta d \\ 0 & i\beta d^\dagger & 2\beta^2 \end{pmatrix} \tag{4.95}$$

where we used the operators d and $d^\dagger$ defined in (4.73). The first term in $H(\alpha,\beta)$ is the Abelian term proportional to the identity, while the second term describes the non-Abelian interaction, depending on α and β, which couples subsequent Landau levels with different spin, as in the U(2) case. Therefore, for each $n \geq 2$, we can identify three families of eigenstates which are constituted by linear superpositions of the states $\psi_{n,m}|-\rangle$, $\psi_{n-1,m}|0\rangle$ and $\psi_{n-2,m}|+\rangle$, where m is related to the angular momentum. In particular, given $n \geq 2$, the corresponding eigenenergies of $H(\alpha,\beta)$ are the solutions ε_n of the following eigenvalues equation (see Fig 4.4 for the case $\alpha = \beta$):

$$\begin{pmatrix} 2\alpha^2 + B(2n-3) & -i2\alpha\sqrt{2B(n-1)} & 0 \\ i2\alpha\sqrt{2B(n-1)} & 2\alpha^2+2\beta^2+B(2n-1) & -i2\beta\sqrt{2Bn} \\ 0 & i2\beta\sqrt{2Bn} & 2\beta^2+B(2n+1) \end{pmatrix} = \varepsilon_n \mathbb{I} \tag{4.96}$$

Like the case of the Jaynes-Cummings coupling, the spin degeneracy of the Landau levels is removed and the eigenstates of (4.95) are also eigenstates of the total angular momentum J.

In analogy with the previously discussed U(2) potential, there are also other eigenstates of the Hamiltonian (4.95) that correspond to the uncoupled states $\psi_{0,m}|-\rangle$ with energy $\varepsilon_0 = 2\beta^2 + B$ and to the family of (unnormalized) "doublet states" defined by:

$$\Phi_m^\pm = \left(B - \alpha^2 \mp \sqrt{(\alpha^2-B)^2 + 8B\beta^2}\right)\psi_{0,m}|0\rangle - i\beta\sqrt{8B}\psi_{1,m}|-\rangle \tag{4.97}$$

with energy:

$$\varepsilon_1^\pm = 2B + 2\beta^2 + \alpha^2 \pm \sqrt{(\alpha^2-B)^2 + 8B\beta^2} \tag{4.98}$$

We can notice that in the limits $\alpha \to 0$ or $\beta \to 0$ we recover the results of the previous case. In fact, if either α or β goes to zero, the resulting gauge potential is an effective U(2) potential of the kind (4.36) and one of the spin states remains decoupled with respect to the others.

Finally Fig. 4.5 shows that it is possible to recover a triple degeneracy of the ground state for particular values of the parameters α and β. The figure shows a triple degeneracy occurring for $B = 1$, $\alpha = \sqrt{(9+\sqrt{73})/6}$ and $\beta = \sqrt{2/3}$ between the uncoupled state and two eigenvectors of (4.96) obtained for $n = 2$ and $n = 3$ at the energy $\varepsilon = \frac{7}{3}B$. The existence of such triple degeneracies implies that, varying the Hamiltonian parameters in a neighborhood of these points, it is possible to detect, in the space defined by α and β, lines of doubly degenerate ground states which intersect the energy eigenvalue ε_0. Moreover in correspondence of such triple degeneracy points, peculiar many-body quantum Hall states may arise, as we will mention in Sec. 4.7.

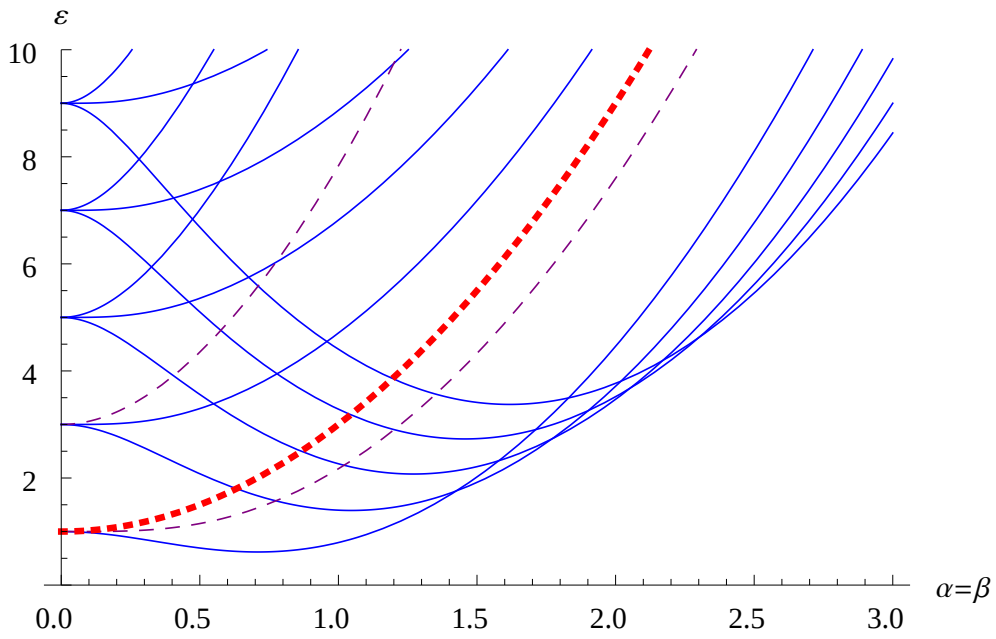

Figure 4.4: The energy levels of the Hamiltonian (4.95) are plotted imposing the constraint $\alpha = \beta$ and rescaling $B = 1$. The blue lines represent the eigenvalues ε_n (4.96), the purple dashed lines represent the energy $\varepsilon_1^{\pm}$ of the doublet states and the dotted red line represents the energy ε_0 of the uncoupled states. One can see that, in the limit $\alpha, \beta \to 0$, the Landau level energies are recovered with a threefold pseudospin degeneracy.

4.3.2 Landau Gauge and Anisotropy

Another possible generalization of the U(2) gauge potential (4.36) is the introduction of anisotropy in the non-Abelian components. This alteration of the single-particle problem corresponds to having both a Rashba and a Dresselhaus spin-orbit interaction with different coefficients. To deal with this problem it is useful to consider the Landau gauge, such that the new potential reads:

$$A_x = \alpha\sigma_x\,, \qquad A_y = \beta\sigma_y + Bx\mathbb{I}; \tag{4.99}$$

the introduction of the anisotropy parameters α and β implies that the minimal coupling Hamiltonian does not fulfill the condition $\mathcal{P}1$ anymore. Nevertheless the single-particle eigenstates can be analytically defined as an infinite series of states in the usual Landau levels [115] and the eigenenergies can be numerically evaluated [103]; in this way it is possible to gain a better insight of the new structure of the deformed Landau levels χ once a small perturbation, given by $\alpha \simeq \beta$, is introduced in the potential 4.36, corresponding to $\alpha = \beta = q$.

In the Landau gauge (4.99) the potential $\vec{A}$ is independent of the coordinate y, its single-particle eigenstates are plane waves in the y direction, $\psi \propto e^{iky}$; therefore they assume the form $\psi = e^{iky}\Psi_n\,(x + k/B)$, where the two-component

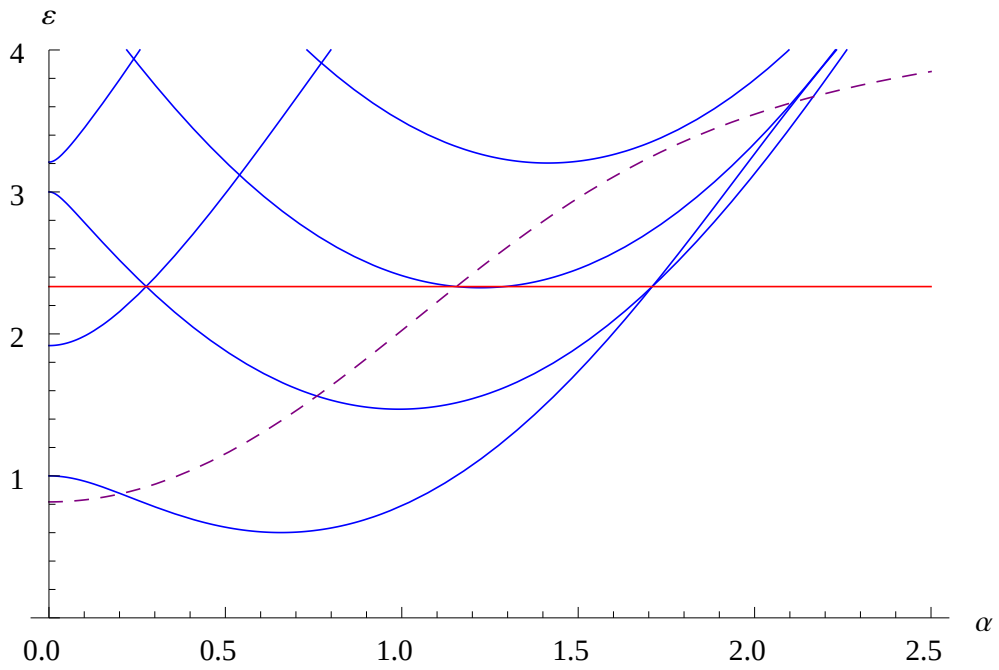

Figure 4.5: The first energy levels of the Hamiltonian (4.95) are plotted as a function of α for $\beta = \sqrt{2/3}$ and $B = 1$. The blue lines represent the eigenvalues ε_n (4.96), the purple dashed line represents the energy ε_1^- of the first doublet states and the red line represents the energy $\varepsilon_0 = 7/3$ of the uncoupled states. For this choice of the parameters a triple degeneracy of the ground states appears for $\alpha = \sqrt{\left(9+\sqrt{73}\right)/6} \simeq 1.71$.

wavefunction Ψ_n and the energy E_n satisfy the equation [103]:

$$E_n \Psi_n(X) = \left[(-i\partial_X + \alpha\sigma_x)^2 + (\beta\sigma_y + BX)^2\right] \Psi_n(X). \tag{4.100}$$

Like the Abelian case, the energy is hence independent of k and we will address the eigenstates as Landau levels, corresponding to the states χ in the symmetric case $\alpha = \beta$.

The previous equation is characterized by a $\mathbb{Z}_2$ symmetry $\Psi_n(x) \to \sigma_z \Psi_n(-x)$, thus, in each Landau level, either the first component is symmetric about $x = -k/B$ and the second antisymmetric ($+-$ symmetry), or vice versa ($-+$ symmetry) [103]. The crossings of the Landau levels in the general case $\alpha \neq \beta$ depend on this symmetry: in general, levels of the same symmetry avoid crossings, with the exceptions given by the values $\alpha = \pm\beta$ that correspond to the pattern of crossings between the χ wavefunctions that we analyzed above. In this symmetric case, in fact, there are conical intersections of the levels with the same $\mathbb{Z}_2$ symmetry that are removed in the the general case with $\alpha \neq \beta$. Levels with opposite symmetry, instead, cross freely in all the cases [103].

Fig. 4.6 shows the comparison between the symmetric case with $a = b$ and the anisotropic case where the crossings between states with the same symmetry

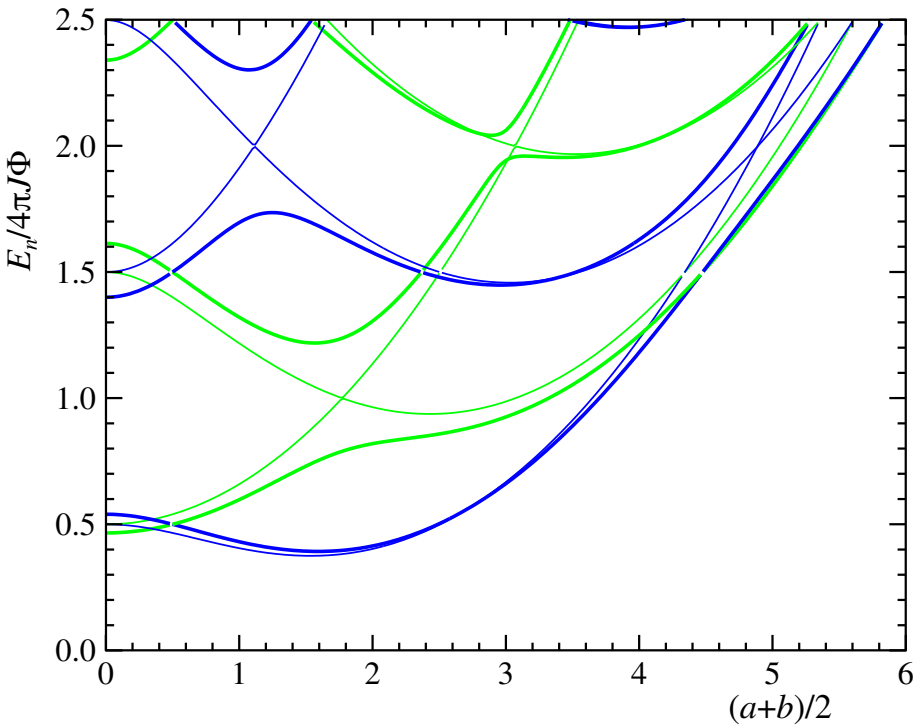

Figure 4.6: Lowest few Landau level energies, and symmetries $+-$ (blue) or $-+$ (green) for $a = b$ (thin lines) and $a = b \pm 1$ (thick lines) [103]. The parameters in the plot are related to the potential (4.99) by $a = \alpha\sqrt{\frac{2\pi}{B}}$, $b = \beta\sqrt{\frac{2\pi}{B}}$, $2\pi\Phi = B$ and J is an overall energy scale. The case $a = b$ corresponds to the spectrum in Fig. 4.1 while for $a \neq b$ the crossings between states with the same symmetry are removed. (Taken from [103]).

are removed. It's important to notice that the lowest Landau levels alternate their symmetry, therefore the crossings between the ground states χ_n^- and χ_{n+1}^- are stable with respect to the anisotropic perturbation. In fact, increasing the Landau level from n to $n+1$ implies a change of the symmetry of the wavefunction Ψ_n and the lowest Landau level for small values of α and β (before the first crossing) shows a positive symmetry [103]. In the next sections we will study the behaviour of cold atomic gases at the degeneracy points of the deformed Landau levels in the symmetric case (4.36); even if the introduction of a small anisotropy implies a displacement of these crossing points, their existence is nevertheless stable under such alteration of the potential and I expect that the main features of the many-body wavefunctions described in Sec. 4.7 survive also in the presence of a small anisotropic perturbation.

4.4 Two–body interaction and deformed Laughlin states

In the previous section we described a single particle in the non–Abelian potential (4.36), now we consider a system of N atoms and we introduce a two–body repulsive interaction. Denoting by g_1 the (dimensionless) scattering length between particles in the same internal state and by g_0 the scattering length between particles in different internal states, we can write the interaction Hamiltonian as:

$$H_I = \sum_{i<j}^{N} \left(g_1 \Pi_1 + g_0 \Pi_0\right) \delta\left(z_i - z_j\right). \tag{4.101}$$

Here Π_1 is the projector over the space in which the particles i and j have parallel spin states ($|\uparrow\uparrow\rangle$ or $|\downarrow\downarrow\rangle$) whereas Π_0 is the projector over the space in which i and j have antiparallel spins ($|\uparrow\downarrow\rangle$ or $|\downarrow\uparrow\rangle$). We will consider both bosonic and fermionic gases, keeping in mind that for fermions it is $g_1 = 0$ [121, 122].

An arbitrary two–particle state, in which both atoms are in χ_1^-, can be described as:

$$\Psi = \mathcal{G}_{1,1}\mathcal{G}_{1,2} P\left(z_1, z_2\right) e^{-B\left(|z_1|^2 + |z_2|^2\right)/4} |\downarrow\downarrow\rangle \tag{4.102}$$

where $\mathcal{G}_{1,i}$, defined in (4.89), refers to the coordinate z_i, and P is generic polynomial in z_1 and z_2. With vanishing inter–species interaction ($g_0 = 0$) and strong intra–species interaction, Ψ has a zero interaction energy if its components $|\uparrow\uparrow\rangle$, $|\downarrow\downarrow\rangle$ vanish when $z_1 \to z_2$: for fermions, this is assured by the Pauli principle; whereas for bosons the strong intra-species regime corresponds to $g_1 \gg B, q^2$ and the two–body wavefunction Ψ has to fulfill the requirements:

$$P\left(z, z\right) = 0\,, \quad \left(\partial_{z_1} + \partial_{z_2}\right) P|_{z_1 = z_2} = 0\,, \quad \partial_{z_1}\partial_{z_2} P|_{z_1 = z_2} = 0 \tag{4.103}$$

Every antisymmetric polynomial $P\left(z_1, z_2\right) = -P\left(z_2, z_1\right)$ obviously satisfies these constraints, and, in general, all the fermionic functions $\Psi\left(z_1, z_2\right)$, antisymmetric by the exchange of the two atoms, guarantee that the intra–species interaction gives a zero energy contribution.

If we also add an inter–species repulsive interaction, such that $g_0 \gg B, q^2$, the two–particle wavefunction (4.102) must satisfy the further constraints

$$\partial_{z_1} P|_{z_1 = z_2} = \partial_{z_2} P|_{z_1 = z_2} = 0 \tag{4.104}$$

in order to be a ground state of H_I. This relations hold, for instance, in the case $P = \left(z_1 - z_2\right)^m$ with $m > 1$. In the case $m = 2$ the inter–species interaction is zero, but not the intra–species one, whereas for $m \geq 3$ every repulsive potential H_I gives a null contribution. In the following we consider the regime given by $g_0 = 0$ and (for bosons) $g_1 \gg B > q^2/3$. Under these conditions we can generalize the previous results for the case of N atoms.

All the fermionic states have a zero interaction energy for intra-species contact repulsions, therefore, essentially, one must distinguish the case of free fermions and repulsive bosons; concerning fermions, a possible ground state of the N–particle

Hamiltonian $\mathcal{H} = \sum_{k=1}^{N} H_k + H_I(g_0 = 0)$, with all the atoms in the χ_1^- space in order to minimize the single–particle energy, is given by:

$$\Psi = \left[\prod_i^N \mathcal{G}_{1,i}\right] \left(\mathcal{A}\left[P_0\left(z_1\right), ..., P_{N-1}\left(z_N\right)\right] e^{-\frac{B}{4}\sum_i^N |z_i|^2} \left|\downarrow\downarrow ... \downarrow\right\rangle \right) \tag{4.105}$$

where $\mathcal{A}$ is the antisymmetrization over all the coordinates z_i and P_m are different polynomials. Generalizing this kind of many-body states, it is easy to define a deformation, due to the non–Abelian potential, of the common Laughlin states. If we choose $P_m(z) = z^m$ with $m = 0, ..., N-1$, we obtain the usual Jastrow factor $\mathcal{A}\left[P_0 ... P_{N-1}\right] = \prod_{i<j}^N (z_i - z_j)$ and, more in general, given a Laughlin wavefunction

$$\Lambda_N^{(m)} = \prod_{i<j}^N (z_i - z_j)^m e^{-\frac{B}{4}\sum_i^N |z_i|^2} \left|\downarrow\downarrow ... \downarrow\right\rangle \tag{4.106}$$

with m odd, the state

$$\Psi^{(m)} = \prod_j^N \mathcal{G}_{1,j} \Lambda_N^{(m)} \tag{4.107}$$

is a ground state of the Hamiltonian $\mathcal{H}$: every atom lies in a superposition of states χ_1^- and the antisymmetric wavefunction causes the intra–species interaction energy to be zero.

However there are also bosonic states, symmetric under the exchange of two atoms, that have a zero intra-species interaction. For instance we can consider $\Psi^{(m)}$ for an even value of $m \geq 4$. In this case for every pair of particle with $z_i \to z_j$ the wavefunction vanishes at least as $(z_i - z_j)^2$, thus the interaction energy (and also its inter-species contribution if $g_0 \neq 0$) is vanishing.

Therefore it is important to notice that the introduction of the non-Abelian gauge potential (in the regime $q^2 < 3B$) implies that the highest density deformed Laughlin state with null interaction energy has a filling factor 1/4 instead of the usual filling factor 1/2 that characterizes systems of rotating bosons [44, 123] with a contact interaction. Thus we expect that the introduction of the SU(2) potential gives rise to the incompressible state $\Psi^{(4)}$, as numerically observed for small value of the chemical potential in the weak-interacting regime [103]; such a state is absent in the case of a pure magnetic field and can be considered as a signature of the effect of the potential (4.36).

The state $\Psi^{(m)}$ describes in general an incompressible fluid of spin-1/2 particles, as it can be shown calculating its norm:

$$\begin{aligned} I = \left\langle \Psi^{(m)} | \Psi^{(m)} \right\rangle &= \left\langle \Lambda_N^{(m)} \right| \prod \mathcal{G}_{1,j}^\dagger \mathcal{G}_{1,j} \left| \Lambda_N^{(m)} \right\rangle = \\ &= \left\langle \Lambda_N^{(m)} \right| \prod_j^N \left(|c_{\uparrow,1}|^2 + |c_{\downarrow,1}|^2 d_j d_j^\dagger + \sigma_{x,j} \left(c_{\uparrow,1}^* c_{\downarrow,1} d_j^\dagger + c_{\uparrow,1} c_{\downarrow,1}^* d_j \right) \right) \left| \Lambda_N^{(m)} \right\rangle = \\ &= \left(|c_{\uparrow,1}|^2 + 8B |c_{\downarrow,1}|^2 \right)^N \left\langle \Lambda_N^{(m)} | \Lambda_N^{(m)} \right\rangle \end{aligned} \tag{4.108}$$

where we considered that all the single-particle states involved in $\Psi^{(m)}$ are in the lowest Landau level and therefore are eigenstates of $dd^\dagger$. Thus the norm I can be easily written in terms of the one of the Laughlin state, and one can apply the usual plasma argument also to $\Psi^{(m)}$. This is also true if we consider quasiholes in the Laughlin state as, for example:

$$\Psi^{(m,k)}_{\zeta_1,\zeta_2} = \prod_i^N \mathcal{G}_{1,i} \left(\prod_i^N (z_i - \zeta_1)^k (z_i - \zeta_2)^k \right) \Lambda^{(m)}_N \tag{4.109}$$

As in the previous case, every atom in the Laughlin state is in the lowest Landau level, therefore the operators $\mathcal{G}_1$ modify only the norm of the states by a constant factor for each atom.

This correspondence highlights the nature of these excitations because it allows us to state that the Berry phase due to the adiabatic exchange of the pair of quasiholes ζ_1 and ζ_2 is the same as the one characterizing the corresponding quasiholes in a simple Laughlin state. This kind of excitations are therefore Abelian anyons and their braiding statistics is ruled by the usual exchange properties of the Abelian states in fractional quantum Hall effect [22].

4.5 Generalization to higher value of q^2/B

So far we referred to the case $q^2 < 3B$ in which the ground state family is constituted by wavefunctions of the kind χ_1^-. However, as shown in Fig. 4.3, for higher values of q different ground states families alternate. Therefore it is necessary to generalize the results of the previous section also for $q^2 \geq 3B$ by defining the family of operators $\mathcal{G}_n$ which allow us to describe every deformed Landau level of the kind χ^-. We can notice from the crossings of the energy levels (4.84) that $\chi^-_{n>1}$ is the ground state family for

$$(2n-1)\,B < q^2 < (2n+1)\,B \tag{4.110}$$

and also its energy ε_n^- varies, in this range of q, from $(2n-1)\,B$ to $(2n+1)\,B$. To describe the ground state family χ_n^- we generalize the operator $\mathcal{G}_1$ (4.89) introducing the operators:

$$\mathcal{G}_n = c_{\uparrow,n}\, d^{\dagger\,(n-1)} \sigma_x + c_{\downarrow,n}\, d^{\dagger\,n} \tag{4.111}$$

where the constants $c_{\uparrow,n}$ and $c_{\downarrow,n}$ are defined in (4.87,4.88); thus, the ground state wavefunctions can be expressed in the form:

$$\chi_n^- = \mathcal{G}_n \left(P(z) e^{-\frac{B}{4}|z|^2} \,|\downarrow\rangle \right) \tag{4.112}$$

Using these expressions it is possible to obtain, following the procedure shown in the case of χ_1^-, the appropriate many-body wavefunctions for every value of B and q, with n chosen in order to satisfy (4.110) (the case of the degeneracy points $q^2 = (2n+1)\,B$ will be analyzed in section 4.7). In particular, for an arbitrary n, all the antisymmetric states given by

$$\Psi^{(m)}_n = \prod_j^N \mathcal{G}_{n,j} \Lambda^{(m)}_N, \tag{4.113}$$

where $\Lambda_N^{(m)}$ is an odd Laughlin state (4.106), are fermionic ground states unaffected by repulsive intra-species contact interactions (here $\mathcal{G}_{n,j}$ indicates the operator $\mathcal{G}_n$ applied to the atom j).

For bosonic wavefunctions in the case of repulsive delta interactions (both intra-species and inter-species) one has to consider the derivatives that are present in the operators $\mathcal{G}_n$ to find a ground state having zero interaction energy. The highest order derivative in $\mathcal{G}_n$ is given by the term ∂_z^n in the $|\downarrow\rangle$ component of each atom. Therefore, to identify the smallest even power m in (4.113) that annihilates a delta interaction, one has to consider for each pair of particles the $|\downarrow\downarrow\rangle$ component: in order to make the repulsive delta interaction null there must be a factor $(z_i - z_j)^m$ with $m > 2n$. Once the polynomial order of the wavefunction (4.113) is high enough to make the interaction in the $|\downarrow\downarrow\rangle$ component vanish, then all the other components also give a null contribution. Therefore, the bosonic wavefunction $\Psi_n^{(2n+2)}$ is the ground state with the smallest polynomial order for a generic repulsive delta interaction.

As a consequence $\Psi_n^{(2n+2)}$ defines the maximum filling factor $\nu_n = 1/(2n+2)$ over which the interaction energy among bosons cannot be zero. In the range (4.110) only states with $\nu < 1/(2n+2)$ can have a null interaction energy for $z_i \to z_j$ in the $|\downarrow\downarrow\rangle_{ij}$ component. This result is coherent with the numerical data obtained in [103], where it is shown that, in the case of $q^2 < 3B$, the Laughlin state with $\nu = 1/2$ has a positive interaction energy, whereas for $\nu = 1/4$ the energy is exactly zero; in this regime, in fact, m must be at least 4 to give a true ground state, as already observed in the previous section. Moreover, the maximum filling factor ν_n decreases as q^2/B increases, therefore the role of interactions becomes more and more important if we consider higher filling factors for high values of q; this could explain why, for $\nu > 1/2 > \nu_n$, there is no numerical evidence of incompressible bosonic states after the first Landau level crossing ($q^2 > 3B$) [103].

4.6 The effect of angular momentum

As mentioned in section 4.2, the single-particle Hamiltonian (4.35) can be considered as the limit of the Hamiltonian H_L (4.44) when the angular velocity Ω approaches the trapping frequency ω; but, so far, we considered only cases in which the condition $\mathcal{P}2$ in section 4.1.3 holds and we neglected an eventual energy contribution of the angular momentum. Nevertheless, this element is important to understand better the physics of the multi-particle states and of their excitations. Therefore, in this section, we analyze the effect of the angular momentum term in the Hamiltonian (4.44) in order to calculate the energy of the states $\Psi_n^{(m)}$ (and their excitations), and the constraints $\Delta = \omega - \Omega$ must satisfy to not spoil the Landau level description.

Let us consider the single-particle Hamiltonian (4.44):

$$H_L = (p + A)^2 - \Delta L_z$$

where $\Delta = \omega - \Omega > 0$. The term proportional to Δ is spin-independent, thus it doesn't affect the non-Abelian contribution H_{na} in (4.72). Using its eigenstates

$\varphi^{\pm}_{n,m}$ (4.77) for $n \geq 1$ we can split H_L into blocks of the form:

$$H_{L,n,m} = 2q^2 + 2Bn - \Delta\left(n - m - \frac{1}{2}\right) + \begin{pmatrix} 2q\sqrt{2Bn} & -B + \frac{\Delta}{2} \\ -B + \frac{\Delta}{2} & -2q\sqrt{2Bn} \end{pmatrix}$$

The eigenenergies of H_L are therefore:

$$\varepsilon^{\pm}_{n,m} = 2Bn + 2q^2 - \Delta\left(n - m - \frac{1}{2}\right) \pm \sqrt{\left(B - \frac{\Delta}{2}\right)^2 + 8q^2Bn} \tag{4.114}$$

and the corresponding unnormalized eigenstates result:

$$\chi^{\pm}_{n,m} = \left(B - \frac{\Delta}{2} + 2q\sqrt{2Bn} \mp \sqrt{\left(B - \frac{\Delta}{2}\right)^2 + 8q^2Bn}\right)\psi_{n-1,m}\,|\uparrow\rangle + \\ + \left(B - \frac{\Delta}{2} - 2q\sqrt{2Bn} \pm \sqrt{\left(B - \frac{\Delta}{2}\right)^2 + 8q^2Bn}\right)\psi_{n,m}\,|\downarrow\rangle\,. \tag{4.115}$$

Besides, the uncoupled eigenstates are not affected by the angular momentum term.

It's important to notice that the coefficients in the definition of the eigenstates do not depend on m. This implies that one can redefine the constants $c_{\uparrow,n}$, $c_{\downarrow,n}$ and the operators $\mathcal{G}_n$ independently of m; moreover, the Landau level structure also holds for H_L (condition $\mathcal{P}1$), and the Landau levels are energetically distinguishable provided that the energy contribution of the angular momentum remains small with respect to the Landau level spacing. In fact, all the energy levels (4.114) present a term which is linear in the total angular momentum $J = n - m - 1/2$ and increases their energy if $J < 0$. Thus the states with lower values of m are favoured. This implies an energy gap Δ for the creation of single-particle quasiholes of the kind (4.91) and 2Δ for (4.92) (for $\zeta = 0$).

In order to understand the stability of the Landau level structure, and thus of the deformed Laughlin states, we must consider a multiparticle wavefunction describing N atoms in a ground state of the kind $\Psi^{(m)}_n$ (4.113) for $2n - 1 < q^2/B < 2n + 1$. In this case an atom corresponding to the highest value of the modulus of the angular momentum term $|J|$ acquires an additional energy $\sim Nm\Delta$ that must be smaller than the gap with the next deformed Landau level. This gap, for values of q^2 far from the degeneracy points, can be calculated by evaluating the energy difference between χ^-_n and χ^-_{n-1} at the crossing point between χ^-_{n-1} and χ^-_{n+1} and it can be approximated by $B/(2n)$. Therefore the Landau level description of the multiparticle states remains accurate if $\Delta \ll B/(2nNm)$.

Let us analyze better the regime characterized by small values of Δ. The deformed Laughlin states $\Psi^{(m)}_n$ must be defined with the appropriate corrections in the operators $\mathcal{G}_n$ (4.111) since the constants $c_\uparrow$ and $c_\downarrow$ must include Δ coherently with (4.115). The corresponding energy contribution of the total angular momentum results, for $\Psi^{(m)}_n$:

$$-\Delta J\Psi^{(m)}_n = \Delta N\left(\frac{mN}{2} - m - n + \frac{1}{2}\right)\Psi^{(m)}_n \approx \Delta m\frac{N^2}{2}\Psi^{(m)}_n. \tag{4.116}$$

Therefore, the Laughlin states with smaller m (and higher density) are energetically favoured: thus, in the case of fermions far from the degeneracy points, the ground states are described by the $\nu = 1$ filling factor states Ψ_n^1, whereas in the case of bosons the ground states are of the form Ψ_n^{2n+2}.

A quasihole in the position $\zeta = 0$

$$\Psi_n^{(m)} = \prod_j^N \mathcal{G}_{n,j} \prod_j^N z_j^k \Lambda_N^{(m)} \tag{4.117}$$

acquires an additional energy $N\Delta k$ with respect to the corresponding ground state, because it changes the angular momentum of each particle by k. This energy can be considered the gap for the creation of a quasihole.

4.7 Degeneracy points and non–Abelian anyons

It is interesting to notice that there are *degeneracy points* corresponding to the values $q^2 = (1 + 2n)\, B$ where the two lowest energy levels cross (possibly generating a first-order phase transition [103]) and the ground state degeneracy of the single particle is doubled. In this case an atom in the ground state can be described by all the superpositions of wavefunctions in χ_n^- and χ_{n+1}^-. However, if we consider the angular momentum term in the Hamiltonian which was described in the previous section, the states with a lower angular are favoured and the variation of the parameter q around the degeneracy points gives rise to a crossover, as we will describe in 4.7.3.

Once we introduce the intra-species interaction between atoms, the doubled degeneracy of the single particle states implies a novel form of the multiparticle ground state which is quite different from (4.105,4.107). Let us consider the case of $q^2 = 3B$ that characterizes the crossing between ground states of particles in χ_1^- and χ_2^- (but our conclusions can be easily generalized to all the crossing points). For the single particle the basis of ground states is defined by the set $\{\mathcal{G}_1 z^m \psi_0(z), \mathcal{G}_2 z^m \psi_0(z),\ \text{with } m \in \mathbb{N}\}$ and, analogously to the previous sections, we must distinguish the case of interacting bosons from that of (free) fermions.

4.7.1 Fermionic gases

Let us analyze first the fermionic gases; in this case the highest density ground state function of the Hamiltonian $\mathcal{H}$ for $2N$ atoms is given by:

$$\Omega_c = \mathcal{A}\left[\mathcal{G}_1\psi_0, \mathcal{G}_1 z\psi_0, \ldots, \mathcal{G}_1 z^{N-1}\psi_0,\ \mathcal{G}_2\psi_0, \mathcal{G}_2 z\psi_0, \ldots, \mathcal{G}_2 z^{N-1}\psi_0\right] |\downarrow\downarrow \ldots \downarrow\rangle \tag{4.118}$$

where $\mathcal{A}$ implements the full antisymmetrization over all the atoms and, because of the doubled degeneracy, this wavefunction describes an atomic gas with filling factor $\nu = 2$. Ω_c is obtained through the Slater determinant of the single-particle wavefunctions with the lowest angular momenta $|J|$, up to the power z^{N-1}; therefore, considering also the angular momentum contribution in the Hamiltonian, it is the true ground state for the system. The doubled degeneracy makes Ω_c very

different from the case (4.105): at the degeneracy points the antisymmetrization hides a clustering of the particles into two sets of N atoms, A and B, that are physically different and refer to states in χ_1^- and in χ_2^-. The two clusters must have the same number of atoms in order to minimize the contribution to the energy given by the angular momentum. Thus, the previous wavefunction can be recast in the following form:

$$\Omega_c = \mathcal{A}\left[\prod_{k\in A}\mathcal{G}_{1,k}\prod_{i<j\in A}(z_i - z_j)\prod_{l\in B}\mathcal{G}_{2,l}\prod_{i<j\in B}(z_i - z_j)\right] e^{-\frac{B}{4}\sum_i^{2N}|z_i|^2}\,|\downarrow\downarrow \ldots \downarrow\rangle\,. \tag{4.119}$$

where we made explicit the Jastrow factor in each cluster and $\mathcal{A}$ refers to the antisymmetrization over all the possible clustering in the sets A and B. In the spirit of the quantum Hall states showing a clustering into two sets (the main example is the Moore and Read (MR) Pfaffian state, see [25, 72]), Ω_c is characterized by the presence of quasihole excitations corresponding to half a quantum flux (and effective charge 1, since $\nu = 2$). These excitations must appear in pairs (see the equation (4.136)), however it is helpful to analyze the two possible wavefunctions they can assume. Such wavefunctions are related to quasiholes in the two different clusters (here we drop the usual Gaussian and spin factors):

$$\sigma_1(\zeta) = \mathcal{A}\left[\prod_A \mathcal{G}_{1,k}\prod_A (z_i - z_j)\prod_A (z_i - \zeta)\prod_B \mathcal{G}_{2,l}\prod_B (z_i - z_j)\right] \tag{4.120}$$

$$\sigma_2(\zeta) = \mathcal{A}\left[\prod_A \mathcal{G}_{1,k}\prod_A (z_i - z_j)\prod_B \mathcal{G}_{2,l}\prod_B (z_i - z_j)\prod_B (z_i - \zeta)\right] \tag{4.121}$$

These quasiholes obey a fermionic statistics: once two of them of the same kind are exchanged, the wavefunction acquires a π phase; however, it is interesting to notice that they show the same fusion rules as the Ising model with defined fermionic parity [124], characterizing the MR state [25, 72], once one defines a third bosonic excitation given by the fusion $\psi \equiv \sigma_1 \times \sigma_2$. From the physical point of view it could be possible to obtain linear superpositions of σ_1 and σ_2 through the interplay between repulsive potentials for the $|\uparrow\rangle$ and $|\downarrow\rangle$ components; one can show that such linear superpositions obey a kind of non-Abelian braiding rules: the exchange of two of them gives a phase π if the two superpositions fuse in the identity channel and a phase 2π if their fusion outcome is ψ (see Sec.. 4.8 for more detail).

In fermionic systems at the degeneracy point $q^2 = 3B$, the ground state Ω_c, characterized by the filling factor $\nu = 2$, is the highest density state obtained with atoms in the Hilbert space spanned by the deformed Landau level χ_1^- and χ_2^-; moreover it minimizes the term in the Hamiltonian proportional to the angular momentum. Nevertheless, in the study of rotating ultracold atomic gases, it is interesting to analyze what happens varying the filling factor, since, in general, such systems present nontrivial phase diagrams as a function of ν [92, 123, 44]. As we have already shown, the doubled degeneracy at this particular value of q^2 provides in a natural way a clustering of the atoms into two sets in order to

minimize $|J|$: each atom can assume a wavefunction which is a superposition of states in χ_1^- and in χ_2^- and the transitions from one to the other are possible; therefore, also for smaller values of the filling factor, we are driven to consider deformed ground states showing a pairing among the atoms that are similar to the ones usually considered in the study of the fractional quantum Hall effect [46].

Let us consider first the filling factor $\nu = 1$; in this case a paired state is built by favouring the creation of coupled atoms in the antisymmetric state obtained by applying the operator $(\mathcal{G}_{1,i}\mathcal{G}_{2,j} - \mathcal{G}_{2,i}\mathcal{G}_{1,j})$ to the pair of atoms (i,j) in the limit $z_i \to z_j$. The corresponding wavefunction for $2N$ particles reads:

$$\Omega_{\rm Hf} = {\rm Hf}\left((\mathcal{G}_{1,i}\mathcal{G}_{2,j} - G_{2,i}G_{1,j})\,\frac{1}{z_i - z_j}\right)\prod_{i<j}^{2N}(z_i - z_j)\,e^{-\frac{B}{4}\sum_i^{2N}|z_i|^2}\,|\downarrow\downarrow \ldots \downarrow\rangle \quad (4.122)$$

where Hf indicates the Haffnian, which is a symmetric version of the Pfaffian defined for a symmetric matrix $M_{ij} = M_{ji}$:

$${\rm Hf}\,(M) = \sum_{\sigma\in\mathcal{P}} M_{\sigma(1),\sigma(2)}M_{\sigma(3),\sigma(4)}\ldots M_{\sigma(2N-1),\sigma(2N)} \quad (4.123)$$

where the sum is over all the permutations of the indices.

The wavefunction $\Omega_{\rm Hf}$ is antisymmetric over all the atoms because it is composed by the symmetric Haffnian and by the antisymmetric Jastrow factor. This implies that intra-species interactions give a zero contribution to the energy and $\Omega_{\rm Hf}$ can be considered a ground state since every atom lies in a superposition of states of χ_1^- and χ_2^-. We must notice, however, that this wavefunction is not zero for $z_i \to z_j$ because of the components with different spin, therefore $\Omega_{\rm Hf}$ is not in general a ground state for inter-species repulsive interactions that require higher powers of the Jastrow factor to give a null contribution.

For $\nu = 1/2$ there are two possible antisymmetric paired states that have been widely analyzed in the literature. The first corresponds to the (deformed) Moore and Read Pfaffian state [25, 72] and the second one corresponds to the Haldane and Rezayi state [125, 25].

The deformed MR pfaffian state can be described by an effective p-wave pairing [46] obtained by applying the operator $(\mathcal{G}_{1,i}\mathcal{G}_{2,j} + \mathcal{G}_{2,i}\mathcal{G}_{1,j})$ which favours a symmetric state (with respect to χ_1^- and χ_2^-) for the pair (i,j) when $z_i \to z_j$. The corresponding wavefunction is:

$$\Omega_{MR} = {\rm Pf}\left((\mathcal{G}_{1,i}\mathcal{G}_{2,j} + \mathcal{G}_{2,i}\mathcal{G}_{1,j})\,\frac{1}{z_i - z_j}\right)\prod_{i<j}^{2N}(z_i - z_j)^2\,e^{-\frac{B}{4}\sum_i^{2N}|z_i|^2}\,|\downarrow\downarrow \ldots \downarrow\rangle \quad (4.124)$$

where Pf is the Pfaffian operator. Also in this case Ω_{MR} is a fermionic wavefunctions unaffected by intra-species contact interactions and it can be considered a ground state since every atom lies in a superposition of states in χ_1^- and χ_2^-. This state shares all the main characteristics of the Moore and Read wavefunctions [25], and, in particular, its excitations are non–Abelian Ising anyons, as shown in [72] where an analogous wavefunction is analyzed. Ω_{MR} can be mapped into the

usual spinless MR state Ψ_{MR} [25, 72] in a way which is similar to Eq. (4.107) for the ground state outside the degeneracy points. Because, for every factor in the Pfaffian, one atoms is in a state in χ_1^- and the other in χ_2^-, the norm of Ω_{MR} is obtained from the one of the Pfaffian state Ψ_{MR} just by multiplying it by a constant value for each pair of atoms:

$$\langle \Omega_{MR} |\, \Omega_{MR} \rangle = \left(|c_{\uparrow,1}|^2 + 8B\, |c_{\downarrow,1}|^2 \right)^N \left(8B\, |c_{\uparrow,2}|^2 + 2(8B)^2\, |c_{\downarrow,2}|^2 \right)^N \langle \Psi_{MR} |\, \Psi_{MR} \rangle \tag{4.125}$$

This constant value can be calculated in a way similar to equation (4.108) and it is an effect of the clustering characterizing the state Ω_{MR}. Equation (4.125) guarantees that also the statistics of the excitations ζ_a and ζ_b of the kind

$$\Omega_{MR}\,(\zeta_a, \zeta_b) = \mathrm{Pf}\left(\frac{\mathcal{G}_{1,i}\mathcal{G}_{2,i}\,(z_i - \zeta_a)\,(z_j - \zeta_b) + i \leftrightarrow j}{z_i - z_j} \right) \Lambda_{2N}^{(2)} \tag{4.126}$$

can be described by Ising anyons as in the case of the Moore and Read state, since the Berry and monodromy phases acquired in the exchange of two excitations coincide.

The other paired ground state at $\nu = 1/2$ is the deformed Haldane and Rezayi state that can be obtained through the introduction of the antisymmetric operator $(\mathcal{G}_{1,i}\mathcal{G}_{2,j} - \mathcal{G}_{2,i}\mathcal{G}_{1,j})$:

$$\Omega_{HR} = \mathrm{Pf}\left((\mathcal{G}_{1,i}\mathcal{G}_{2,j} - \mathcal{G}_{2,i}\mathcal{G}_{1,j})\, \frac{1}{(z_i - z_j)^2} \right) \prod_{i<j}^{2N} (z_i - z_j)^2\, e^{-\frac{B}{4}\sum_i^{2N} |z_i|^2} \,|\downarrow\downarrow \ldots \downarrow\rangle \tag{4.127}$$

This state has a total angular momentum $|J|$ which is lower than that of Ω_{MR} so that, in principle, it is energetically favoured if we consider the single-particle Hamiltonian (4.44). However the Haldane and Rezayi state represents the critical point between a weak and a strong coupling phase in a fermionic system with an effective d-wave pairing [46], therefore it is considered to be a gapless state whose excitations are described by a non-unitary conformal field theory [126] which is unfit to define an incompressible state. Nevertheless it constitutes the ground state of the interaction given by a hollow core Hamiltonian that can be expressed in terms of Haldane pseudopotentials as we will analyze in Sec. 4.10.

Finally, to extend this discussion about the (free) fermionic gases it is worth noticing that all the states presented can also be retrieved for the generic degeneracy point between states in χ_n^- and χ_{n+1}^- by substituting the operators $\mathcal{G}_1$ and $\mathcal{G}_2$ with $\mathcal{G}_n$ and $\mathcal{G}_{n+1}$. This is true in the case of free fermions (i.e., with $g_0 = 0$), whereas the introduction of strong interactions, such as an inter-species contact repulsion, brings to different scenarios presenting deformed Halperin states, similar to the one we will present for the bosonic gases, whose exponents and filling factors also depend on the value of n.

To conclude our description of the fermionic states at the degeneracy points, it is worth noticing that, in the presence of a U(3) gauge potential of the kind analyzed in 4.3.1, there are also triple degeneracy points (see Fig. 4.5). In this case it is natural to assume that a clustering of the atoms in three subsets may

happen, giving rise to a deformed $k = 3$ Read-Rezayi state [70, 73] at $\nu = \frac{3}{5}$. The key aspect of this fermionic state is that its excitations obey the statistics of Fibonacci anyons, that, as we saw in the previous chapters, could provide a basis for a universal topological quantum computation.

4.7.2 Bosonic gases

The analysis of these degenerate points can also be applied to bosonic gases. As described in section 4.5 the state $\Psi_n^{(m)}$ (4.113) is a ground state of both the intra-species and the inter-species interactions for every $m > 2n$, therefore $\Psi_n^{(2n+2)}$ is the bosonic wavefunction with zero interaction energy that minimizes the polynomial order. At the point $q^2 = 3B$ one has a superposition of states in χ_1^- and in χ_2^- and, as in the previous case, we can describe the related multiparticle ground state through the clustering in two corresponding subsets A and B. The resulting ground state, dropping the usual Gaussian and spin factors, is:

$$\Omega_b = \mathcal{S}\left[\prod_{k\in A}\mathcal{G}_{1,k}\prod_{i<j\in A}(z_i-z_j)^4\prod_{l\in B}\mathcal{G}_{2,l}\prod_{i<j\in B}(z_i-z_j)^6\prod_{k\in A,l\in B}(z_k-z_l)^4\right] = \\ = \mathcal{S}\left[\prod_{k\in A}\mathcal{G}_{1,k}\prod_{l\in B}\mathcal{G}_{2,l}\prod_{i<j\in B}(z_i-z_j)^2\right]\Lambda_{2N}^{(4)} \quad (4.128)$$

where the symmetrization over all the atoms is necessary to have a bosonic state and $\Lambda^{(4)}$ is the generalized Laughlin state (4.106). The exponents of the Jastrow factors are defined considering that the lowest-order polynomial term for an atom in A is given by the first derivative included in $\mathcal{G}_1$ whereas in B it is given by the second derivative in $\mathcal{G}_2$. Therefore Ω_b vanishes at least as $(z_i - z_j)$ whenever $z_i \to z_j$ for every pair of atoms, and the intra-species interaction energy is zero. Ω_b is characterized by a filling factor $\nu = 2/9$ and it is built by the symmetrization of the Halperin state $\Psi(4, 6, 4)$. The interaction term between atoms in different clusters is determined in order to satisfy the zero interaction energy constraint:

$$\prod_{k\in A,l\in B}\partial_{z_k}\partial_{z_l}^2(z_k-z_l)^4 \propto (z_k-z_l)$$

The Ω_b filling factor, $\nu = 2/9$, is therefore the highest possible filling factor that guarantees a null interaction energy for bosons at the point $q^2 = 3B$.

We conclude this section by observing that considering different degeneracy points, $q^2 = (2n + 1)B$, the ground states for intra–species repulsions are defined as deformed Halperin states $\Psi(2n + 2, 2n + 4, 2n + 2)$, which are characterized by lower filling factors.

4.7.3 Crossover at a degeneracy point

So far we considered the non-Abelian component of the potential at the exact value $q^2 = (2n+1)B$ which is characterized by a perfect degeneracy of the deformed Landau levels χ_n^- and χ_{n+1}^- and implies that the population of atoms must be equally

distributed into these levels in order to minimize the total angular momentum of the system and thus its total energy. If the parameter q^2 is slightly detuned from these degeneracy points, however, the deformed Landau level with a lower energy will present an increase in population balancing the small energy difference arising between the two state families.

Let us consider, in particular, a system showing a filling factor $\nu_n = 1/m_n$ on the n^{th} Landau level, and let us suppose that q^2 is slightly higher than $(2n+1)B$, so that $\varepsilon^-_{n,m} > \varepsilon^-_{n+1,m}$. To fill the gap between χ^-_n and χ^-_{n+1} there must be an imbalance $M = N_{n+1} - N_n$ between the population of atoms in χ^-_{n+1} and χ^-_n, such that

$$\varepsilon^-_{n+1,\, Mm_{n+1}} \approx \varepsilon^-_{n,0}.$$

Considering the energy eigenvalues given by equation (4.114) one obtains:

$$Mm_{n+1}\Delta \approx \delta q^2 \left.\frac{d\left(\varepsilon^-_{n,0} - \varepsilon^-_{n+1,0}\right)}{dq^2}\right|_{q^2=(2n+1)B} \approx \left(\frac{1}{4n+3} + \frac{1}{4n+1}\right)\delta q^2 \tag{4.129}$$

where δq^2 is the displacement of q^2 from the degeneracy point and we imposed $\Delta \ll B$ in the second approximation. In order to obtain a system described by the deformed Hall states defined above for the degeneracy point at $q^2 = 3B$, the imbalance M must be negligible with respect to the total number of atoms N and, in particular, one obtains the following degeneracy condition on the displacement δq^2 around $3B$:

$$\frac{12}{35}\left|\delta q^2\right| \ll \frac{N}{\nu}\Delta < \left(9 - \sqrt{73}\right) B \approx 0.46B \tag{4.130}$$

where ν is the total filling factor of the system and the further constraint for $N\Delta$ is derived from the energy difference with the third Landau level, χ^-_3, in such a way that all the atoms lie only in the two lower Landau levels. If δq^2 exceeds the previous limit the imbalance M grows until only the population in the lower Landau level is left; therefore the displacement δq^2 drives a crossover between different regimes characterized by wavefunctions in χ^-_n and χ^-_{n+1} such as the deformed Laughlin states in (4.113) and only in the regime defined by the condition (4.130) Hall states presenting particles in both the deformed Landau levels can be present.

4.8 Ω_c and its excitations

In this section we investigate the properties of the fermionic ground state Ω_c (4.119), which minimizes the total angular momentum $|J|$ at the first degeneracy point $q^2 = 3B$, and its excitations. For a system of $2N$ atoms, Ω_c can be written as the following correlation function:

$$\Omega_c = \left\langle : \mathcal{O}_{bg} \prod_i^{2N} \mathcal{V}(z_k) : \right\rangle e^{-\frac{B}{4}\sum_i^{2N}|z_i|^2} \left|\downarrow\downarrow \ldots \downarrow\right\rangle \tag{4.131}$$

where we introduced the vertex operators:

$$\mathcal{V}(Z_k) =: \left(\mathcal{G}_{1,k} c_1 e^{i\frac{\varphi_1}{\sqrt{2}}} + \mathcal{G}_{2,k} c_2 e^{-i\frac{\varphi_1}{\sqrt{2}}}\right) e^{i\frac{\varphi_2}{\sqrt{2}}} : \tag{4.132}$$

and the background charge operator $\mathcal{O}_{bg}$. The vertex operators $\mathcal{V}$ depend on two independent massless bosonic field $\varphi_1(z)$ and $\varphi_2(z)$, defined by

$$\langle \varphi_i(z_1)\varphi_j(z_2)\rangle = -\delta_{ij} \ln(z_1 - z_2), \tag{4.133}$$

and on two Klein factors defined by $\{c_i, c_j\} = 2\delta_{ij}$. Finally the background charge operator depends only on φ_2 and is given by:

$$\mathcal{O}_{bg} = \lim_{z\to\infty} z^{2N^2} : e^{-i\sqrt{2}N\varphi_2} : \tag{4.134}$$

$\mathcal{O}_{bg}$ is defined to guarantee that only the correlations of terms with the same number of atoms in χ_1^- and χ_2^- don't vanish, while the Klein factors c_i ensure that the antisymmetrization in (4.119) is correctly developed. Therefore we can consider φ_1 as the "topological" bosonic field, while φ_2 plays the role of the "charge" field that needs to be compensated by the background charge.

As in the case of the Moore and Read state [124, 127], it is natural to introduce two kinds of elementary quasihole excitations: σ_1 that pierces the χ_1^- states (4.120) and σ_2 that pierces the χ_2^- states (4.121). These excitations can be described with the introduction of the following operators:

$$\sigma_1 =: e^{i\frac{\varphi_1}{\sqrt{2}} + i\frac{\varphi_2}{\sqrt{2}}} :, \qquad \sigma_2 =: e^{-i\frac{\varphi_1}{\sqrt{2}} + i\frac{\varphi_2}{\sqrt{2}}} : \tag{4.135}$$

However, due to their different terms in the topological field φ_1, the quasiholes σ_1 and σ_2 can be inserted only in pairs $\sigma_1(\zeta_a)\sigma_2(\zeta_b)$ as in the case of the Ising operators with definite fermionic parity σ_+ and σ_- in the Moore and Read state [124]. In the case of $2M$ excitations one obtains:

$$\Omega_{qh} = \mathcal{A}\left[\prod_{k\in A}\mathcal{G}_{1,k}\prod_{i<j\in A}(z_i - z_j)\prod_{i\in A}\prod_{h=1}^{M}(z_i - \zeta_h)\cdot \right.$$
$$\left.\prod_{l\in B}\mathcal{G}_{2,l}\prod_{i<j\in B}(z_i - z_j)\prod_{i\in B}\prod_{h=M+1}^{2M}(z_i - \zeta_h)\right] e^{-\frac{B}{4}\sum_i^{2N}|z_i|^2} |\downarrow\downarrow \ldots \downarrow\rangle \tag{4.136}$$

We can calculate the operator product expansion of the operators σ:

$$\sigma_1(\zeta_1) \times \sigma_1(\zeta_2) = (\zeta_1 - \zeta_2) : e^{i\sqrt{2}\varphi_1 + i\sqrt{2}\varphi_2} : \sim (\zeta_1 - \zeta_2)\mathbb{I} \tag{4.137}$$
$$\sigma_2(\zeta_1) \times \sigma_2(\zeta_2) = (\zeta_1 - \zeta_2) : e^{-i\sqrt{2}\varphi_1 + i\sqrt{2}\varphi_2} : \sim (\zeta_1 - \zeta_2)\mathbb{I} \tag{4.138}$$

and

$$\sigma_1 \times \sigma_2 = e^{i\sqrt{2}\varphi_2} \equiv \psi \tag{4.139}$$

The first two equations state that the vertex operators σ_i describes (Majorana) fermions and the terms σ_i^2 must be considered in the topological sector of the identity

$$\mathbb{I} \sim : e^{\pm i\sqrt{2}\varphi_1 + i\sqrt{2}\varphi_2} : \tag{4.140}$$

because they introduce just an excitation of the ground state Ω_c which is bosonic with respect to the atoms and does not affect their phases. The product $\sigma_1 \times \sigma_2$, instead, defines a new kind of excitation, ψ, that describes the quasihole in the wavefunction:

$$\Omega_{qh}(\zeta) = \mathcal{A}\left[\prod_{k\in A}\mathcal{G}_{1,k}\prod_{l\in B}\mathcal{G}_{2,l}\cdot \prod_{i<j\in A}(z_i - z_j)\prod_{i<j\in B}(z_i - z_j)\prod_{i=1}^{2N}(z_i - \zeta)\right] e^{-\frac{B}{4}\sum_i^{2N}|z_i|^2}\,|\downarrow\downarrow \ldots \downarrow\rangle \quad (4.141)$$

We can consider the operator product expansions involving ψ:

$$\psi \times \psi \sim (\zeta_1 - \zeta_2)^2\,\mathbb{I} \quad (4.142)$$
$$\psi \times \sigma_1 \sim (\zeta_1 - \zeta_2)\,\sigma_2 \quad (4.143)$$
$$\psi \times \sigma_2 \sim (\zeta_1 - \zeta_2)\,\sigma_1 \quad (4.144)$$

In particular one can notice from (4.142) that the excitation ψ is a boson whereas the σ_i excitations acquire a phase π when they are exchanged with a ψ. We can summarize the previous OPE with the following non trivial fusion rules:

$$\sigma_1 \times \sigma_1 = \mathbb{I} \qquad \sigma_2 \times \sigma_2 = \mathbb{I} \qquad \psi \times \psi = \mathbb{I} \quad (4.145)$$
$$\sigma_1 \times \psi = \sigma_2 \qquad \sigma_2 \times \psi = \sigma_1 \quad (4.146)$$

These are the well known fusion rules of the excitations of Kitaev's toric code [27] but the statistics that describes the Ω_c quasiholes is different from the one of the toric code Abelian anyons.

We can consider σ_1 and σ_2 as elementary topological excitations for the state Ω_c. From the physical point of view, however, the quasiholes can be obtained through a delta repulsive potential affecting the $|\uparrow\rangle$ or $|\downarrow\rangle$ component of the atoms, as we mentioned in Sec. 4.3. The resulting quasiholes, which are characterized by a zero in the density of the two spin components, are respectively:

$$\Omega_{\uparrow}(\zeta) = \mathcal{A}\left[\prod_{k\in A}\mathcal{G}_{1,k}\prod_{l\in B}\mathcal{G}_{2,l}\prod_{i<j\in A}(z_i - z_j)\prod_{i<j\in B}(z_i - z_j)\cdot \prod_{i\in A}(z_i - \zeta)\prod_{j\in B}(z_i - \zeta)^2\right] e^{-\frac{B}{4}\sum_i^{2N}|z_i|^2}\,|\downarrow\downarrow \ldots \downarrow\rangle = \sigma_1 \times \sigma_2^2 \sim \sigma_1 \quad (4.147)$$

$$\Omega_{\downarrow}(\zeta) = \mathcal{A}\left[\prod_{k\in A}\mathcal{G}_{1,k}\prod_{l\in B}\mathcal{G}_{2,l}\prod_{i<j\in A}(z_i - z_j)\prod_{i<j\in B}(z_i - z_j)\cdot \prod_{i\in A}(z_i - \zeta)^2\prod_{j\in B}(z_i - \zeta)^3\right] e^{-\frac{B}{4}\sum_i^{2N}|z_i|^2}\,|\downarrow\downarrow \ldots \downarrow\rangle = \sigma_1^2 \times \sigma_2^3 \sim \sigma_2, \quad (4.148)$$

where the last simplification concerns the topological sectors and it is dictated by the previous fusion rules. Therefore the two physical quasiholes $\Omega_\uparrow$ and $\Omega_\downarrow$ belong respectively to the topological sectors of σ_1 and σ_2, since they are obtained from the wavefunctions (4.120) and (4.121) by applying the topologically trivial operators σ_i^2. Thus the application of a localized repulsion for either the $|\uparrow\rangle$ or the $|\downarrow\rangle$ component implies the creation of the fermionic excitations σ_1 and σ_2.

As we mentioned before, however, the σ_i vertex operators remind the two chiral spin fields σ_+ and σ_- of the Ising model in the Ramond sector [124] which generate the quasiholes in the MR state. Using the same procedure shown in [128] we can build a non-Abelian anyon (corresponding to the Ising one in the Pfaffian state) using a superposition of σ_1 and σ_2. Therefore we define:

$$\sigma \equiv \frac{\sigma_1 + \sigma_2}{\sqrt{2}} \tag{4.149}$$

The fusion rules for σ result

$$\sigma \times \sigma = (\zeta_1 - \zeta_2)\, \mathbb{I} + \psi \tag{4.150}$$

$$\sigma \times \psi = (\zeta_1 - \zeta_2)\, \sigma \tag{4.151}$$

and show the non-Abelian nature of σ whose quantum dimension is $\sqrt{2}$ as in the Moore and Read case. We can notice that the alternative linear combination $(\sigma_1 - \sigma_2)/\sqrt{2}$ brings to equivalent results. Such linear superposition of the elementary quasiholes may be obtained through the interplay of repulsive potentials for the two different internal state components.

However σ does not describe the usual Ising anyon since its braiding rules are different because of the different conformal weight of the vertex operators with respect to the usual primary field in the Ising minimal model. In particular we can consider the case of four σ excitations in Ω_c that can be described by two independent topological states: in fact, dividing in two pairs the four non-Abelian anyons, the fusion of the two pairs must be described by the same topological sector ψ or $\mathbb{I}$ as in the MR case, which corresponds to the Ising model shown in Sec. 2.3.

In particular the unitary operator describing a braiding ρ_1 of a pair of σ's can be deduced by the relation (4.150). Considering the case of four σ's, the exchange of two anyons in the same couple is described by ρ_1 whereas the exchange of anyons in different couples is described by the operator ρ_2, which is linked to ρ_1 by the associativity matrix $F_\sigma^{\sigma\sigma\sigma}$:

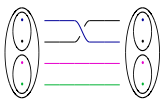

$$\rho_1 = \begin{pmatrix} -1 & 0 \\ 0 & 1 \end{pmatrix},$$

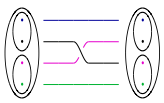

$$\rho_2 = F \rho_1 F^{-1}$$

where ρ_1 is expressed in the basis $(\mathbb{I}, \psi)$. Imposing the Yang - Baxter relation $\rho_1\rho_2\rho_1 = \rho_2\rho_1\rho_2$ one can obtain the following results:

$$\rho_1 = \begin{pmatrix} -1 & 0 \\ 0 & 1 \end{pmatrix}; \qquad \rho_2 = \begin{pmatrix} 1/2 & -\sqrt{3}/2 \\ -\sqrt{3}/2 & -1/2 \end{pmatrix}; \qquad F = \begin{pmatrix} 1/2 & \sqrt{3}/2 \\ \sqrt{3}/2 & -1/2 \end{pmatrix} \tag{4.152}$$

The braidings ρ_i are characterized by the relation $\rho_i^2 = \mathbb{I}$ and they generate a finite subgroup of SU(2) that is not sufficient for a universal quantum computation as in the case of the Ising non-Abelian anyons.

4.9 Haldane pseudopotentials for χ

So far we considered only strong contact interactions and we determined exact ground states characterized by a zero interaction energy. However our analysis can be extended considering more generic interactions between the atoms in different deformed Landau levels through the use of the Haldane pseudopotentials. Such parameters provide us a useful tool to compare the energy acquired as effect of a weak interaction by the many-body ground states we analyzed above. In particular the Haldane pseudopotentials measure the interaction energy between a pair of atoms with relative angular momentum m, and thus, analyzing which relative angular momenta are allowed in a given many-body ground state, allow us to obtain new information about both the states in the non-degenerate regime and the ones at the first crossing point such as the deformed Pfaffian and Haldane-Rezayi states.

In particular let us consider an interaction potential between two atoms with spin s and s' of the form:

$$V_{ss'} = V(r_i - r_j) \left|ss'\right\rangle \left\langle ss'\right| \propto \int d^2q V(|q|) e^{i\vec{q}(\vec{r}_i - \vec{r}_j)} \left|ss'\right\rangle \left\langle ss'\right| \tag{4.153}$$

This potential is invariant under rotations and translations and must be symmetric under the exchange $s \leftrightarrow s'$.

We are interested in calculating the interaction terms involving two atoms in different families. A generic matrix elements can be written as:

$$\begin{aligned} W^{a,b} = \left\langle \chi^-_{a,m_3}\chi^-_{b,m_4}\right| V \left|\chi^-_{a,m_1}\chi^-_{b,m_2}\right\rangle = \\ = |\alpha_{\uparrow,a}\alpha_{\uparrow,b}|^2 \left\langle \psi_{a-1,m_3}\psi_{b-1,m_4}\right| V_{\uparrow\uparrow} \left|\psi_{a-1,m_1}\psi_{b-1,m_2}\right\rangle + \\ + |\alpha_{\downarrow,a}\alpha_{\downarrow,b}|^2 \left\langle \psi_{a,m_3}\psi_{b,m_4}\right| V_{\downarrow\downarrow} \left|\psi_{a,m_1}\psi_{b,m_2}\right\rangle + \\ + |\alpha_{\uparrow,a}\alpha_{\downarrow,b}|^2 \left\langle \psi_{a-1,m_3}\psi_{b,m_4}\right| V_{\uparrow\downarrow} \left|\psi_{a-1,m_1}\psi_{b,m_2}\right\rangle + \\ + |\alpha_{\downarrow,a}\alpha_{\uparrow,b}|^2 \left\langle \psi_{a,m_3}\psi_{b-1,m_4}\right| V_{\downarrow\uparrow} \left|\psi_{a,m_1}\psi_{b-1,m_2}\right\rangle \end{aligned} \tag{4.154}$$

where $\alpha_{s,n}(q, B)$ is the normalized coefficient of the component s of the wavefunction χ_n^- in (4.83).

Following Jain [129] it is possible to express the matrix elements of the usual Landau levels as functions of the ones in the lowest Landau level and, in particular:

$$\begin{aligned}\left\langle \psi_{n,m_3}\psi_{n',m_4}\right| e^{i\vec{q}(\vec{r}_i-\vec{r}_j)} \left|\psi_{n,m_1}\psi_{n',m_2}\right\rangle = \\ = L_n\left(\frac{q^2}{2}\right) L_{n'}\left(\frac{q^2}{2}\right) \left\langle \psi_{0,m_3}\psi_{0,m_4}\right| e^{i\vec{q}(\vec{r}_i-\vec{r}_j)} \left|\psi_{0,m_1}\psi_{0,m_2}\right\rangle \end{aligned} \quad (4.155)$$

where L_n are Laguerre polynomials.

Since the potential depends only on the distance between the two atoms, to evaluate the matrix element referring to the lowest Landau level it is convenient to introduce the center of mass coordinate Z and the relative coordinate z of the two atoms:

$$Z = \frac{z_1+z_2}{2}, \qquad z = z_1 - z_2 \quad (4.156)$$

It is possible to show that the Hamiltonian for a system of two atoms decouples in these coordinates [129] and, in particular, one can rewrite the two-body wavefunction of the atoms with *relative angular momentum* m in the lowest Landau level in the following way:

$$\phi_m = C_m\,(z_1-z_2)^m\, e^{-\frac{B}{4}\left(|z_1|^2+|z_2|^2\right)} = C_m z^m e^{-\frac{B}{2}|Z|^2-\frac{B}{8}|z|^2} \quad (4.157)$$

where C_m is the proper normalization. Considering the matrix element on the right-hand side of (4.155), every wavefunction of the kind $\psi_{0,m_1}\psi_{0,m_2}$ can be decomposed in terms of wavefunctions $Z^M\phi_m$, but all the terms in the center of mass coordinates Z factor out and don't contribute to the evaluation of the matrix element because the potential depends only on z. Therefore only the factors in the relative coordinate provide nontrivial results and it is convenient to consider the following matrix elements:

$$\left\langle \phi_{m'}\right| e^{i\left(\frac{q}{2}z+\frac{\bar{q}}{2}\bar{z}\right)} \left|\phi_m\right\rangle = \delta_{m,m'} e^{-|q|^2} \sum_{j=0}^{m} (-q\bar{q})^j \frac{m!}{j!^2\,(m-j)!} = \delta_{m,m'} e^{-|q|^2} L_m\left(|q|^2\right) \quad (4.158)$$

with $q = q_x + iq_y$ and $\bar{q} = q_x - iq_y$. The first equality is obtained by decomposing z and $\bar{z}$ in the usual ladder operators but considering that the Gaussian component of the wavefunctions in z differs by a factor 2 in the exponent. The equation (4.155) can be proved with the same procedure [129].

Finally all the terms in the generic matrix element $W^{a,b}$ in (4.154) can be decomposed in the same way in terms characterized by a relative angular momentum (in the lowest Landau level) m. Therefore the potential $V(q^2)$ can be expressed as a series of Laguerre polynomial $L_m(q^2)$ corresponding to the Haldane pseudopotentials. To analyze the behaviour of the many-body ground states in the non-degenerate regime we consider the case $a = b = n$:

$$\begin{aligned} W_m^{n,n} = \left\langle \chi_n^- \chi_n^-\right| V_m \left|\chi_n^- \chi_n^-\right\rangle = \\ = \left|\alpha_{\uparrow,n}\alpha_{\uparrow,n}\right|^2 V_{m,\uparrow\uparrow}^{n-1,n-1} + \left|\alpha_{\downarrow,n}\alpha_{\downarrow,n}\right|^2 V_{m,\downarrow\downarrow}^{n,n} + 2\left|\alpha_{\uparrow,n}\alpha_{\downarrow,n}\right|^2 V_{m,\uparrow\downarrow}^{n,n-1} \end{aligned} \quad (4.159)$$

where the Haldane potentials $V_m^{n,n'}$ in the rotational invariant case are obtained considering the equations (4.155) and (4.158):

$$V_m^{n,n'} \propto \int q\, dq\, V(q)\, L_n\left(\frac{q^2}{2}\right) L_{n'}\left(\frac{q^2}{2}\right) L_m\left(q^2\right) e^{-q^2} \tag{4.160}$$

Since all the atoms in the many body ground states belong to the same deformed Landau level χ_n^-, the symmetry of the wavefunctions depends only on the relative angular momentum m and only odd (even) values of m must be considered for fermionic (bosonic) systems.

At the degeneracy points, instead, we must consider also the interactions of atoms belonging to different deformed Landau levels such that $a = b - 1 = n$. For instance, in the case $q^2 = 3B$, the interactions between two atoms in χ_1^- and χ_2^- are defined by the following terms:

$$\begin{aligned} W_m^{1,2} = \left\langle \chi_1^- \chi_2^- \right| V_m \left| \chi_1^- \chi_2^- \right\rangle = |\alpha_{\uparrow,1}\alpha_{\uparrow,2}|^2 V_{m,\uparrow\uparrow}^{0,1} + |\alpha_{\downarrow,1}\alpha_{\downarrow,2}|^2 V_{m,\downarrow\downarrow}^{1,2} + \\ + |\alpha_{\uparrow,1}\alpha_{\downarrow,2}|^2 V_{m,\uparrow\downarrow}^{0,2} + |\alpha_{\downarrow,1}\alpha_{\uparrow,2}|^2 V_{m,\uparrow\downarrow}^{1,1} \end{aligned} \tag{4.161}$$

It is important to notice that both even and odd values of the relative angular momentum are allowed in the pseudopotentials $V_{m,\uparrow\uparrow}^{n,n'}$ and $V_{m,\downarrow\downarrow}^{n,n'}$ for $n \neq n'$ since we are dealing with atoms in different Landau levels and both even and odd powers of the relative coordinate z can be present. In the case of delta interaction in the intra-species component, however, the antisymmetric wavefunctions guarantee that the contributions from $V_{m,\uparrow\uparrow}^{n,n'}$ and $V_{m,\downarrow\downarrow}^{n,n'}$ cancel out.

4.10 Weak inter-species repulsive contact interaction

In the previous study of the quantum Hall states we considered the case of strong intra-species interactions that, for fermions, is equivalent to free atoms. Using the Haldane pseudopotentials it is possible to get a deeper insight on the effects of the introduction of a weak repulsive inter-species delta interaction, whose intensity must be small compared to the gap between different Landau levels to avoid level mixing. The two-body inter-species potential we introduce assumes the following constant value in momentum space:

$$V_{\uparrow\downarrow}(q) = 2\pi v > 0\,, \qquad V_{\uparrow,\uparrow} = V_{\downarrow,\downarrow} = 0 \tag{4.162}$$

where $q = |\vec{q}|$. The choice for $V_{\uparrow,\uparrow}$ and $V_{\downarrow,\downarrow}$ corresponds to the fact that fermionic wavefunctions are ground states for intra-species interactions.

From the counting of the derivatives in the operators $\mathcal{G}_n$ it is easy to show that, for strong inter-species interaction in a fermionic system, the ground state of a system far from the degeneracy points is a deformed Laughlin state of the kind $\Psi_n^{(2n+1)}$, whereas at the degeneracy point $q^2 = 3B$, the fermionic ground state assumes a form similar to (4.128) obtained by the antisymmetrization of a deformed Halperin state $\Psi(3,5,3)$ with filling factor $\nu = 2/7$.

In the following we will consider instead the case of weak inter-species interaction such that the interaction energy of the state is lower than their total angular

momentum contribution. Let us investigate first the non-degenerate regime; for the wavefunctions χ_1^- which are the lowest Landau level for $0 < q' \equiv q/\sqrt{B} < \sqrt{3}$, the pseudopotentials (4.159) result:

$$W_0^{1,1} = W_1^{1,1} = \frac{q'}{1+8q'} v\,, \qquad W_{m>1}^{1,1} = 0. \tag{4.163}$$

The terms for relative angular momenta higher than 1 are zero as expected by the derivative counting (here we included also the even values of m that are significant for bosonic gases), therefore the deformed Laughlin state $\Psi_0^{(3)}$ at $\nu = 1/3$ is the highest density ground state for contact inter-species repulsions at $q^2 < 3B$.

For the wavefunctions χ_2^-, which constitute the lowest Landau level for $\sqrt{3} < q' \equiv q/\sqrt{B} < \sqrt{5}$, the pseudopotentials are instead:

$$W_0^{2,2} = W_3^{2,2} = \frac{3q'}{2+32q'} v\,, \quad W_1^{2,2} = W_2^{2,2} = \frac{q'}{2+32q'} v\,, \quad W_{m>3}^{2,2} = 0. \tag{4.164}$$

In this deformed Landau level, the terms of relative angular momenta higher than 3 vanish as expected by the counting of derivatives in the wavefunctions. Moreover, it is interesting to notice that the pseudopotentials for χ_2^- do not decrease monotonically with m, as in the case of the Coulomb potential in the first excited Landau level; in particular $W_1^{2,2} < W_3^{2,2}$, so that the pairs of atoms with relative angular momentum $m = 1$ are energetically favoured with respect to the ones with $m = 3$, which could have important consequences in the structures of the many-body states for $3B < q^2 < 5B$.

Finally, at the degeneracy point $q^2 = 3B$ (see Fig. 4.7) one recovers the following values for the pseudopotentials (the label (b) indicates the bosonic case):

$q^2 = 3B$	$m = 0$	$m = 1$	$m = 2$	$m = 3$	$m \geq 4$
$W_m^{1,2}$	$5v/56$	$9v/140$	$5v/56$	0	0
$W_m^{1,1}$	$3v/25^{(b)}$	$3v/25$	0	0	0
$W_m^{2,2}$	$9v/98^{(b)}$	$3v/98$	$3v/98^{(b)}$	$9v/98$	0

In particular the pseudopotentials of the kind $W^{1,2}$ help us to compare the energy of the deformed Moore and Read state Ω_{MR} and of the deformed Haldane and Rezayi state Ω_{HR}. As we described in the previous section both of them are characterized by a filling factor $\nu = 1/2$ but the first one, Ω_{MR}, is defined as a "triplet" wavefunction for atoms in χ_1^- and χ_2^-. Therefore it is a zero energy state with respect to the pseudopotential W_0 whereas it acquires energy if $W_1 > 0$; instead the second one, Ω_{HR}, is built as a 'singlet' wavefunction and it is the ground state for the "hollow core" Hamiltonian given by $W_0 = 0$ and $W_1 \neq 0$ and it acquires a positive energy if $W_0 > 0$.

From the results of the previous table we have that $W_0^{1,2} > W_1^{1,2}$ and, in particular, $W_0^{1,2}/W_1^{1,2} \simeq 1.39$; therefore the energy contribution of pairs in the "singlet" component are higher than the ones in the "triplet component". If we assume that all the energy contribution provided to Ω_{MR} and Ω_{HR} are the same for all the other pairs of atoms (either pairs in the same deformed Landau level or pairs with

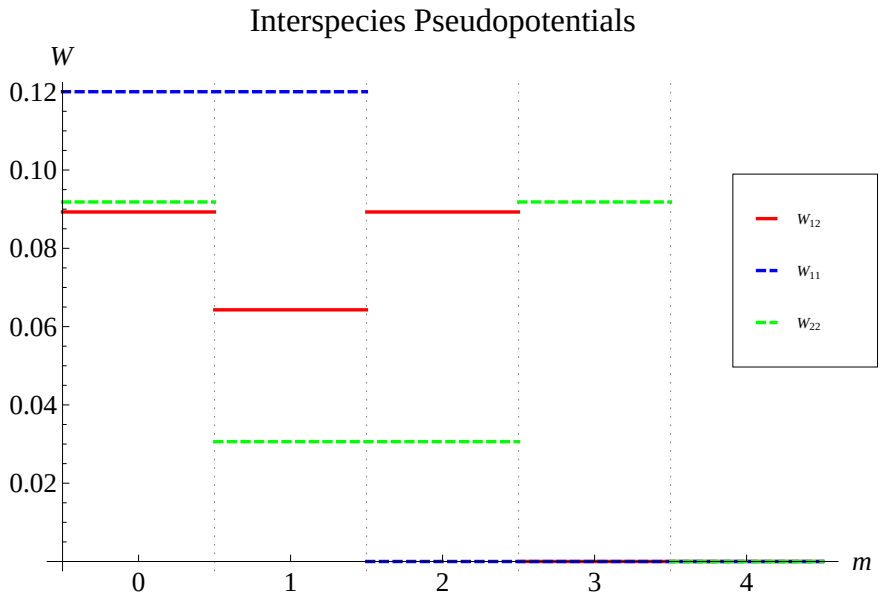

Figure 4.7: Pseudopotentials for an inter-species contact interaction at the degeneracy point $q^2 = 3B$. The red lines represent the value of W_{12} which is zero for $m > 2$; the blue and green dotted lines correspond respectively to the pseudopotentials W_{11} and W_{22} that must be considered in fermionic (odd $m = 1, 3$) or bosonic ($m = 0, 2$) cases.

$m > 1$), then we must conclude that an inter-species contact repulsion energetically favours the deformed Moore and Read state with respect to the Haldane and Rezayi wavefunction. However it is important to consider also the angular momentum contribution that, instead, is lower for Ω_{HR} by the quantity $N\Delta/2$. Our conclusion is that a weak inter-species interaction could fill this energy gap at filling factor $\nu = 1/2$, making the deformed Moore and Read state the ground state of the system.

Finally we must notice that the contact inter-species repulsion is also characterized by a positive energy value for the "singlet" pairs at $m = 2$, $W_2^{1,2} > W_1^{1,2} > 0$. This result implies that such components cannot be present in the degenerate spectrum of the quasihole excitations of the ground states at $\nu = 1/2$. Therefore the excitation spectrum of the Moore and Read state is favoured by the inter-species repulsion with respect to the spectrum of the Abelian deformed Helperin state $\Psi(3, 3, 1)$, as shown in [72].

4.11 Concluding remarks

In this chapter we analyzed cold atomic gases characterized by the interplay of an artificial magnetic field and a uniform non-Abelian SU(2) potential, equivalent to a spin-orbit coupling. The presence of the magnetic field breaks the time reversal

symmetry, therefore all the systems investigated belong to the universality class of the quantum Hall effect and we showed that it is possible to build a mapping between the deformed Landau levels, obtained as an effect of the pseudospin mixing, and the usual unpolarized states. At the level of many-body states, such mapping preserve the Berry phases related to the exchanges of pairs of quasiholes and, thus, their excitation statistics.

We investigated the effect of general homogeneous non-Abelian SU(2) potential and we detected three classes of (quadratic) Hamiltonians preserving an analytically defined Landau level structure, whose eigenstates are expressed as a finite linear combination of the eigenstates of a particle in a magnetic field. The first class corresponds to an Abelian $U(1) \times U(1)$ gauge potential and it refers to uncoupled internal states, whereas the other two are characterized by a truly non-Abelian $U(2)$ gauge potential and correspond to different kinds of Jaynes-Cummings models.

The spin degeneracy of the single-particle Hamiltonian is in general lifted by this kind of interaction; however, there are crossing points of the Landau levels where such degeneracy is recovered. Thanks to this feature non-Abelian gauge potentials could provide a useful playground to investigate the transition (or the crossover) between fully polarized and spinful quantum Hall systems, or equivalently, between monolayer and bilayer setups.

Moreover we analyzed the effect of an angular moment term on the stability of the Landau level structure and of the deformed Laughlin states and we provided an estimate of the values of the angular momentum such that the Landau level description of the multiparticle states remains accurate. We also gave results for $U(3)$ gauge potentials acting on a three–component gas, pointing out that it is possible to have lines of degeneracy points of the Landau levels and triple degeneracies in the spectrum.

In this work we considered only contact interactions, well-suited to ultracold atoms; however the Haldane pseudopotentials we presented constitute the basic tools to introduce also long range potentials such as dipolar interactions. Different kinds of interaction could in principle stabilize different kinds of strongly correlated states, supplying the opportunity of obtaining different topological states.

The setup we described is based on the possibility of simulating non-Abelian gauge potentials through Raman couplings in tripod atoms; however the results we obtained are general and characterize every system described by a gauge-equivalent potential. Since in the last year different experimental setups have been realized to implement a spin-orbit coupling in Bose-Einstein condensate [112, 113] and there are also promising attempts to obtain effective magnetic and electric fields in ultracold atom gases [91, 130], we hope that in the near future it will be possible to experimentally verify the results here exposed.

Summary

Even if the experimental realization of a topological quantum computer is an extremely challenging task whose achievement appears unlikely in a near future, it is incontrovertible that the study of topological order benefited from the theoretical investigation of anyons under the light of fault-tolerant quantum computation.

The work exposed in this thesis is an example of how topological quantum computation can both inspire advances in quantum computation and be a compelling motivation for the study of new strongly correlated quantum systems such as the ones offered by interacting ultracold atoms.

From the point of view of quantum computation I proposed in Chapter 3 a new and efficient algorithm, the quantum hashing, to approximate every target gate in SU(2) in terms of elementary operators in a universal basis. Such approach is naturally applied to describe single-qubit gates as braids of Fibonacci anyons, and, in such frame, I showed that the hashing procedure allows to overcome the technical difficulties of the brute-force approach in reaching high accuracies and it is more efficient than the Solovay-Kitaev algorithm.

The quantum hashing is based, in general, on the composition rules of a subgroup of the target space SU(2). In Chapter 3 I mainly adopted the icosahedral group, the largest polyhedral subgroup; however I presented also the comparison with the results obtained with the cubic group and, in general, the efficiency of the quantum hashing can be estimated through a connection with the random matrix theory.

Dealing with non-Abelian anyons, one of the main mathematical elements of the the anyonic models presented in Chapter 2 is the exponential growth of the Hilbert space with the number of elements considered. Therefore, beside the well-known quantum Hall states presenting non-Abelian excitations, it is quite straightforward to assume that a possible route in the quest for non-Abelian anyons is to consider systems constituted by multicomponent particles, characterized by an exponentially large Hilbert space. Hence, in Chapter 4, I chose, on one side, to examine ultracold atomic gases with a pseudospin degree of freedom and, on the other, to involve such pseudospin in the dynamics of the system through a non-Abelian gauge potential, given the possibility of experimentally realizing such setups.

The homogeneous artificial non-Abelian gauge potentials I considered are equivalent to spin-orbit couplings affecting the ultracold atoms. Interestingly enough, this is the key element that characterizes the innovative studies of another family of topological condensed matter systems, the topological insulators and superconductors, which, under well defined conditions, bring to the presence

of Majorana fermions corresponding to non-Abelian Ising anyons.

In Chapter 4 I investigated the effect of U(2) gauge potentials over the quantum Hall system provided by a rotating ultracold gas. In particular I addressed the problem of determining classes of homogeneous non-Abelian potentials preserving the Landau level structure, which is a necessary condition to enter the quantum Hall regime. We analyzed a particular potential, gauge-equivalent to both the Rashba and the Dresselhaus spin-orbit coupling, whose energy eigenstates can be analytically determined through the mapping to a Jaynes-Cummings model and give rise to deformed Landau levels.

These deformed Landau levels can be mapped to the usual spin-polarized Landau levels of the quantum Hall systems and I showed that the introduction of strong contact interactions in the system, which well describe the interactions between neutral atoms, brings in general to deformed Laughlin states presenting Abelian anyons as quasiholes.

There are, however, degeneracy points of the deformed Landau levels that are characterized by a richer set of fractional quantum Hall ground states that include also deformed non-Abelian states such as the Moore and Read and the Haldane and Rezayi states; moreover, more general interactions can be examined through the study of Haldane pseudopotentials.

Considering the fast progress of the last years in the experimental simulation of artificial magnetic field and spin-orbit couplings in ultracold Bose-Einstein condensates, I hope that the systems analyzed in this thesis could offer a new possibility of creating non-Abelian anyons and open new opportunities towards the realization of a topological quantum computer.

Appendix A

Best approximation in a set of braids

In this Appendix we derive the distribution of the approximation to a gate in a given set of N braids in the vicinity of the identity. While it is sufficient for the discussions in the main text, this derivation can be generalized to more generic cases. Let us assume that the targeted gate is $g_0 = U(\hat{l}, \phi_0)$ as defined in Eq. (3.5). The distance between g_0 and the identity is $s_0 = 2\sin(\phi_0/4) \approx \phi_0/2$ for small ϕ_0. We then search for, in a given set of braids either with a distribution as given in Eq. (3.14) or from a generated random matrix distribution as discussed in Sec. 3.2.2, the one with the shortest distance to the target.

We consider an arbitrary braid with representation $g = U(\hat{m}, \phi)$ in a collection with a distribution $p(s)$ of the distance to the identity $s = 2\sin(\phi/4)$. We define

$$P(x) = \int_0^x p(s)ds, \tag{A.1}$$

which is the probability of having a distance less than $x \leq \sqrt{2}$. Obviously $P(x)$ is a monotonically increasing function bound by $P(0) = 0$ and $P(\sqrt{2}) = 1$. The distance $d(g_0, g)$ between g and g_0 is the same as that between $g_0^{-1}g$ and the identity. To the first order in ϕ and ϕ_0 (as we assume all braids/gates are in the vicinity of the identity braid) we have, from Eq. (3.7)

$$d(g_0, g) \approx \sqrt{s^2 + s_0^2 - 2(\hat{l}\cdot\hat{m})s_0 s} = \left|\left|s\hat{m} - s_0\hat{l}\right|\right|, \tag{A.2}$$

which is bound by $s + s_0$ and $|s - s_0|$. We can see that the chance to find a braid that is close to g_0 is large when $p(s)$ peaks around s_0. If we denote the probability of having no braids within a distance of t by $Q(t)$, the probability of having the braid with the shortest distance between t and $t + dt$ is

$$Q(t) - Q(t + dt) = Q(t)\left\langle Ndt\int_0^{\sqrt{2}} p(s)ds\delta\left(t - d(g_0, g)\right)\right\rangle, \tag{A.3}$$

where the angular brackets imply the angular average of the averaged number of

braids with a distance between t and $t+dt$. Therefore,

$$-\frac{d\ln Q(t)}{dt} = N\left\langle \int_0^{\sqrt{2}} p(s)ds\delta\left(t-d(g_0,g)\right)\right\rangle. \tag{A.4}$$

As an example, we consider $s_0 = 0$ (i.e., with the full SU(2) rotation symmetry of the distribution), in which case

$$-\ln Q(t) = N\int_0^t p(s)ds = NP(t), \tag{A.5}$$

or $Q(t) = \exp[-NP(t)]$. $NP(t)$ is the expected number of braids with a distance to the identity less than t. The differential probability of having the braid with the nearest distance between t and $t+dt$ is, therefore,

$$q(t) \equiv -\frac{dQ(t)}{dt} = N\frac{dP(t)}{dt}e^{-NP(t)} = Np(t)e^{-NP(t)}. \tag{A.6}$$

Combining the results with Eq. (3.14), we estimate for the brute-force search

$$q_{BF}(t;L) = N(L)p_{BF}(t)e^{-N(L)P_{BF}(t)} \tag{A.7}$$

with an average distance

$$\bar{d}(L) = \frac{\pi^{1/3}\left[\Gamma\left(\frac{1}{3}\right) - \Gamma\left(\frac{1}{3}, \frac{8\sqrt{2}N(L)}{3\pi}\right)\right]}{6^{2/3}[N(L)]^{1/3}} \tag{A.8}$$

where $\Gamma(a,x)$ is the incomplete gamma function

$$\Gamma(a,x) = \int_x^\infty dt t^{a-1}e^{-t}. \tag{A.9}$$

In the large L limit, $\bar{d}(L) \approx 1.021e^{-L/5.970}$. This is the result quoted in Eq. (3.15).

The general distribution (A.6) can be used also to roughly evaluate the error reduction factor f of the iterations of the hashing procedure. By substituting the Wigner-Dyson distribution (3.22) with average value s_0 inside (A.6), one obtains the following approximation for the average value ε_i of the error of the output braid $\tilde{T}_i$ at the i^{th} iteration:

$$\varepsilon_i \approx \bar{d}\,(N,s_0) = s_0\int_0^\infty dt\, Nt^3 e^{-\frac{4t^2}{\pi}-\frac{32N}{\pi^2}\int_0^t ds\, s^2 e^{-\frac{4s^2}{\pi}}} \approx \frac{\pi^{1/3}\Gamma\left(\frac{1}{3}\right)s_0}{2\cdot 6^{2/3}N^{1/3}} \approx 0.87\frac{s_0}{N^{1/3}} \tag{A.10}$$

where the approximation of the integral has been calculated through a series expansion for large N, coherently with the required values of the icosahedral and cubic groups, 60^3 and 24^4. Considering $s_0 \sim \sqrt{n+1}\varepsilon_{i-1}$, Eq. (A.10) justifies the factor $f \sim \frac{N^{1/3}}{\sqrt{n+1}} = 30$ assumed in Sec. 3.2.2 and verified by the average data in Table 3.2. The correct numerical prefactor in f, however, cannot be exactly determined by the previous equation since the mesh $\mathcal{S}(L_i,n)$ used in the iteration of the hashing procedure results centered in the unitary operator corresponding to the braid $\tilde{T}_{i-1}$, and not in the target gate T as supposed by the application of the distribution (A.6). This discrepancy, in our opinion, should increase the previous prefactor 0.87 according to the value $f \sim 30$ shown by the data in Table 3.2.

Bibliography

[1] M. Burrello, H. Xu, G. Mussardo, and X. Wan, Phys. Rev. Lett. **104**, 160502 (2010).

[2] M. Burrello, G. Mussardo, and X. Wan, New J. Phys. **13**, 025023 (2011).

[3] M. Burrello and A. Trombettoni, Phys. Rev. Lett. **105**, 125304 (2010).

[4] M. Burrello and A. Trombettoni, arXiv:1108.0839 (2011).

[5] K. von Klitzing, G. Dorda, and M. Pepper, Phys. Rev. Lett. **45**, 494 (1980).

[6] R. B. Laughlin, Phys. Rev. B **23**, 5632 (1981).

[7] D. J. Thouless, M. Kohmoto, M. P. Nightingale, and M. den Nijs, Phys. Rev. Lett. **49**, 405 (1982).

[8] Q. Niu, D. J. Thouless, and Y.-S. Wu, Phys. Rev. B **31**, 3372 (1985).

[9] D. C. Tsui, H. L. Stormer, and A. C. Gossard, Phys. Rev. Lett. **48**, 1559 (1982).

[10] X. G. Wen, Adv. Phys. **44**, 405 (1995).

[11] A. Zee, L. N. Phys. **456**, 99 (1995).

[12] A. Y. Kitaev, Ann. Phys. **321**, 2 (2006).

[13] A. Lopez and E. Fradkin, Phys. Rev. B **44**, 5246 (1991).

[14] S. C. Zhang, Int. Jour. Mod. Phys. B **6**, 25 (1992).

[15] E. Witten, Comm. Math. Phys. **117**, 353 (1988).

[16] E. Witten, Comm. Math. Phys. **121**, 351 (1989).

[17] L. H. Kauffman and S. J. Lomonaco Jr., New J. Phys. **6**, 134 (2004).

[18] M. A. Levin and X. G. Wen, Phys. Rev. B **71**, 045110 (2005).

[19] L. Fidkowski *et al.*, Comm. Math. Phys. **287**, 805 (2009).

[20] C. Nayak *et al.*, Rev. Mod. Phys. **80**, 1083 (2008).

[21] R. B. Laughlin, Phys. Rev. Lett. **50**, 1395 (1983).

[22] D. Arovas, J. R. Schrieffer, and F. Wilczek, Phys. Rev. Lett. **53**, 722 (1984).

[23] J. K. Jain, Phys. Rev. Lett. **63**, 199 (1989).

[24] R. Willett *et al.*, Phys. Rev. Lett. **59**, 1776 (1987).

[25] G. Moore and N. Read, Nucl. Phys. B **360**, 362 (1991).

[26] P. Di Francesco, P. Mathieu, and D. Senechal, *Conformal Field Theory* (Springer Verlag, New York, 1996).

[27] A. Y. Kitaev, Ann. Phys. **303**, 2 (2003).

[28] P. Fendley and E. Fradkin, Phys. Rev. B **72**, 024412 (2005).

[29] P. Fendley, Jour. Phys. A: Math. Gen. **39**, 15445 (2006).

[30] P. Fendley, Ann. Phys. **323**, 3113 (2008).

[31] F. Burnell and S. H. Simon, Ann. Phys. **325**, 2550 (2010).

[32] M. H. Freedman, A. Kitaev, and Z. Wang, Comm. Math. Phys. **227**, 587 (2002).

[33] M. H. Freedman, M. J. Larsen, and Z. Wang, Comm. Math. Phys. **227**, 605 (2002).

[34] M. H. Freedman, M. J. Larsen, and Z. Wang, Comm. Math. Phys. **228**, 177 (2002).

[35] A. Marzuoli and M. Rasetti, Phys. Lett. A **306**, 79 (2002).

[36] A. Marzuoli and M. Rasetti, Ann. of Phys. **318**, 345 (2005).

[37] N. E. Bonesteel, L. Hormozi, G. Zikos, and S. H. Simon, Phys. Rev. Lett. **95**, 140503 (2005).

[38] S. H. Simon *et al.*, Phys. Rev. Lett. **96**, 070503 (2006).

[39] L. Hormozi, G. Zikos, N. E. Bonesteel, and S. H. Simon, Phys. Rev. B **75**, 165310 (2007).

[40] L. Hormozi, N. E. Bonesteel, and S. H. Simon, Phys. Rev. Lett. **103**, 160501 (2009).

[41] H. Xu and X. Wan, Phys. Rev. A **78**, 042325 (2008).

[42] H. Xu and X. Wan, Phys. Rev. A **80**, 012306 (2009).

[43] G. K. Brennen and J. K. Pachos, Proc. R. Soc. A **464**, 1 (2008).

[44] N. R. Cooper, Adv. Phys. **57**, 539 (2008).

[45] S. Das Sarma, C. Nayak, and S. Tewari, Phys. Rev. B **73**, 220502 (2006).

[46] N. Read and D. Green, Phys. Rev. B **61**, 10267 (2000).

[47] M. Z. Hasan and C. L. Kane, Rev. Mod. Phys. **82**, 3045 (2010).

[48] S. Ryu, A. P. Schnyder, A. Furusaki, and A. W. W. Ludwig, New J. Phys. **12**, 065010 (2010).

[49] L. Fu and C. L. Kane, Phys. Rev. Lett. **100**, 096407 (2008).

[50] J. Alicea *et al.*, Nat. Phys **7**, 412 (2011).

[51] R. M. Lutchyn, J. D. Sau, and S. Das Sarma, Phys. Rev. Lett. **105**, 077001 (2010).

[52] J. Preskill, Lecture Notes on Topological Quantum Computation, available online at www.theory.caltech.edu/ preskill/ph219/topological.pdf.

[53] F. Wilczek, Phys. Rev. Lett. **48**, 1144 (1982).

[54] V. J. Goldman and B. Su, Science **267**, 1010 (1995).

[55] S. M. Girvin, Séminaire Poincaré **2**, 53 (2004).

[56] A. Stern, Ann. Phys. **323**, 204 (2008).

[57] M. O. Goerbig, arXiv:0909.1998 (2009).

[58] P. H. Bonderson, Non-Abelian Anyons and Interferometry, PhD Thesis, 2007, available online at http://thesis.library.caltech.edu/2447/.

[59] R. De Picciotto *et al.*, Nature **389**, 162 (1997).

[60] M. Dolev *et al.*, Nat. **452**, 829 (2008).

[61] R. L. Willett, L. N. Pfeiffer, and K. W. West, PNAS **106**, 8853 (2009).

[62] R. L. Willett, L. N. Pfeiffer, and K. W. West, Phys. Rev. B **82**, 205301 (2010).

[63] S. Trebst, M. Troyer, Z. Wang, and A. W. W. Ludwig, Prog. Theor. Phys. Suppl. **176**, 384 (2008).

[64] J. Ruseckas, G. Juzeliūnas, P. Öhberg, and M. Fleischhauer, Phys. Rev. Lett. **95**, 010404 (2005).

[65] G. Mussardo, *Statistical Field Theory* (Oxford University Press, Oxford, 2009).

[66] E. Ardonne *et al.*, New J. Phys. **13**, 045006 (2011).

[67] V. S. Dotsenko and V. Fateev, Nucl. Phys. B **240**, 312 (1984).

[68] A. Feiguin *et al.*, Phys. Rev. Lett. **98**, 160409 (2007).

[69] S. Trebst *et al.*, Phys. Rev. Lett. **101**, 050401 (2008).

[70] N. Read and E. Rezayi, Phys. Rev. B **59**, 8084 (1999).

[71] E. Ardonne and K. Schoutens, Phys. Rev. Lett. **82**, 5096 (1999).

[72] C. Nayak and F. Wilczek, Nucl. Phys. B **479**, 529 (1996).

[73] A. Cappelli, L. S. Georgiev, and I. T. Todorov, Nucl. Phys. B **599**, 499 (2001).

[74] J. S. Xia *et al.*, Phys. Rev. Lett. **93**, 176809 (2004).

[75] J. K. Slingerland and F. A. Bais, Nucl. Phys. B **612**, 229 (2001).

[76] E. Ardonne, N. Read, E. Rezayi, and K. Schoutens, Nucl. Phys. B **607**, 549 (2001).

[77] B. Halperin, Helv. Phys. Acta **56**, 75 (1983).

[78] E. Ardonne and K. Schoutens, Ann. Phys. **322**, 201 (2007).

[79] M. A. Nielsen and I. L. Chuang, *Quantum Computation and Quantum Information* (Cambridge University Press, Cambridge, 2000).

[80] D. P. Di Vincenzo, Phys. Rev. A **51**, 1015 (1995).

[81] Y. A. Kitaev, A. H. Shen, and M. N. Vyalyi, *Classical and Quantum Computation* (American Mathematical Society, Providence, RI, 2002).

[82] C. M. Dawson and M. A. Nielsen, Quantum Inf. Comput. **6**, 81 (2006).

[83] C. Rebbi, Phys. Rev. D **21**, 3350 (1980).

[84] D. Petcher and D. H. Weingarten, Phys. Rev. D **22**, 2465 (1980).

[85] G. Bhanot, K. Bitar, and R. Salvador, Phys. Lett. B **188**, 246 (1987).

[86] R. Mosseri, J. Phys. A: Math. Theor. **41**, 175302 (2008).

[87] Object-oriented source codes are available for download at http://sites.google.com/site/braidanyons/.

[88] M. L. Mehta, *Random Matrices*, 3^{rd} ed. (Elsevier, San Diego, CA, 2004).

[89] M. Aguado, G. K. Brennen, F. Verstraete, and J. I. Cirac, Phys. Rev. Lett. **101**, 260501 (2008).

[90] I. Bloch, J. Dalibard, and W. Zwerger, Rev. Mod. Phys. **80**, 885 (2008).

[91] Y. J. Lin *et al.*, Nat. **462**, 628 (2009).

[92] N. R. Cooper, N. K. Wilkin, and J. M. F. Gunn, Phys. Rev. Lett. **87**, 120405 (2001).

[93] N. Gemelke, E. Sarajlic, and S. Chu, arXiv:1007.2677 (2010).

[94] J. Dalibard, F. Gerbier, G. Juzeliūnas, and P. Öhberg, arXiv:1008.5378 (2010).

[95] G. Juzeliūnas, J. Ruseckas, and J. Dalibard, Phys. Rev. A **81**, 053403 (2010).

[96] K. Osterloh *et al.*, Phys. Rev. Lett. **95**, 010403 (2005).

[97] J. Larson and S. Levin, Phys. Rev. Lett. **103**, 013602 (2009).

[98] Z. Lan *et al.*, arXiv:1102.5283 (2011).

[99] I. I. Satija, D. C. Dakin, and C. W. Clark, Phys. Rev. Lett. **97**, 216401 (2006).

[100] I. I. Satija, D. C. Dakin, J. Y. Vaishnav, and C. W. Clark, Phys. Rev. A **77**, 043410 (2008).

[101] N. Goldman, A. Kubasiak, P. Gaspard, and M. Lewenstein, Phys. Rev. A **79**, 023624 (2009).

[102] N. Goldman *et al.*, Phys. Rev. Lett. **103**, 035301 (2009).

[103] R. N. Palmer and J. K. Pachos, New J. Phys. **13**, 065002 (2011).

[104] L. Mazza *et al.*, arXiv:1105.0932 (2011).

[105] L.-H. Lu and Y.-Q. Li, Phys. Rev. A **76**, 023410 (2007).

[106] A. Jacob, P. Öhberg, G. Juzeliūnas, and L. Santos, App. Phys. B **89**, 439 (2007).

[107] A. Jacob, P. Öhberg, G. Juzeliūnas, and L. Santos, New J. Phys. **10**, 045022 (2008).

[108] J. Larson and E. Sjöqvist, Phys. Rev. A **79**, 043627 (2009).

[109] A. Bermudez *et al.*, New J. Phys. **12**, 033041 (2010).

[110] M. Merkl, G. Juzeliūnas, and P. Öhberg, EPJD **59**, 257 (2010), 10.1140/epjd/e2010-00134-4.

[111] B. Estienne, S. M. Haaker, and K. Schoutens, New J. Phys. **13**, 045012 (2011).

[112] Y. J. Lin, K. Jiménez-García, and I. B. Spielman, Nat. **471**, 83 (2011).

[113] Z. Fu *et al.*, arXiv:1106.0199 (2011).

[114] B. A. Bernevig and S.-C. Zhang, Phys. Rev. Lett. **96**, 106802 (2006).

[115] D. Zhang, J. Phys A: Math. Gen. **39**, L477 (2006).

[116] C. C. Gerry, Phys. Rev. A **37**, 2683 (1988).

[117] Y. Brihaye and A. Nininahazwe, J. Phys A: Math. Gen. **39**, 9817 (2006).

[118] L. S. Brown and W. L. Weisberger, Nucl. Phys. B **157**, 285 (1979).

[119] J. Radic, T. Sedrakyan, I. Spielman, and V. Galitski, arXiv:1108.4212 (2011).

[120] A. H. C. Neto *et al.*, Rev. Mod. Phys. **81**, 109 (2009).

[121] L. P. Pitaveskii and S. Stringari, *Bose-Einstein condensation* (Clarendon Press, Oxford, 2003).

[122] C. J. Pethick and H. Smith, *Bose-Einstein condensation in dilute alkali gases* (Cambridge University Press, Cambridge, 2008).

[123] N. R. Cooper, F. J. M. van Lankvelt, J. W. Reijnders, and K. Schoutens, Phys. Rev. A **72**, 063622 (2005).

[124] L. S. Georgiev, J. Phys. A **42**, 225203 (2009).

[125] F. D. M. Haldane and E. H. Rezayi, Phys. Rev. Lett. **60**, 956 (1988).

[126] V. Gurarie, M. Flohr, and C. Nayak, Nucl. Phys. B **498**, 513 (1997).

[127] T. H. Hansson, M. Hermanns, and S. Viefers, Phys. Rev. B **80**, 165330 (2009).

[128] J. R. Wootton, V. Lahtinen, Z. Wang, and J. K. Pachos, Phys. Rev. B **78**, 161102 (2008).

[129] J. K. Jain, *Composite fermions* (Cambridge University Press, Cambridge, 2007).

[130] Y. J. Lin *et al.*, Nat. Phys **7**, 531 (2011).